Modelling and Simulation of MD 500E Helicopter Drive System

تصميم ومحاكاة نظام ناقل الحركة لطائرة المروحية طراز MD 500

by

AHMED AL MANSOORI

Dissertation submitted in fulfilment
of the requirements for the degree of
MSc SYSTEMS ENGINEERING
at
The British University in Dubai

November 2018

DECLARATION

I warrant that the content of this research is the direct result of my own work and that any use made in it of published or unpublished copyright material falls within the limits permitted by international copyright conventions.

I understand that a copy of my research will be deposited in the University Library for permanent retention.

I hereby agree that the material mentioned above for which I am author and copyright holder may be copied and distributed by The British University in Dubai for the purposes of research, private study or education and that The British University in Dubai may recover from purchasers the costs incurred in such copying and distribution, where appropriate.

I understand that The British University in Dubai may make a digital copy available in the institutional repository.

I understand that I may apply to the University to retain the right to withhold or to restrict access to my thesis for a period which shall not normally exceed four calendar years from the congregation at which the degree is conferred, the length of the period to be specified in the application, together with the precise reasons for making that application.

Signature of the student

COPYRIGHT AND INFORMATION TO USERS

Abstract

The primary aim of this study is to study the helicopter driveline system response of the helicopter model MD 500E. In order to meet the aims of this study, a mathematical model has been derived from the system from the physical description of the helicopter available. Lumped, finite element and hybrid, distributed-lumped parameter procedures developed by R Whalley, M Ebrahimi and Z Jamil paper “The Torsional response of rotor systems” are employed to represent the system of concern in efforts aimed at increasing accuracy, integrity and computational efficiency. The simulation was done using the Matlab Simulink platform. From the simulation, predictions can be made about how the helicopter’s drive shaft will behave under specific conditions. The results revealed that the three models share identical steady-state response and only vary in transient behaviour. In addition, it was observed that the hybrid, distributed-lumped model showed high accuracy and good integrity and computational efficiency in comparison to the lumped model as well as finite elements model.

خلاصة البحث

تهدف هذه الدراسة بشكل أساسي إلى دراسة استجابة نظام خط ناقل الحركة لطائرة المروحية طراز MD 500E. من أجل تحقيق ذلك، تم اشتقاق معادلات رياضية لتمثيل النموذج الفيزيائي المتوفر للهليكوبتر. بالإضافة إلى ذلك، تم تطوير نموذج النظام ومحاكاته باستخدام برنامج Matlab Simulink. ومن خلال هذه المحاكاة، يمكن إجراء تنبؤات حول الكيفية التي سيتصرف بها عمود ناقل الحركة لطائرة المروحية طراز MD 500Eفي ظروف محددة.

يتم النظر في الاستجابة الالتوائية لنظام خط ناقل الحركة لطائرة المروحية (MD 500E) المكونة من محرك توربين، وعمود ناقل حرك رئيسي، وصندوق تروس الرئيسي، وعمود ناقل حركة دوران المروحة الرئيسية وصندوق تروس المروحة الرئيسية والمروحة الرئيسية، وعمود ناقل حركة دوران مروحة الذيل، ومروحة الذيل. تم استخدام تصميم العناصر المجمعة والعناصر المتفردة والهجينة المطوّرة من قبل R Whalley و M Ebrahimi و Z Jamil لتمثيل النظام وذلك كجزء من الاهتمامات في الجهود الرامية إلى زيادة الدقة والنزاهة والفعالية الحسابية.

Dedication

"Simulations and a rapid, iterative approach enabled us to minimise the unknowns and ensure that we had established enough margin that when we ran into a surprise, we could continue to have a safe flight test program—and run it with unprecedented efficiency." - David KingBell Helicopter

Acknowledgments

I would first like to thanks to my dissertation supervisor, Dr Alaa A-Ameer of the Faculty of Engineering and Information Technology at the British University in Dubai. The door to Dr Alaa A-Ameer office was always open whenever I ran into a trouble spot or had a question with reference to system modelling. He consistently allowed this dissertation to be my own work but steered me in the right direction whenever he thought I needed it.

I would also like to say thanks to all my mentors and professors who have taught me and helped me in my road to professional development.

In the final analysis, I must express my very profound gratitude to my family for providing me with unfailing support and continuous encouragement throughout my years of study and through the process of modelling and writing this dissertation. This accomplishment would not have been possible without them. Thank you all.

Ahmed Mohamed Al Mansoori

Contents

List of Figures

List of Tables

List of Notations and Abbreviations:

ATSB	Australian Transport Safety Bureau
AD	Anno Domini: a Latin phrase meaning “in the year of the lord”
BC	Before Jesus Christ
C	Shaft compliance
C_1, C_2	Viscous damping coefficients
C_d	Damping coefficient (bearing friction)
D	Diameter of the shafts
Di	Inside diameter
D_o	Outside diameter
E	Young’s Modulus
fpm	Feet per minutes
G	Modulus of rigidity (shear modulus)
Hp	Hours power
J	Polar moment of inertia of shafts
K	Torsional stiffnesses
K	Gain constant
L	Shaft lengths
MD	McDonnell Douglas
M	Mass
MR	Main Rotor
P	power
SUC	System under consideration
S	Laplace variable
Tr	Tail rotor

T	Shaft torque
T	Time
Ω	Angular velocities
τ	Shaft shear stress
A	Angle of twist
Ω	Resonant frequency
P	Shaft density
Ξ	Characteristic impedance

Chapter I

Introduction

1.1. Research Background

From the late fifties to early sixties, there has been an increase in the gas turbines, and its applications to helicopter began during this time. Due to this, helicopter driveline design and technology underwent substantial change. Not only that, the effect was seen in the drive input speeds as well which saw an increase from 2,500 to around 20,000 rpm. The power that was needed to be absorbed also grew threefold. This proved to be highly challenging, and by the early eighties, there was a requirement for reduced noise, weight, safety, costs and other factors in helicopters.

The rotational speed of the power unit is very high. However, a lower speed is essential for driving the main and tail rotor. Several mechanical gearboxes are part of a conventional helicopter drive train for this purpose. The power is transmitted from the engine to the main rotor and tail rotor. The speed of the engine or the input is reduced by the gearbox to avoid the same speed being generated as the output.

1.2. Helicopter Drive System Overview

1.2.1. Engine

The engine supplies the power in the form of torque and transfers it to other components of the helicopter. The power is provided by the engine in the form of torque at a

specific angular velocity which is then transferred to the rotors at a different angular velocity. The difference in the torque angular velocity is due to the fact that the engine's velocity is faster than what the components are safe to handle, hence, to avoid damage to the fundamental components of the helicopter, the engine supplies the torque at a different, reduced angular velocity.

The gas turbine engine is one of the most widely used engine type in helicopters. It is also called Turboshaft Engine. This type of engine is designed to produce more shaft rotation rather than thrust power and is used in applications requiring a light-weight, high-power output and high-reliability situations. This makes it highly applicable in helicopters.

The engine consists of two sections: gas generator and power section which rotate at varying speeds relative to one another. The key feature of the turboshaft engine is that it drives a transmission which is structurally separated from the engine. Some larger helicopters can use two or more turboshaft engines for redundancy.

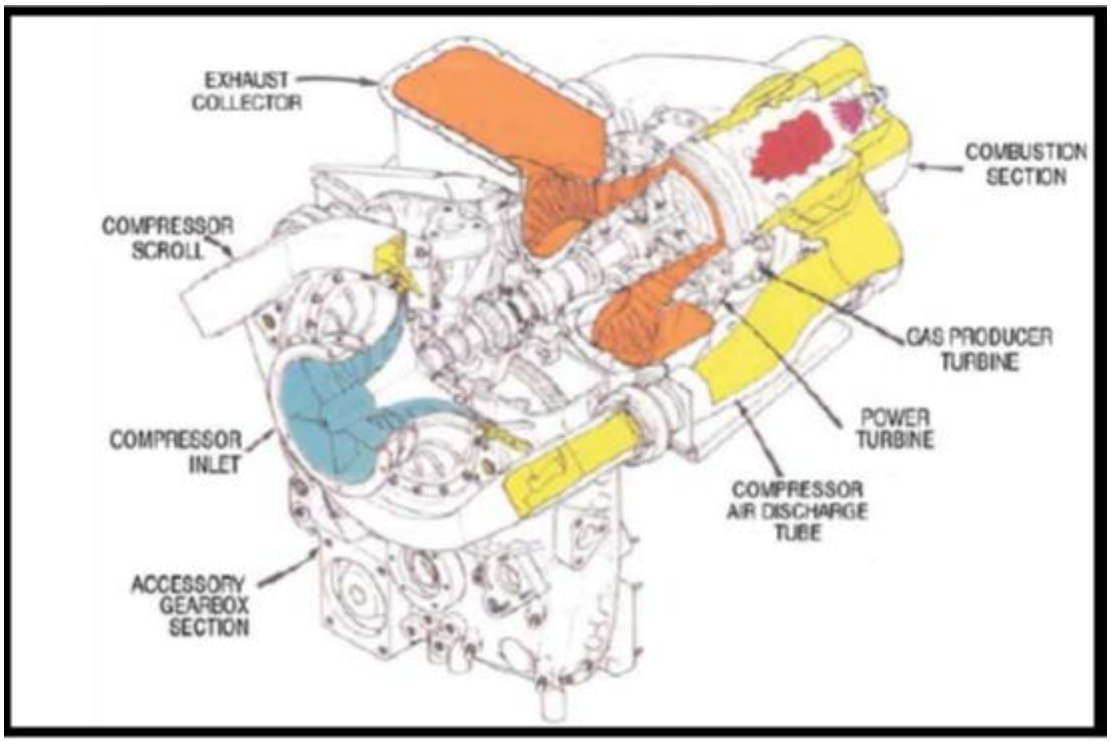

Figure 1 Typical Rolls-Royce Model 250 Turboshaft Engine Cross Section

(Source: "MD500"2018)

1.2.2. Drive shaft

A drive shaft is a component that is used for the transmission of the torque and subsequent rotation. A drive shaft is usually connected to other components. Drive shafts are highly subjected to effects of torque such as shear stress and torsion which are dependent on the input torque and the load. Therefore it can be stated that the drive shaft is designed to strong and robust to withstand the effects of torque while not being too heavy which can lead to an increase in the inertia.

Figure 2 MD500E Main Drive Shaft (Source: "MD500E"2018)

In a helicopter, the main drive shaft is connected between the engine and the main transmission while the tail rotor shaft is between the main transmission and the tail rotor. The Main rotor shaft is between the main rotor and the main rotor transmission.

1.2.3. Transmission gear

Power is transferred to other components of the helicopter like the main rotor, the tail rotor and other components through the transmission which is also known as the main gearbox. The primary purpose of the gearbox is to reduce the rpm output of the engine and render it suitable for the main and tail rotors of a helicopter. For example, when an engine generates rpm of 6,000 as the output reduction happens so that the main rotor operates at a reduced speed of 450 rpm.

Some of the primary functions of the main transmission gear are provided below:

1. In an effort to drive the rotor mast, the transmission gear leads to the change in angle to the drive and reduces the speed using a chain of spiral bevel gears and planetary gears.
2. When the engine is stopped or is generating outputs that are below the rotor driving speed, the transmission is disconnected from the engine to allow the main rotor and the gear train to rotate independently.
3. Supported by bearings, the tail rotor is driven through the shaft by the secondary gear train.
4. One (or two) gearboxes are responsible for the transmission of power to the tail rotor. The transmission delivers a gear ratio of 1:1 and also provides a change in the angle of 42 degrees.
5. There is a 90-degree gearbox which generates a change angle of 90 degrees and also delivers gear reduction.
6. The tail rotor quill is also driven by the transmission. In addition, the hydraulic pump quill, the rotor tachometer, the cockpit blower quill and several other components are driven by the transmission.

1.2.4. Tail Rotor gearbox

The tail rotor gearbox, also called the 90^0 Gearbox, is located at the top of the vertical fin. Some of the helicopter models have this gearbox near the vertical fin. This gearbox serves a primary purpose of providing a 90^0 transition in the speed and drive reduction. This reduction is provided between the output and input shaft. The pitch change mechanisms are also situated within this gearbox.

Figure 3 Tail Rotor Gear Box

1.2.5. Main rotor

The main rotor system is a crucial part of the helicopter system which allows the helicopter to fly by generating sufficient lift. This system comprises of a blade, a mast, a hub and a rotor. Due to their being a number of ways of attaching the rotor blades to the main rotor hub, there are different classifications to be made: rigid, semi-rigid or fully articulated.

1.3.Tail rotor Drive Shaft Failure (MD369E)

It was reported by the Australian Transport Safety Bureau (2005), that the McDonnell Douglas Hughes 369E helicopter had a failure of the tail rotor. The damage to the aircraft happened when the tail rotor and the helicopter completely separated. While no clear damage to the tail or main rotor system was found, the tail was broken. The helicopter model had a five-blade rotor system which was accompanied by a four-blade anti-torque system. The incident occurred when the helicopter was in-flight in a climb to cruise. Due to it being at a sufficiently low-altitude, the pilot was able to engage in an emergency landing action. A close inspection by the ATSB revealed that the accident happened due to a localised buckling

which leads to total fracture of the rear tail due to torsional overload. The structure did not reveal any pre-existing fault or contact damage and had a good serviceability record.

In terms of structure, the helicopter is powered by a single gas turbine engine. The lift force was provided by the main rotor which comprised of five blades, and the anti-torque is delivered by the four-blade tail rotor. The tail rotor drive shaft was connected to the transmission which delivered the relevant torsional power. The dimensions of the failed drive shaft were as follows: 3.96m in length, a wall thickness of 1.20 mm and the outer diameter of 70mm. The shape of the shaft was such that it tapered off at the ends and flanges attached the shaft to the flexible joint couplings. A damper was attached to the centre in an effort to reduce the lateral flex and the vibrations during the flight.

After the failure happened, there was a close examination of the servicing and repairing of the helicopter. It was identified that the helicopter was well in its desired operating state. There were no known internal issues or problems that had caused such a failure in the shaft. The report stated that only the history of a tail rotor system failure occurred when a foreign object, such as a bird or vegetation got stuck in the tail rotor. In addition, there were reported cases when a gross mechanical failure took place during the operation.

The fractured tail rotor drive shaft is presented in the below figure.

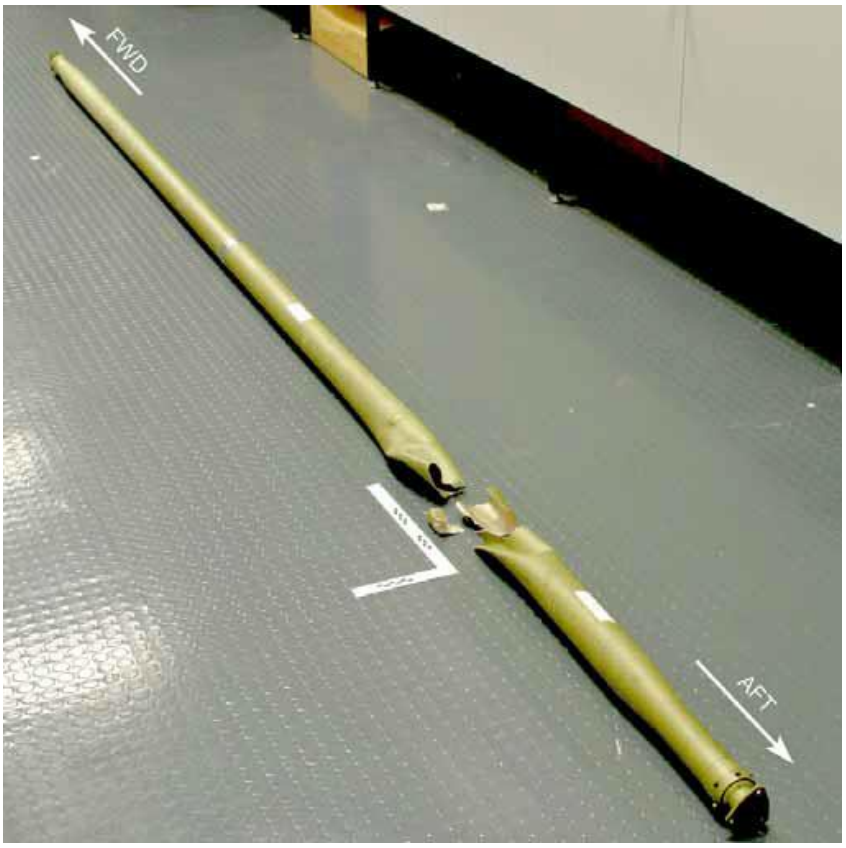

Figure 4 Damaged Tail Rotor Shaft Optical Examination (Source: "ATSB"2005)

In the above figure, the fracture occurred towards the rear end of the tail rotor gearbox connection. The estimated distance from the rear end was estimated at about 760 mm. The shaft had separated into a total of four pieces with the two of them being smaller fragments and other two being the shaft tubes. The smaller and the larger sections of the shaft had shown, upon closer visual inspection, that the damage was in the form of bending. It was suggested by the report that this bending and the subsequent damage that occurred was due to torsional loading and buckling which was experienced by the shaft. After a closer examination, it was discovered that there were fractures on the surface of the shaft which

were consistent with the type of fractures generated due to shear stress type failures. There was also no previous fatigue crack noticed, and the shaft was in otherwise good condition.

The report released by the ATSB (2005) hypothesised that the tail could have been subjected to a "localised transient loading condition above that of its intended design" (p.10). The report stated that there could have been the generation of a rotational resistance of the assembly. Several possibilities were outlined in the report: bird strike, tail rotor impact, gross malfunction of the rotor gearbox system, and the failure of the drive shaft bearings.

1.4. OH 58A Overview

The MD 500E is an upgraded model of the OH 58A helicopter. The OH 58A served both commercial and military needs while the MD 500E serves as a primary observational helicopter.

According to a report published by Lewicki and Coy (1987), the OH 58A was subjected to a study in which the vibration characteristics were studied. Several vibration tests were performed on the main rotor transmission. The helicopter was a single engine helicopter which was used in both military and commercial use. In the military perspective, it was considered a light-observational helicopter. It had a bevel gear which was mounted on the bearings (duplex and roller). The justification of this study was provided in the form of understanding the vibration and the helicopter noise. The source of noise in the helicopter is from two sources: internal and external. The internal noise is caused due to the vibration which is generated by the transmission of the gears. This internal noise contributes to discomfort to the passengers and has the potential to reduce the pilot's efficiency. On the

other hand, the external noise is generated due to the rotor blades, the engine and the exhaust. External noise can lead to noise pollution and add to the discomfort of the people. The usual manner of reducing the internal noise is by using soundproofing foam and other materials with sound absorbing properties inside the cabin of the helicopter. However, the issue with this method is that it creates weight and hence the power needs to increase to accommodate the added weight. This creates a cycle where no effective solution can be found due to the critical nature of the weight to power ratio. In addition, the vibration that is generated also causes an increase in the noise. Thus, seeing as an external solution is not possible, the attention was diverted to fix the noise at the source itself. It was identified in the report by Lewicki and Coy (1987), that the transmission is the primary source of the noise and the transmission. Furthermore, shaft deflections, bearing misalignments, and gear profile issues will lead to an increase in the noise profile. Not only that, but these issues can also lead to increased dynamic loading and harmful vibrations. The absence of appropriate control of vibration can even lead to transmission failures which can be rather damaging. The authors stated that whenever vibration analysis has been carried out, there have been huge vibrations associated with these transmissions. This poses a greater in-flight risk to the safety of the passengers, the helicopter and the pilot in the case of a failure due to shaft deflections, or dynamic loading caused by these vibrations.

During the analysis that was conducted by Lewicki and Coy (1987), it was found that the speed increased the vibrations by a substantial level. It was observed that the vibrations increased until a resonant point was achieved. After this, the resonance decreased when the speed reached to levels above the resonance. In addition, it was also detected that the

vibration was at the highest point at the spiral bevel gear's meshing frequency. In essence, the results of the above study conducted by Lewicki and Coy showed that as the speed increased, the transmission increased which then caused an increase in the vibrations and the resonance frequency.

1.5. McDonnell Douglas MD 500E overview

The MD helicopters form part of a series that is in production from 1967 and are used for military operations as well as light civilian use. The MD 500E has the following applications: aerial photography, aerial survey, air rescue, firing fighting, police air support, and various other applications in the fields of petroleum, paramilitary, forestry and construction engineering.

The rotor system of the MD 500E is unique to itself and uses a static mast that is rigidly attached to the fuselage. This allows the transfer of all the dynamic loads through the mast rather than the transmission. Designed for optimum safety, the inner drive shaft transmits the engine torque to the main hub. This also allows the helicopter to maintain light weight and facilitate better flight control. Structurally, the MD 500E's rotor system is composed of a five-blade, fully articulated main rotor assembly. Fastened to the main hub using laminated steel strap sets, the rotor blades, pitch housings and the links are feathered to contain the blade centrifugal loading. The steel strap sets allow the centrifugal loads to be countered by force from the two, opposite blades. This leads to a very light centrifugal load. The main rotor blade is turned using the V-legs of the strap set as driving members.

Feathering and flapping of the blades are allowed due to the strap sets' configuration. The main rotor blades are retained to the main rotor hub using captive cam-handle-type blade retention bolts.

The recent design practices in the light helicopters are the use of a single primary rotor transmission, and this is what MD 500E also follows. The engine and the main rotor shaft are separated by four reduction stages. The output speed of the engine is reduced by helical gears (from 35,350 rpm to 6,060 rpm in two stages) at the input of the gearbox.

Power is extracted from the helical gear which provides an offset between the bevel pinion axis and the engine which will extract the power from the final helical gear. Spiral bevel (19/71 reduction) in the transmission is the first-stage gearing. This delivers a speed of approximately 1,622 rpm to the sun gear of the planetary unit with a fixed ring. Providing a final reduction of 4:67:1, this planetary ring generates a speed of 347.5 rpm to the main shaft and the planet carrier. This design is featured by self-aligning bearings in the pinions of the planet, a flexible radial ring gear, and cantilever support for the bevel gear with which the overall height can be reduced.

Driveline modelling is an important method for understanding the dynamics of the driveline. The tail rotor drive shaft of this helicopter comes equipped with dampers which serve to reduce the vibration that takes place in the tail rotor drive system.

1.6. Research Problem Statement

This research covers modelling of MD500E helicopter drive train systems comprising jet Engine, Engine drive shaft, main gears, main rotor gears, tail rotor gear,

Main rotor drive shaft, Tail rotor drive shaft, Main rotor and Tail rotor. Lumped, finite element and hybrid, distributed-lumped parameter procedures developed by R Whalley, M Ebrahimi and Z Jamil paper “The Torsional response of rotor systems “are employed to represent the system of concern in efforts aimed at studying accuracy, integrity and computational efficiency.

1.7. Research Aims and Objectives

The primary objectives of this dissertation are as follows:

- Derive a complete mathematical model for the MD500E helicopter drive train using lumped, finite element and hybrid, distributed-lumped techniques.
- Compare between lumped, finite elements and hybrid, distributed-lumped techniques in accuracy, integrity and computational efficiency.
- Generate the system block diagram.
- Define the system parameters.
- Analysis system model performance

1.8.Project Outline

- Review of various mathematical modelling methods
- Obtain helicopter driveline physical parameter from MD500E helicopter design specification
- Calculating and estimating of helicopter drivetrain model constant value

- Derived the helicopter drivetrain models based on *Whalley, Ebrahimi & Jamil 2005 paper*
- Simulate the mathematical models
- Discusses the simulation result

1.9.Research Dissertation Organization

This Dissertation is organised in five chapters which include the following:

Chapter1: Introduction

This chapter is the introduction to this project. It includes brief sections on the helicopter in question (MD 500E), the old model of the same helicopter which has been decommissioned (OH 58A), helicopter drive line overview which takes into account various relevant components of the helicopter and finally, this chapter also includes a section on a case of MD helicopter shaft failure in a helicopter cause due to shear stress and torsional loading.

Chapter 2: Literature Review

Chapter 2 covers the important literature review of mathematical model fundamentals describing various methods of modelling of helicopter driveline including lumped model, finite element model and hybrid, distributed-lumped parameter model.

Chapter3: Modeling of MD500E Helicopter driveline

In this chapter, MD 500 E helicopter driveline physical parameter is identified, and model constant value is calculated. Furthermore, three different drivetrain models are derived (lumped model, finite element model and hybrid, distributed-lumped parameter model.

Chapter4: Simulation Result and Discussion

The models derived in Chapter 3 are used to simulate helicopter drivetrain response in time domain and frequency domain. In addition, the performance of subject models is compared in accuracy, integrity and computational efficiency.

Chapter5: Conclusion

In chapter 5, the work accomplished is summarized, and several recommendations are made for possible future work on this topic.

Furthermore, this dissertation includes an abstract in both Arabic and English languages.

Chapter II

Literature review

2.1. Mathematical Model Fundamentals Review

Schichl (2004) stated that mathematical modelling has been around since early 30,000 BC where the first numbers have been documented. Fast forwarding to 2,000 BC, some of the cultures already had the knowledge of mathematics and were using mathematical; modelling. Geometry, developed in the 600 BC was one of the first methods of trying to understand reality using mathematical principles on a wide scale. Pythagoras is said to have developed the theory of numbers, and in 300 BC, Euclid developed a book which contained as much mathematical knowledge as was known at the time. The first applied mathematicians, Erathosthenes, in 250 BC computed the circumference of the Earth using a geometrical-mathematical model. A mathematical model was developed in the 250 AD which introduced the concepts of Algebra and the idea of a 'variable'. In 150 AD, the mathematical model of the solar system was developed which are still valid today due to the contributions of Newton and Einstein (Schichl, 2004).

Galbraith and Clatworthy (1990) have defined mathematical modelling as the process for solving real-life situations or problems using mathematics. Cheng (2001) stated that in mathematical modelling a problem or situation is transformed into a mathematical equation and solved using mathematics. Berry and Houston (1995) define mathematical modelling as a method of solving problems using mathematics.

There are several applications of mathematical modelling across many technologies and scientific fields (Kaiser & Sriraman, 2006). According to Hazelrigg (1999), the early mechanical engineers used a method of trial and error primarily to see what worked and what doesn't. The author stated that on moving from iconic models (small-scale representations such as a model bridge) to analogue models (using one system to represent another as is the case in F=ma), engineers have in the final analysis settled on symbolic models (using symbols to denote physical quantities). The main significance of symbolic modelling (henceforth, modelling) is that it allows the engineer to reduce uncertainty in highly complex systems by allowing to make guesses at certain variables, as stated by Hazelrigg. In addition, mathematical modelling can help engineers change the variables and understand the real world in a better manner as well as make predictions. Therefore, it can be stated that modelling carries the following benefits for mechanical engineers:

- Enables a complex understanding of a system
- Allows the testing of various inputs and measuring the system's outputs
- Provides input into the extreme working conditions of a system.

Broadly speaking, there are two types of modelling procedures: experimental and theoretical. Theoretical modelling is done by first developing a set of assumptions with reference to a known object or a system (Achinstein, 1965). In addition, he stated that a theoretical model will often ascribe a structure, reference, or inner structure which will then be used to explain some or all of its properties. Experimental modelling, also known as System Identification, is where the information with reference to the system is unavailable and when the properties of the system are undefined to some extent (Ljung, 1997). According

to the author, this type of modelling is also referred to as Black-box modelling. In contrast, theoretical modelling is known as White-box model. An intersection of white-box and black-box reveals a grey-box model which is depicted in Figure 4 below.

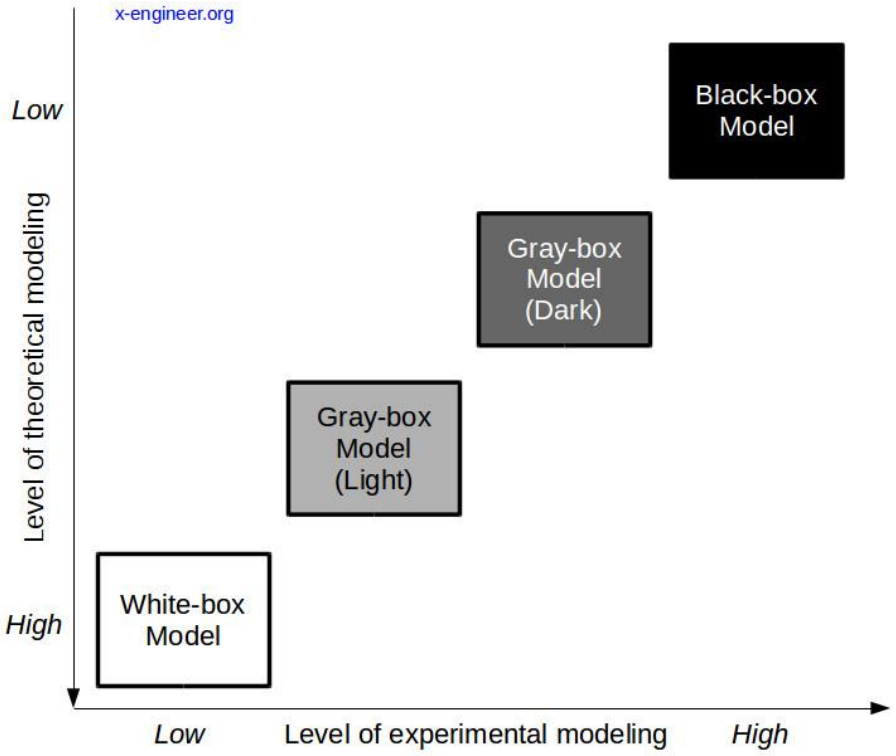

Figure 5 Different Methods of Mathematical modelling (Source: "x-engineer.org"2018)

This research is based on the principles of theoretical modelling.

2.2.The System Model

The term system has come to mean several things in the modern world. However, for the objectives of this study, the definition suggested by Gordon (1969) who said that a system is an assembly of several objects joined together in a pre-defined manner with some

interconnectedness or interaction. The brief history and the wider applications of modelling discussed earlier. Typically, engineers and mathematicians have used various methods of developing system models which are then used to carry out investigations, plan systems and processes, and study various systems.

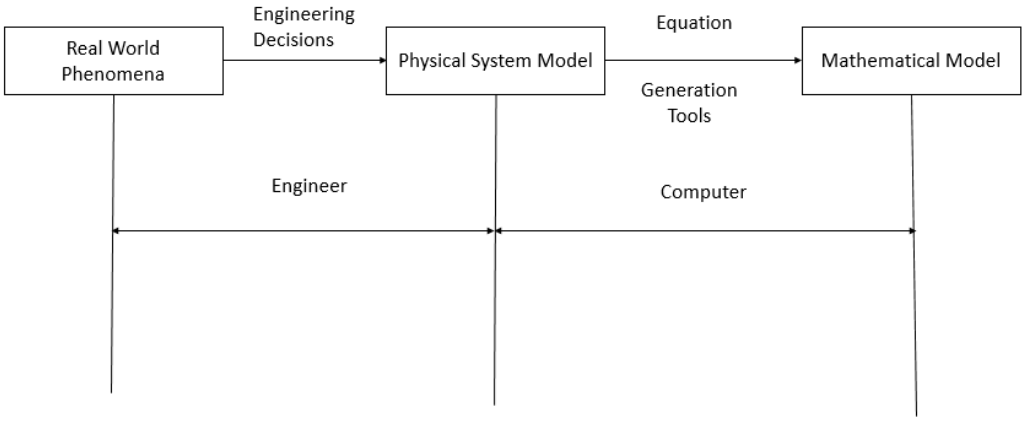

Figure 6 Physical System Modelling

Modelling of systems can be done in an entirely physical manner or done in an entirely mathematical or abstract manner. In essence, Karnopp and Rosenberg (1983) have determined that the system model represents a simplified reality. It is the use of abstract or simplified construction to create a system model which can then allow us to study and predict how the system might behave under different conditions.

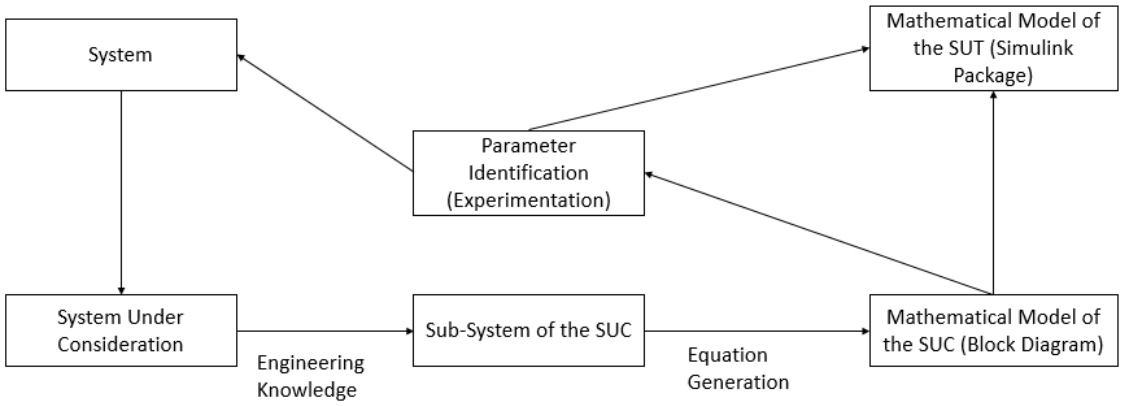

Figure 7 Modelling Procedure

However, Stein and Louca (1995) have stated that since the system model is only an abstract that is over-simplified, it can only be used for understanding and predicting minor parts of its behaviour but not the entire behaviour as a whole. In addition, it is noteworthy that a mathematical model is not an exact representation of the physical system and it is only a simplified abstraction of the same. While a physical model will be a more accurate representation of the system as a whole, it is time-consuming to develop and costly. Therefore, mathematical models are preferred.

A mathematical model takes the form of equations which depicts the relationship between the various elements of the physical system. The model essentially has four components that are linked together. The first element is the dependent variable, which is what best represents the behaviour of the system. The independent variable is the external dimension of space and time which can influence the behaviour of the system. Parameters are constants which reflect the composition or the property of the system. Any external influences which change the system in any way are known as forcing functions.

In order to develop a system model, there are two primary approaches:

- The system is divided into various elements which form the basis for the development of the mathematical equation or model.
- The system is subjected to an experiment, results of the experiment are obtained, and then a mathematical model is built based on the information.

There are several types of system models which are briefly discussed below.

2.3. Linear and Non-linear Models

According to Hale and Lasalle (1963), the history of differential equations began with Newton. The authors delineate two primary types of models: linear and non-linear. To put simply, non-linear equations (models) are those for which the principle of superposition does not hold true. To make a simple comparison between linear and non-linear systems, the authors presented the following first order equations respectively:

$y' = -y \quad (1)$

$y' = -y(1-y) \quad (2)$

The solution for (1) will be $y = ae^{-t}$ where 'a' is any arbitrary constant. On the contrary, the solution for (2) will be $y = a/(1-a+ae^{-t}) * e^{-t}$. Therefore, it can be observed that even the most simplest non-linear model will have more than one solution which can also become unbounded in some cases (Hale and Lasalle, 1963).

Most of the systems are non-linear, but the mathematical models are built with the assumption that all the elements that form the system are linear. The basic idea of linearity is that the input/output is a straight line. In this research, the systems are being simplified into a linear system due to non-linear systems being too complex to handle.

2.4. Static and Dynamic Models

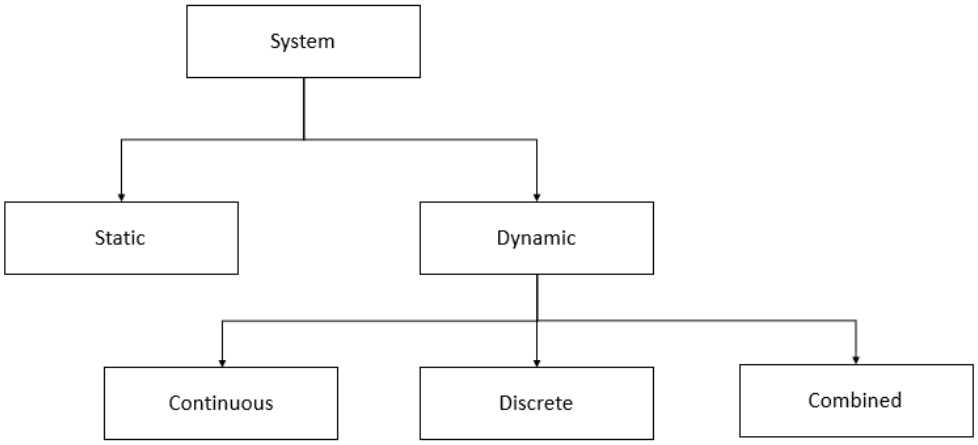

Figure 8 Types of System Models

In simple terms, a dynamic system is one where the changes are not applied immediately (Astrom & Murray, 2018). The authors provided the example of a moving car not changing its speed immediately when the pedal has been pressed. Therefore, it can be said that a dynamic model is one where the behaviour changes with time. In contrast, a static system is time-invariant.

Both the models are expressed in differential equations. This research is a dynamic system response. The ideal order that a dynamic mechanical system has should be zero (n=0).

However, since this is a real time-dependent system, there is no zero-order system, and most of the systems are either first or second degree.

The relationship between the input and output in a dynamic system can be represented by this ordinary differential equation:

$$a_n \frac{d^n y}{dt^n} + a_{n-1} \frac{d^{n-1} y}{dt^{n-1}} + \dots + a_2 \frac{d^2 y}{dt^2} + a_1 \frac{dy}{dt} + a_0 y = bx \qquad (3)$$

where 'n' is the order of the equation, x is the input and y is the output. a_0, a_1, a_2, …, an represent the coefficients of the equation.

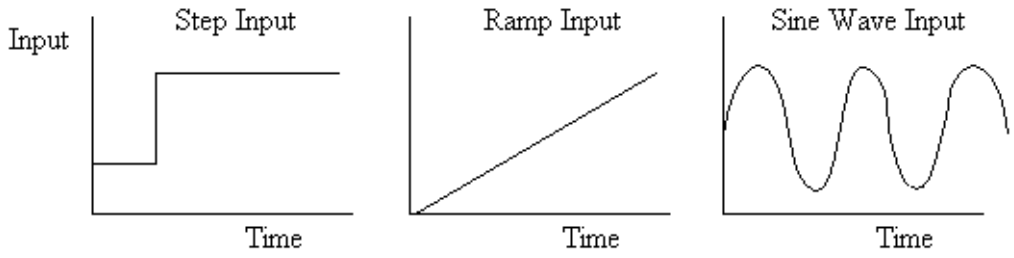

Figure 9 Types of inputs for dynamic system response test

The dynamic system response is usually tested using one of the four types of inputs: Step input, Impulse input, ramp input and sinusoidal input. Step input represents a sudden change that was made in the input at time t=0 which will allow the measurement of the time response of the dynamic system. The Impulse input will represent a sudden increase in the input at a random time interval over a very short time. The Ramp input sees an exponential increase in the input starting at t=0, and sinusoidal input is where the input is a function of the sine wave with a frequency of f and amplitude A.

There are some features of a dynamic system model. Any dynamic model which follows the physical laws of nature is developed using non-linear differential equations. In addition, when these non-linear equations are in the proximity of an operating point, they assume the properties and behaviour of linear equations.

2.5. Explicit and Implicit Model

To put simply, an explicit model is one where all the input parameters of the known, therefore, the output parameters are computed with a finite set of calculations. The opposite is true for an implicit model which does not have the output parameters and the input parameters need to solved using an iterative method.

2.6. Deterministic and Probabilistic (Stochastic) Model

Meiss (2007) stated that a deterministic system is one where there is no randomness, one where the same results are obtained with a given set of conditions. In this model, every single variable set is predetermined by the previous sets and parameters in the model. In other words, these types of models have elements which are clearly specified which leads to an accurate identification of the model’s behaviour, in a given scenario.

In contrast, a stochastic model is one where there is a lot of randomness, and no defined set of variables are present. In this model, the variable states are dependent on the probability distributions and not on specific values. In simpler terms, the model's input variables or coefficients are not well-known, and the model is represented in the form of probability distributions.

2.7. Lumped Parameter Models

A lumped parameter model is defined as a system in which the dependent variables are functions of time. In this regard, a lumped model can be thought to provide a simplification of the behaviour of the physical systems into an approximated behavioural model that forms a topological system of entities. Due to this, the lumped model can be solved using ordinary differential equations and therefore is an important consideration.

There are two primary simplifying assumptions that are made for lumped parameter models in mechanical systems:

1. All the mechanical objects are solid bodies with rigidity
2. The interactions that take place between these rigid bodies are only through dampers, springs, and kinematic pairs.

The mechanical rotatory shaft system of a helicopter can be reduced to a number of interconnected rigid bodies (shafts and rotors) with bearings. The usage of rotors and shafts on bearings is widespread in the aerospace industry. The rotors have a very high RPM and are subjected to high-frequency stress. There are several loach changes, and violent perturbations that are experienced by the rotor, shaft and bearing systems which can lead to damaging vibrations, increased wear and generation of noise (Whalley, Ebrahimi, & Jamil, 2005). Representing these components in the form of differential equations can allow the testing of various properties like stiffness, resonance, mass/inertia and frictional dissipation. However, Whalley, Ebrahimi and Jamil (2005) pointed out that resonance predictions

become increasingly inaccurate in a lumped parameter model if there is an increase in the spatial dispersion of the system.

2.8. Finite Elements Model

For the modern engineers, Finite Element Analysis has become one of the most valued tools. Digital transformation and the current advances in the technology have created the way for advanced and highly sophisticated finite elements software today. Just within this decade, there has been a tremendous increase in the usage, no doubt caused by the increased accuracy and strength of the finite elements software.

In accordance with this, the use of finite element analysis has become more widely acceptable especially in the calculation of fatigue and stress of any aircraft part. This is because of the fact that with the increased technological capabilities, the finite element analysis software can create 3D models and allow the engineers to carry out a myriad number of tests.

Conducting a fatigue analysis on various helicopter components is a widespread practice. For example, Schaff carried out such an analysis on the tail rotor spar of a helicopter. Using finite element analysis, a composite of the tail rotor was created. In the composite model, Schaff used a layered shell element. This allowed the strength and stiffness properties to be used. In addition, Schaff established a residual strength relation which allows assumptions to be made to the effect that the strength decreases without change after being equal to the original, static value. The strength decreases until a failure is induced. Here, the failure is defined as the maximum stress failure criteria.

The results of the fatigue relations and residual strengths are compared to the damaged regions and the failure criterion. These damaged regions can be degraded with adjustments made to the stiffness matrix of the finite elements model. Fatigue causes a lot of damage which can be due to several factors such as material flaws, design flaws, any manufacturing defects, and loads. However, the instances where a sudden event caused the failure are present. Finite element analysis can be used even in this situation. For example, Colombo identified the fatigue life of the helicopter tail rotor transmission which was put under sudden ballistic damage using the finite element model. In this analysis, the helicopter was made to perform an emergency manoeuvre during a normal flight which lasted for 30 minutes. The emergency was created when the shaft of the tail rotor was impacted upon by a ballistic projectile. The model was used as a means to allow the simulation of the crack generation as soon as the shaft was hit by the ballistic projectile. This model allowed the generation of an estimate of how much time was needed to reach failure of the shaft.

Finite Elements model represents the breakdown of complex systems into smaller, finite elements which can be analysed using partial differential equations. In terms of mathematical modelling, the Finite Element Model will allow for the computation of how different parts of a mechanical system behave under different conditions. In design engineering, Finite Elements Analysis is important to determine the performance of key areas in the mechanical systems and identify any weak spots.

Where the Lumped Parameter model shows an oversimplification of a complex mechanical system, the Finite Elements model allows for complexities and follows a discretisation method for analysis. First developed by Rhul and Booker (1972) for rotor

systems, the Finite Elements Model allows the breakdown of one complex system of shaft-rotor-bearing into several smaller nodal sections interconnected at two or more points. Figure 4 shows a Finite Model Analysis of a shaft under stress, as an example.

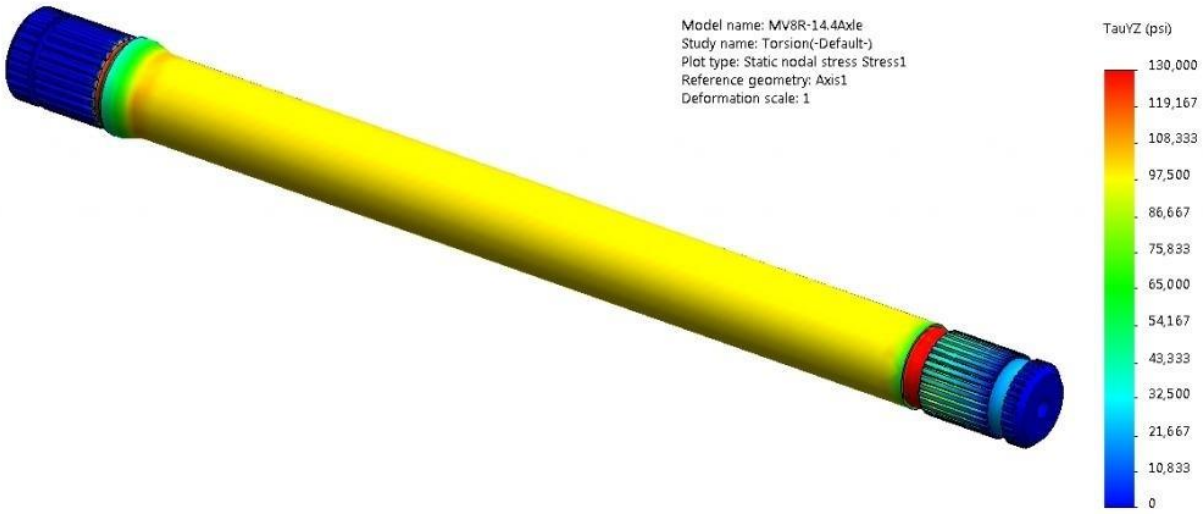

Figure 10 Example of Finite Element Analysis of shaft torsional response

(Source: Veershetty 2018)

Nelson and McVaugh (1976) developed a finite element model for a rotatory shaft system for both the static and dynamic frame of reference. The authors found that the dynamic frame is beneficial in the analysis of isotropic systems as it can allow the two planes of motion to be considered as two separate elements. In addition, the static frame can allow for the computational analysis of damping and stiffness. In conclusion, the authors identified that the finite element model could be applied for the identifying stability, critical speeds, shear stress deformation, internal damping, etc.

Whalley, Ebrahimi, and Jamil (2005) classified the Finite Element model as a step-up from the simplified lumped model. They noted that as the values of mass, stiffness matrix and damping increases, the Finite Element Analysis will increase the number of eigenvalues and eigenvectors.

2.9. Hybrid Distributed-Lumped Model

Distributed systems are not only functions of time but also have a spatial dimension, unlike the lumped model which is simply a function of time. Whalley (1988) stated that despite the fact that mechanical systems are constructed using several complex structures the models rarely depict the same complexity and mainly work to avoid the complexities. To this end, the author developed a distributed-lumped hybrid model which carries lumped sections and other sections that are distributed and solved using a combination of partial and ordinary differential equations.

2.10. Shaft Model

A three-dimensional load is experienced by a transmission shaft which then experiences a combination of torsional, bending, compression, and axial tension loads. The maximum shear theory states that fatigue from loads is the primary reason for the shaft failures. The transmission shafting is designed to remain hollow with the ratio of diameter to thickness being as high as possible. The torsional loads occur on the tail rotor and engine drive. The following equation represents the torsional shear stress which can carry torsional loads:

$f_s = T_r/J$

where

f_s is the torsional shear stress

T is torque

r is the radial distance from the stress point

J is the polar moment of inertia and is given by the following equation: $J = \Pi(D^4 - d^4) / 32$

The outside diameter will experience the most shear stress. This will be the greatest value possible of the local moment and the stress concentration factor K_s and is given by the following equation:

$$f_{smax} = \frac{16TK_sD}{\Pi(D^4 - d^4)}$$

The sharp narrowing of a shaft diameter is the critical area of the shaft and faces an increased stress. This increased stress is denoted by a stress concentration factor of K_s. The endurance limit is given by half the yield strength according to the maximum shear stress theory.

2.10.1. Critical Speeds

'Critical speeds' appears to be one of the major challenges that is encountered by shaft design. Large centrifugal forces are created by the residual imbalances as a direct result of the shaft speed. The rotating shaft is bent as a result of the large centrifugal forces and is then counteracted by the elastic forces present in the shaft.

As the critical speed increases, the shaft's bent mass travels towards the centreline till the sgat begins to rotate with reference to its axis. The shaft's operations carried out at a lower speed than the critical speed is known as sub-critical speed where if the operations takes place above the critical speed, it is called supercritical. In order to maintain the safety of the operation, the sub-critical operation must not exceed more than 30% of the critical speed, and supercritical must not exceed more than 10%. The drive shafts which connect the engines and the gearbox are operated within or below the critical speeds. Damping is a necessity if a shaft is designed to operate above the critical speed during the run-up.

In the case of shafts that have a zero moment restraint on the bearings and have a uniform mass distribution no bending will occur. Such a situation is observed in the tail rotor drive shaft which links the primary transmission to tail rotor gearbox. The modelling of such a shaft is carried out with a beam of a particular length. Here, the bearings are in place to provide support to the ends.

The critical speed is a function of the length between supports and the mean radius of the tube, is denoted by the critical speed N_c and is expressed in rpm as:

$$N_c = \frac{30\Pi^3}{2\Pi L^2}\sqrt{\frac{4gE\Pi\,(D^4 - d^4)}{64\Pi\rho\,(D^2 - d^2)}}$$

Where L is the shaft length; g is 386.4 in/sec^2; E is the modulus of elasticity; ρ is the density; D is the outside diameter and d is the inside diameter.

2.10.2. Shaft Materials

The use of lightweight aluminium and titanium alloys can provide a greater strength due to the possibility of a higher diameter to thickness ratio. For example, the Boeing HLH uses an aluminium alloy for almost all of the shafts except the main rotor shaft. Here, the titanium allow is used so that the strength can allow the withstanding of larger aerodynamic loads. The model used in this thesis uses the aluminium allow T7075 and Titanium Forging 6A1-4V.

2.11. Helicopter gear

2.11.1. Spur Gears in Helicopter Transmissions

Figure 11 Spur Gears (Sources: "Howstuffworks"2018)

The spur gear is usually used in the helicopter's transmission gear. The spur gear generated torque between the parallel axis through its teeth. They generate more noise than

other types of gears due to its low contact ratio. However, the primary benefit of a spur gear is that it does not generate axial loads or thrusts like other types of gears do, in particular, bevel or helical gears. This feature of the spur gear also allows for reduced weight of the gearbox and removes the requirement for thrust bearings. In addition, this makes the spur gear the perfect choice for planetary configurations.

The spur gear does not generate really high speeds, but it can have a maximum velocity of 20,000 feet per minute in an aerospace application. However, this does create a high level of noise.

2.11.2. Helical Gears in Helicopter Transmissions

Figure 12 Helical Gears (Source:" Howstuffworks"2018)

The helical gears are different than the spur gears as they have a helix angle between 15-30 degrees. This gear generates a radial as well as an axial load on the bearings associated with it. In contrast, the spur gear has an angle of zero degrees. Additionally, the helical gear

is longer due to the angled tooth of the tooth face. This, in turn, enhances load sharing which then allows for a smoother mesh, noise reduction, better speed handling and better horsepower. Furthermore, this also enhances the contact ratios.

However, despite the benefits mentioned above the Helicopter Engineering Preliminary Design Handbook (HEPDH) advises against the use of helical gears in the helicopter transmissions. This is due to the fact that even if the helical gears have a stronger and better load carrying capability than a spur gear of the same size, the overall structure is not any lighter. In addition, there is an effect of thrust on the bearings' mounting which must be taken into account. In essence, there are no clear benefits of using spur gears over helical gears .

2.11.3. Bevel Gears in Helicopter Transmissions

Figure 13 Bevel Gears (Source: "accu"2018)

Bevel gears offer the fundamental means to switch directions between two or more intersecting axis. Between the intersecting axes, there is a shaft angle of 0^0 and 115^o with the

most common angle being 90º. There are two main types of bevel gears: Straight bevel with radial teeth and spiral bevel with curved teeth.

The primary difference between the straight bevel and spiral bevel is the difference in the pitch line velocity. Where the straight bevel velocity is less than 1,000 fpm, on the other hand, spiral bevel gears can reach more than 30,000 fpm. This proves to be a challenge for helicopter drive systems. Spiral bevel gears, on the other hand, offer a better contact area which can allow for a smaller gear pitch and an enhanced bending strength. Furthermore, the three-dimensionality of the spiral bevel requires several bearing restraints and generates loads in all directions. There are some other types of bevel gears like Zerol, but the spiral bevel is the most suitable for the power and speed requirements of a helicopter drive system.

2.12. Helicopter Rotor

The semirigid rotor system comprises of two blades that are rigidly mounted to the two hub. There is something known as a teethering hinge, which simply means that the rotor hub is allowed to tilt with respect to the rotor shaft. The teethering hinge allows the blades to flap in order as one goes up the other goes down. A benefit of this design is the fact that the lag forces are absorbed as there is no vertical hinge. This model also feathers and has a feathering hinge to allow its blades to change the pitch angle.

In this system, the centre of gravity is located below the mast. This is also called underslinging, and it helps in the elimination of any geometric imbalances. However, a primary drawback of this system is that the rotors are susceptible to mast bumping which means that the flaps cause shear in the mast. This is the result of excessive rotor flapping

which can lead to violent contacts and can cause separation of the mast and the rotors. An increased risk of excessive flapping can be found when flying through turbulence at a very high altitude and high speeds.

The Rigid motor system is where the blades are rigidly attached to the hub, but there are no flapping or lag hinges.

The blades of a rigid system can be feathered even if they cannot flap. The rigid system is not prone to mast bumping and is more responsive. This is due to the rigidity of the joints between the rotor and the fuselage which reduces oscillation and allows the helicopter to move as one unit. However, while this does improve the safety in turbulent flight conditions, it does decrease the quality of the flight as the vibrations are felt through the entire fuselage.

The Fully Articulated rotor system, on the other hand, is where each blade can lead/lag, flap and feather independent of one another. This type of system is found in helicopters which have more than two main rotor blades. A Fully Articulated system allows for better control as each blade is highly responsive to the inputs.

Another part of the helicopter is the Swash Plate Assembly which allows the conversion of inputs from pilots to rotatory inputs on the rotor blades. The Freewheeling system is another part of the helicopter. The lift in a helicopter is generated by the rotatory blades, and hence, these blades need to be in motion in the case of an engine failure as a safety measure. The Freewheeling unit in a helicopter disengage the engine and the rotors to

allow the rotors to continue spinning at normal speeds. The Antitorque system of the helicopter is a unite which is used to maintain the directional control of the helicopter.

2.13. Time Domain and Frequency Domain Analysis

Simply put, time domain analysis is the analysis of the system with respect to time and frequency domain analysis is the analysis of the system with respect to frequency.

In a time domain analysis, the interpretation of the output is direct and works on mathematical models derived from Laplace transformation. For such an analysis, considerations should be made for the transient state response and the steady state response. The two most used methods for stability analysis are the Routh Hurtwitz criteria and the Root Locus method. The performance of the system in a time domain analysis can be measured using the rise/peak times, the damping factor, the settling time, and the steady state error.

In contrast, the frequency domain analysis is an indirect interpretation, and if there is a sinusoidal input, the frequency response will be in steady state. The stability analysis of the systems is conducted using Bode plot, Pole placement as well as the Nyquist plot. The system's performance can be measured using the bandwidth analysis, resonance frequency, gain/phase margin, and resonance peak overshoot.

The frequency response of a system could be used for the testing of the system elements. To do this, the amplitude ratio and the phase difference can be calculated for every test frequency.

Bode Diagram is an alternative to Nyquist plots and offer a log gain, log frequency and log phase plots. This Bode Diagram has a linear dB and deg scale on the Y axis and the log scale of frequency on the X axis.

In this study, the time domain and frequency domain analysis are used because of the fact that these methods are complementary in nature and add robustness to the study. The analysis can be applied once the transfer function of the system is known.

2.14. Underdamped/ Critically damped / Overdamped Systems

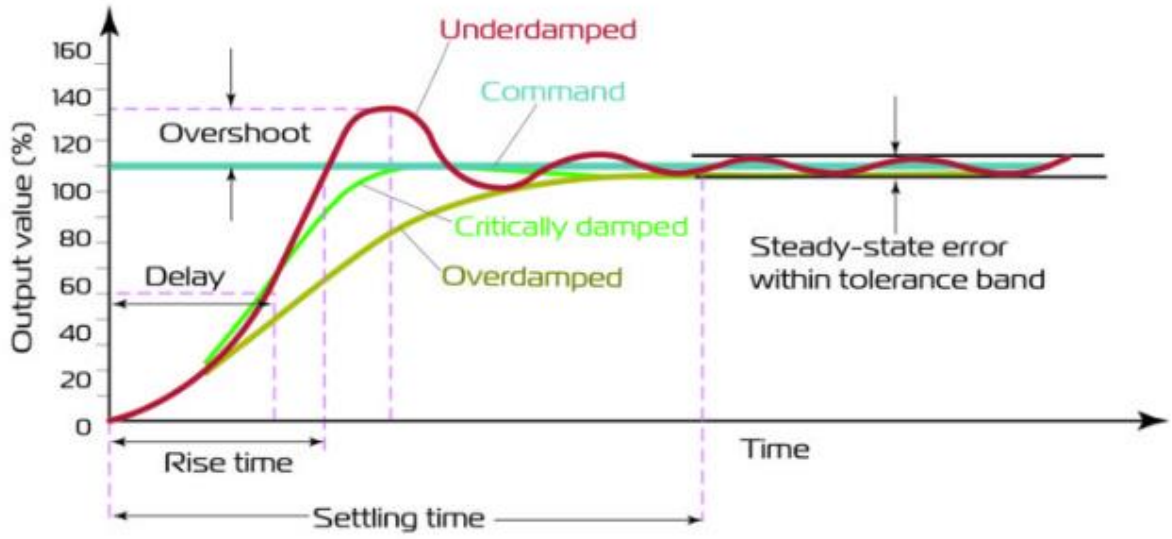

Figure 14 showing Underdamped/Critically damped/Overdamped Systems

(Source: "Motioncontroltips"2018)

In a time, response diagram, the underdamped system overextends from the target position and then finds the position. The critically damped system, however, approaches the

target position without overreaching, while the overdamped system misses the target position because of the fact that of its slow approach.

Several frequency and time domain plots have the same manner of depicting which category the system falls into. For example, the underdamped system almost certainly shows a peaking response whereas the critically damped system has no response until some frequency where it decreases away from zero dB. In the final analysis, the overdamped system decreases away from zero dB gradually and starts the fall earlier. It is of great importance to know how to identify under, over or critically damped system due to the fact that it speaks with reference to the stability of the system.

2.14.1. Bandwidth

Bandwidth is the measure of how good a system functions or how fast the response it.

2.14.2. Gain and Phase Margins

Gain and Phase Margins are a degree of system stability. However, the usage of stability is primarily due to the ease of use rather than the accuracy. The system's open loop frequency response is used in the measurement of the Gain and Phase Margins. It is also essential to remark that these cannot be measured from a closed loop response. In order to quantify the phase margins of a system, the point at which the open loop amplitude exceeds 0dB needs to be identified. At this point, the open loop phase response needs to be identified. The phase margin is the above distance 180^0 which the response reads. An

important point to perceive is that the gain and phase margins are always reported together in a pair.

2.15. System Instability

System instability can cause a complete shutdown of the system. In some circumstances, a system may be susceptible to instability where even if there is a lack of unbalance effects, substantial noise can be generated along with stress which can lead to more fatigue.

In an ideal linear system, the value of the vibrations can become infinity. However, shaft vibrations are reduced because of the fact that of the non-linearity of the systems. These system instabilities can arise from a number of sources which include internal friction, aerodynamic forces and shaft stiffness asymmetry.

2.16. Resonant Frequencies

Resonance is the amplification of vibration of any rotating system. Any given mechanical structure resonates at certain frequencies if the natural state is excited. According to Whalley, Ebrahimi and Jamil (2005), dynamic excitations in drive designs, are a prevalent issue which then, necessitates subsequent investigations; the reason being the reduction of damaging vibrations, heat, wear, and noise. Resonant frequencies are a major issue in this regard. This is because of the fact that even if there is a small change in the excitation, it can result in mechanical failure by causing output changes that are dynamically large.

2.17. Shear Stress

When there is twisting force or torque acting on a shaft system, shear stress is produced. A rotating shaft can produce torsional vibration because of the fact that the force of friction at the bearings can decrease when the shaft rotates due to the lesser value of the dynamic friction in comparison to the static fiction (Catling & De Barr, 1956).

Chapter III

Modelling of Helicopter driveline

3.1. Introduction

In this chapter, Mc-Dannell Douglas MD500E helicopter drive-train is model as lumped, finite element and hybrid, distributed-lumped based on the method developed by R Whalley, M Ebrahimi and Z Jamil paper “The Torsional response of rotor systems”. According to Pettersson (1996), for the development of a driveline model, Newton’s second law is to be used in line with several assumptions with reference to the workings of the parts of the driveline.

3.2. Assumptions

Major assumptions for this dissertation include:

1. Main rotor and tail rotor shafts are uniform
2. Bearing frictions at the load and drive ends of the shaft
3. Main and tail Rotor air resistance are estimated and added to the damping frictions on the load end to simplify the model
4. Gear efficacy estimated and multiplied by the gear ratio to simplify the model.
5. Helicopter main and tail rotor blades are considered as long thin rod to simplify calculation of the rotor moment of inertia.

3.3. MD 500 E helicopter physical parameter

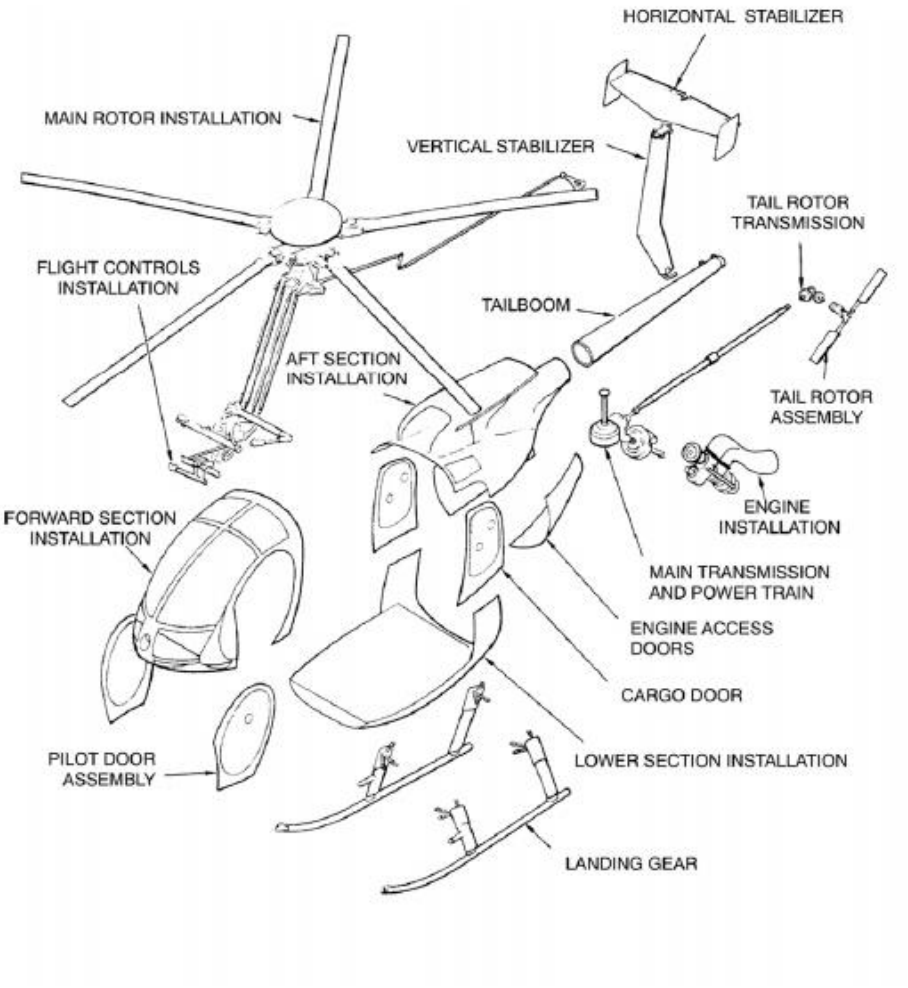

Figure 15 MD 500E Helicopter Major Components (Source Helicopters - MD 500E" 2018)

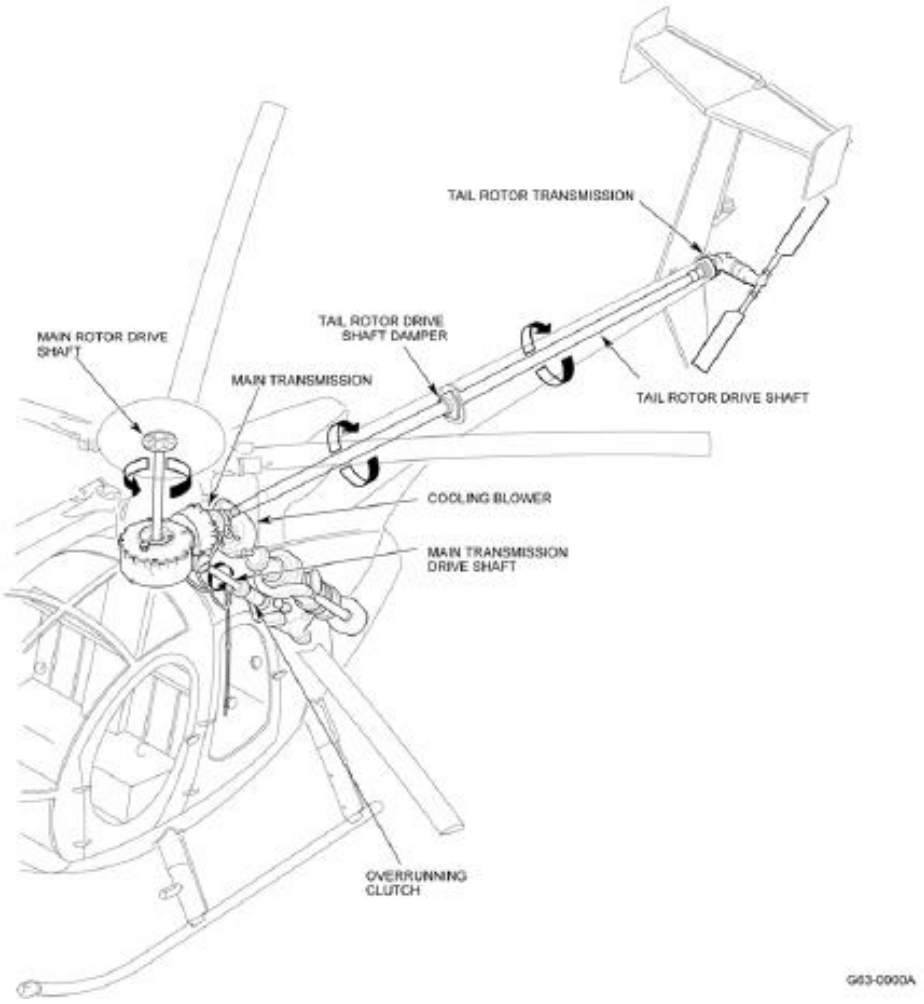

Figure 16 MD 500 Helicopter Drive System (Source Helicopters - MD 500E" 2018)

3.3.1. MD 500 helicopter Dimensions

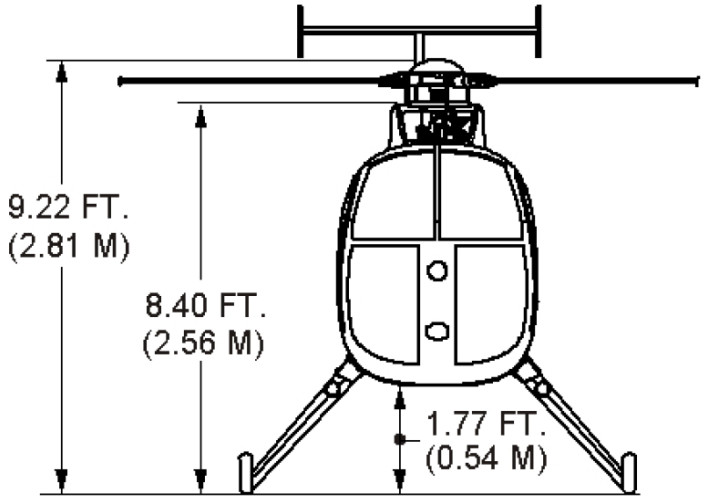

Figure 17 MD 500 helicopter Dimensions front view (Source Helicopters - MD 500E" 2018)

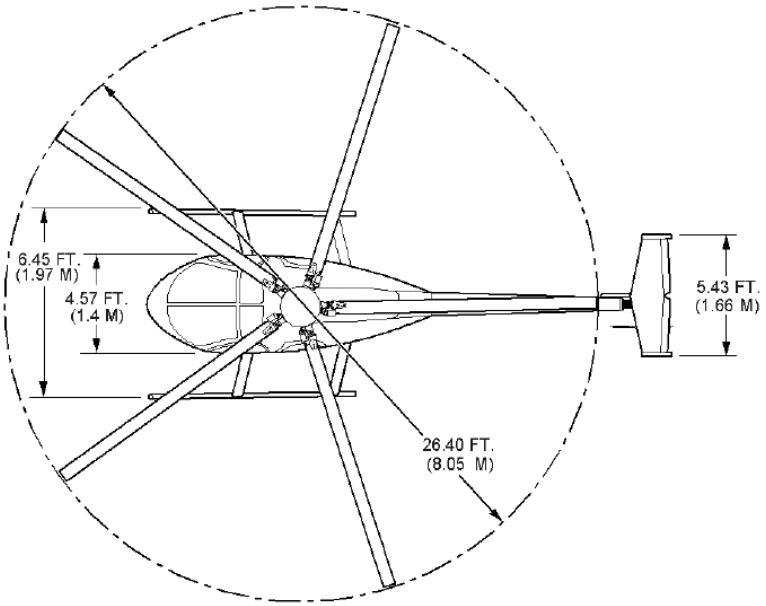

Figure 18 MD 500 helicopter Dimensions top view (Source Helicopters - MD 500E" 2018)

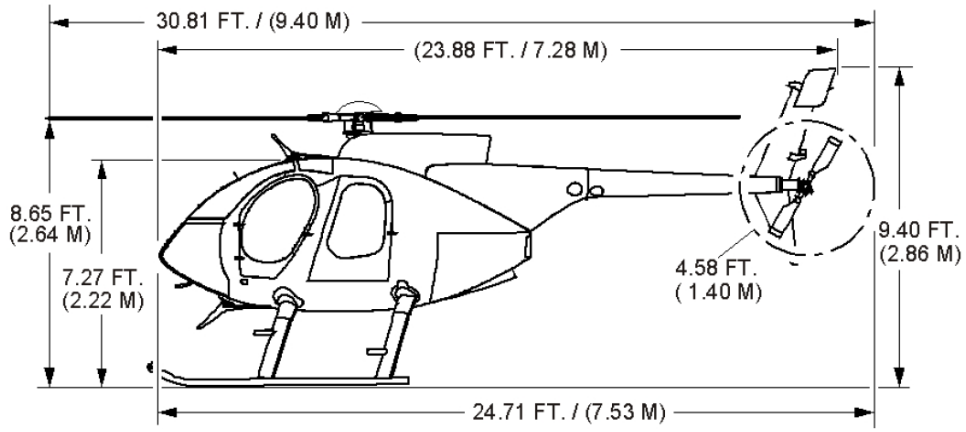

Figure 19 MD 500 helicopter Dimensions side view (Source Helicopters - MD 500E" 2018)

The below summary of MD500E helicopter drivetrain physical parameter are obtain from MD500E helicopter technical manual:

Summary of MD 500 E helicopter drivetrain physical parameter	
Main Rotor	
Number of blades	N=5
Length of blade	L=4.03 m
Mass of each blade	M=16.6 kg
Tail Rotor	
Number of blades	N=4
Length of blade	L=0.7m
Mass of each blade	M=.1.4 kg
Main rotor hub	
Mass of main rotor hub	M=20 kg
Radius	R=0.3 m
Main Rotor drive shaft	
Length	L=0.34m
Tail Rotor drive shaft	
Length	L=3.96m

Table 1 MD 500E Helicopter drive system Physical property

The below schematic layout of MD500E helicopter drivetrain is developed from MD500E helicopter technical manual:

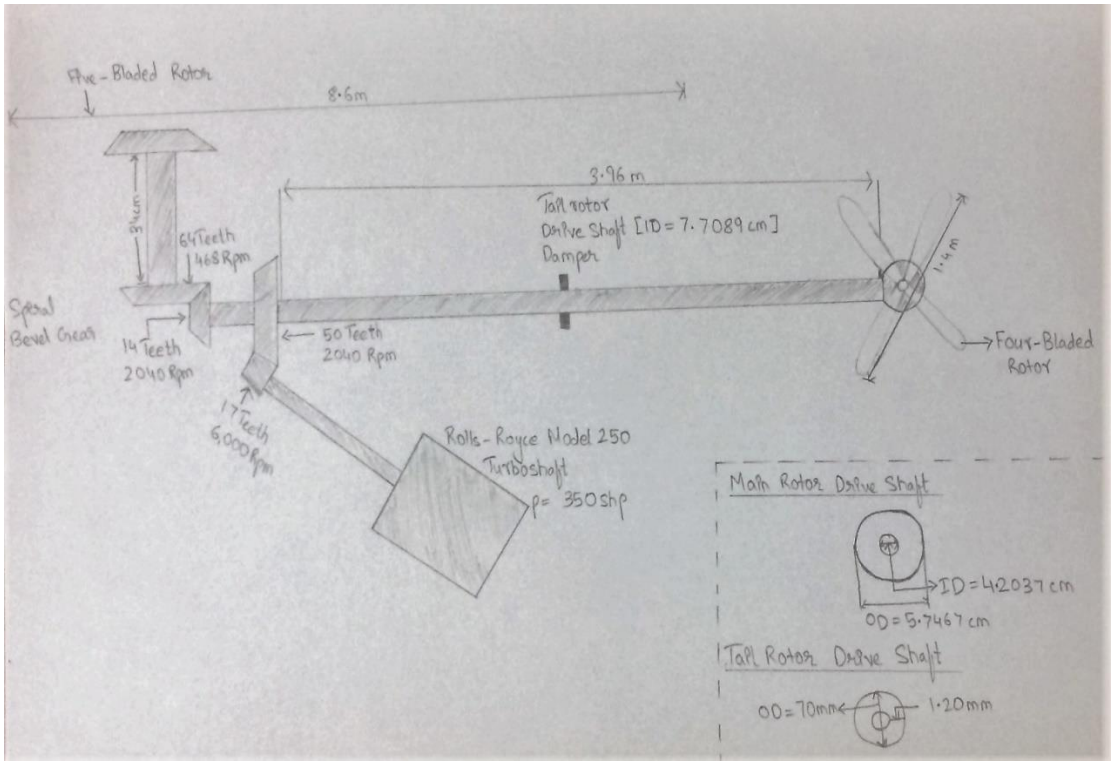

Figure 20 schematic layout of MD 500E Helicopter drive system

3.4.Lumped Parameter Model

In this section, lumped Parameter Model for MD500E helicopter drivetrain is developed based on method developed by R Whalley, M Ebrahimi and Z Jamil paper "The Torsional response of rotor systems".

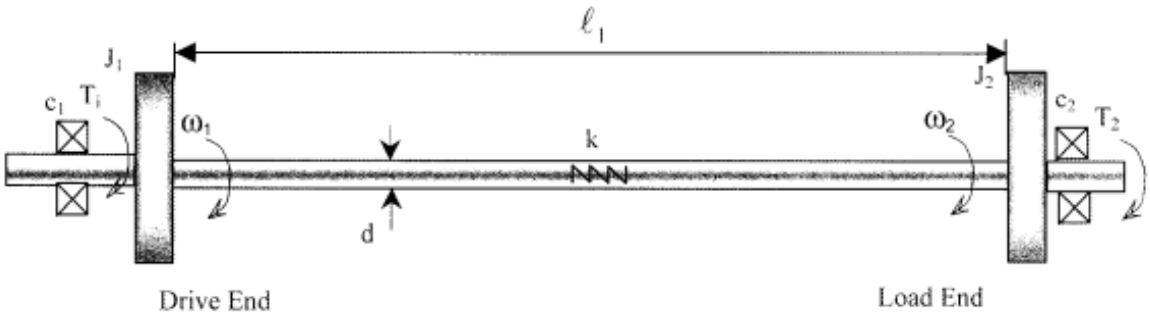

Figure 21 lumped parameter model (source: Whalley, Ebrahimi & Jamil 2005)

Tail Rotor governing equations

$$T_{mt}(t) = J_{tr1}D^2\theta_{tr1}(t) + C_{tr1}D\theta_{tr1}(t) + K_{tr}(\theta_{tr1}(t) - \theta_{tr2}(t))$$

(1)

$$T_{tr2}(t) = J_{tr2}D^2\theta_{tr2}(t) + C_{tr2}D\theta_{tr2}(t) + K_{tr}(\theta_{tr1}(t) - \theta_{tr2}(t))$$

(2)

Where D =d/dt

Following the Laplace transformation with zero initial conditions and with $T_2(t)=0$, equations (1) and (2), become

$$\begin{pmatrix} w_{tr1}(s) \\ w_{tr2}(s) \end{pmatrix} = \frac{\begin{pmatrix} J_{tr2}s^2 + C_{tr2}s + k_{tr} & k_{tr} \\ k_{tr} & J_{tr1}s^2 + C_{tr1}s + k_{tr} \end{pmatrix}}{\square(s)} \begin{pmatrix} T_{mt}(s) \\ 0 \end{pmatrix}$$

(3)

Hence:

$$\begin{pmatrix} w_{tr1}(s) \\ w_{tr2}(s) \end{pmatrix} = \begin{pmatrix} J_{tr2}s^2 + C_{tr2}s + k_{tr} \\ k_{tr} \end{pmatrix}_{s=iw} T_{mt}(s) / \square(s)$$

(4)

Where

$$\square(s) = J_{tr1}J_{tr2}s^3 + (J_{tr1}C_{tr2} + J_{tr2}C_{tr1})s^2 + (J_{tr1}k_{tr} + J_{tr2}k_{tr} + C_{tr1}C_{tr2})s + (C_{tr1} + C_{tr2})k_{tr}$$

Main Rotor governing equations

$$T_{mrt}(t) = J_{mr1}D^2\theta_{mr1}(t) + C_{mr1}D\theta_{mr1}(t) + K_{mr}(\theta_{mr1}(t) - \theta_{mr2}(t))$$

(5)

$$T_{mr2}(t) = J_{mr2}D^2\theta_{mr2}(t) + C_{mr2}D\theta_{mr2}(t) + K_{mr}(\theta_{mr1}(t) - \theta_{mr2}(t))$$

(6)

Where D =d/dt

Following the Laplace transformation with zero initial conditions and with $T_{mr2}(t)=0$, equations (5) and (6), become

$$\begin{pmatrix} w_{mr1}(s) \\ w_{mr2}(s) \end{pmatrix} = \frac{\begin{pmatrix} J_{mr2}s^2 + C_{mr2}s + k_{mr} & k_{mr} \\ k_{mr} & J_{mr1}s^2 + C_{mr1}s + k_{mr} \end{pmatrix}}{\Delta(s)} \begin{pmatrix} T_{mrt}(s) \\ 0 \end{pmatrix}$$

(7)

Hence:

$$\begin{pmatrix} w_{mr1}(s) \\ w_{mr2}(s) \end{pmatrix} = \begin{pmatrix} J_{mr2}s^2 + C_{mr2}s + k_{mr} \\ k_{mr} \end{pmatrix}_{s=iw} T_{mrt}(s) / \Delta(s)$$

(8)

Where,

$$\Delta(s) = J_{mr1}J_{mr2}s^3 + (J_{mr1}C_{mr2} + J_{mr2}C_{mr1})s^2 + (J_{mr1}k_{mr} + J_{mr2}k_{mr} + C_{mr1}C_{mr2})s + (C_{mr1} + C_{mr2})k_{mr}$$

3.4.1. Lumped models block diagram

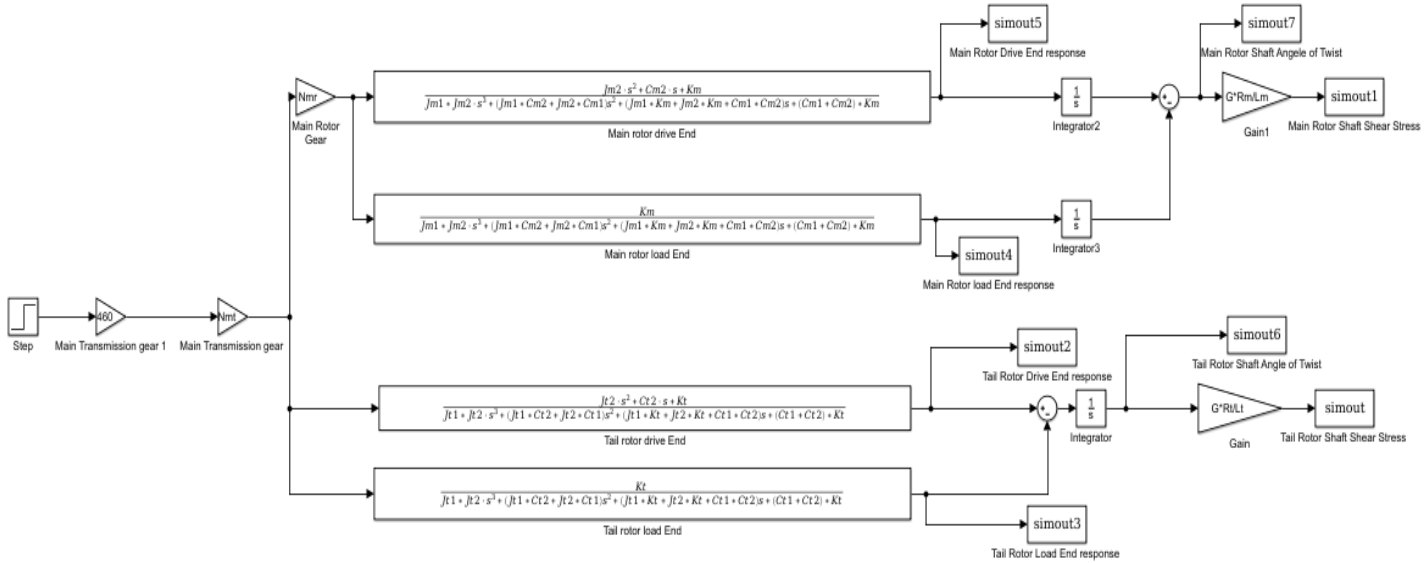

Figure 22 Lumped models block diagram

3.5.Finite element Model (Five sections)

In this section, Finite element Model for MD500 E helicopter is developed based on method developed by R Whalley, M Ebrahimi and Z Jamil paper "The Torsional response of rotor systems". Tail Rotor and Main Rotor shaft are divided to five sections each in an effort to improve prediction accuracy.

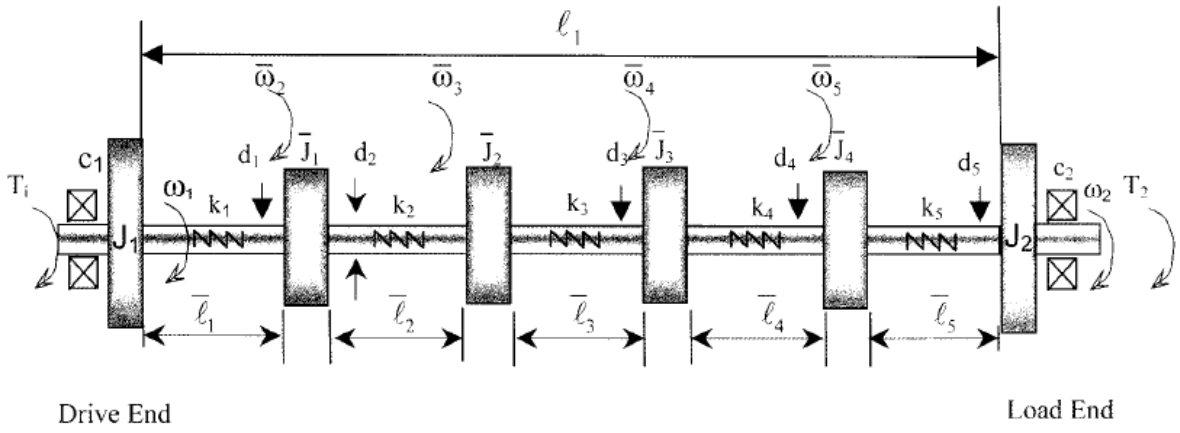

Figure 23 Finite element model five sections ***(source: Whalley, Ebrahimi & Jamil 2005)***

$$
\begin{aligned}
T_{mt}(t) &= J_{tr1}D^2\theta_{tr1}(t) + C_{tr1}D\theta_{tr1}(t) + k_{tr1}(\theta_{tr1}(t) - \overline{\theta_{tr2}}(t)) \\
0 &= \overline{J}_{tr1}D^2\overline{\theta}_{tr2}(t) + k_{tr2}(\overline{\theta}_{tr2}(t) - \overline{\theta_{tr3}}(t)) + k_{tr1}(\theta_{tr1}(t) - \overline{\theta_{tr2}}(t)) \\
0 &= \overline{J}_{tr2}D^2\overline{\theta}_{tr3}(t) + k_{tr3}(\overline{\theta}_{tr3}(t) - \overline{\theta_{tr4}}(t)) + k_{tr2}(\overline{\theta}_{tr2}(t) - \overline{\theta_{tr2}}(t)) \\
0 &= \overline{J}_{tr3}D^2\overline{\theta}_{tr4}(t) + k_{tr4}(\overline{\theta}_{tr4}(t) - \overline{\theta_{tr3}}(t)) + k_{tr3}(\overline{\theta}_{tr3}(t) - \overline{\theta_{tr2}}(t)) \\
0 &= \overline{J}_{tr4}D^2\overline{\theta}_{tr5}(t) + k_{tr5}(\overline{\theta}_{tr5}(t) - \overline{\theta_{tr4}}(t)) + k_{tr4}(\overline{\theta}_{tr4}(t) - \overline{\theta_{tr2}}(t)) \\
0 &= \overline{J}_{tr5}D^2\overline{\theta}_{tr2}(t) + C_{tr2}D\theta_{tr2}(t) + k_{tr5}(\overline{\theta}_{tr5}(t) - \theta_{tr3}(t))
\end{aligned}
$$

(9)

Where $D\overline{\theta}_j(t) = \overline{\omega_j}(t), 2 \le j \le 5 - and - D\theta_k(t) = \omega_k(t), 1 \le k \le 2.$ Following Laplace transformation, with zero initial conditions equations (15) become:

$$
\begin{bmatrix} T_{mt}(S) & 0 & 0 & 0 & 0 & 0 \end{bmatrix}^T = \begin{bmatrix} J_{tr}s^2 + C_{tr}s + K_{tr} \end{bmatrix} \times \begin{bmatrix} \theta_{tr1}(s) & \overline{\theta}_{tr2}(s) & \overline{\theta}_{tr3}(s) & \overline{\theta}_{tr4}(s) & \overline{\theta}_{tr5}(s) & \overline{\theta}_{tr2}(s) \end{bmatrix}^T
$$

(10)

$$
k_{tr} = \begin{bmatrix}
k_{tr1} & -k_{tr1} & 0 & 0 & \cdots & 0 \\
-k_{tr1} & k_{tr1} + k_{tr2} & -k_{tr2} & 0 & \cdots & 0 \\
0 & -k_{tr2} & k_{tr2} + k_{tr3} & -k_{tr3} & \cdots & 0 \\
\vdots & 0 & & & & \vdots \\
\vdots & \vdots & & & & -k_{tr3} \\
0 & 0 & \cdots & 0 & -k_{tr5} & -k_{tr5}
\end{bmatrix}
$$

(11)

$$
J_{tr} = Diag(J_{tr1}, \overline{J}_{tr1}, \overline{J}_{tr2}, \overline{J}_{tr3}, \overline{J}_{tr4}, J_{tr2})
$$

$$
C_{tr} = Diag(C_{tr1}, 0, 0, 0, 0, C_{tr2})
$$

If all the shaft sections are equal in length and diameter, then:

$\overline{J}_{tr1} = \overline{J}_{tr2} = \overline{J}_{tr3} = \overline{J}_{tr4} = \overline{J}_{tr}$ and $k_{tr1} = k_{tr2} = k_{tr3} = k_{tr4} = k_{tr5} = k_{tr}$

The time response, frequency response characteristics for the subject system may be calculated from:

$$\omega_{tr}(s) = s\left[J_{tr}s^2 + C_{tr}s + k_{tr} \right]^{-1} \begin{bmatrix} T_{mt} & 0 & 0 & 0 & 0 & 0 \end{bmatrix}^T$$

(12)

Where

$$\omega_{tr}(s) = \begin{bmatrix} \omega_{tr1}(s) & \overline{\omega}_{tr2}(s) & \overline{\omega_{tr3}}(s) & \overline{\omega_{tr4}}(s) & \overline{\omega}_{tr5}(s) & \omega_{tr2}(s) \end{bmatrix}^T$$

(13)

Therefore, it can be stated that,

$$\frac{\omega_{tr1}(s)}{T_{mt}} = \frac{num1}{\square_1(s)}$$

(14)

$$\frac{\omega_{tr2}(s)}{T_{mt}} = \frac{k^5}{\square_1(s)}$$

(15)

Where:

$$num1 = s^{10}J_{tr}^4 J_{tr2} + s^9 J_{tr}^4 C_{tr2} + s^8(8k_{tr}J_{tr}^3 J_{tr2} + kJ_{tr}^4) + s^7 8k_{tr}J_{tr}^3 C_{tr2} +$$
$$s^6(7J_{tr}^3 k_{tr}^2 + 21k_{tr}^2 J_{tr2}) + s^5 21k_{tr}^2 J_{tr}^2 C_{tr2} + s^4(15J_{tr}^2 k_{tr}^3 + 20k_{tr}^3 J_{tr} J_{tr2}) +$$
$$s^3 20k_{tr}^3 J_{tr} C_{tr2} + s^2(5k_{tr}^4 J_{tr2} + 10k_{tr}^4 J_{tr}) + 5k_{tr}^4 C_{tr2} s + k_{tr}^5$$

(16)

$$\square_1(s) = J_{tr1}J_{tr}^4 J_{tr2}s^{11} + s^{11}(C_{tr1}J_{tr}^4 J_{tr2} + J_{tr1}J_{tr}^4 C_{tr2})$$
$$+s^9(k_{tr}J_{tr}^4 J_{tr2} + 8k_{tr}J_{tr1}J_{tr}^3 J_{tr2} + k_{tr}J_{tr1}J_{tr}^4 + C_{tr1}J_{tr}^4 C_{tr2})$$
$$+s^8(k_{tr}C_{tr1}J_{tr}^4 + 8k_{tr}C_{tr1}J_{tr}^3 J_{tr2} + 8k_{tr}J_{tr}^3 C_{tr2} + k_{tr}J_{tr}^4 C_{tr2})$$
$$+s^7(7J_{tr1}J_{tr}^3 k_{tr} + 21k_{tr}^2 J_{tr1}J_{tr}^2 J_{tr2} + k_{tr}^2 J_{tr}^4 + 8k_{tr}C_{tr1}J_{tr}^3 C_{tr2} + 7k_{tr}^3 J_{tr}^3 J_{tr2})$$
$$+s^6(21k_{tr}^2 J_{tr1}J_{tr1}^2 C_{tr2} + 7C_{tr1}J_{tr}^3 k_{tr}^2 + 21k_{tr}^2 C_{tr1}J_{tr}^2 J_{tr2} + 7k_{tr}^2 J_{tr}^3 C_{tr2})$$
$$+s^5(15k_{tr}^3 J_{tr}^2 J_{tr2} + 20k_{tr}^3 J_{tr1}J_{tr}J_{tr2} + 6J_{tr}^3 k_{tr}^3 + 15k_{tr}^3 J_{tr1}J_{tr}^2 + 21k_{tr}^2 C_{tr1}J_{tr}^2 C_{tr2})$$
$$+s^4(15k_{tr}^3 J_{tr1}J_{tr}^2 + 15k_{tr}^3 J_{tr}^2 C_{tr2} + 20k_{tr}^3 C_{tr1}J_{tr}J_{tr2} + 20k_{tr}^3 J_{tr1}J_{tr}C_{tr2})$$
$$+s^3(5k_{tr}^4 J_{tr1}J_{tr2} + 20k_{tr}^3 C_{tr1}J_{tr}C_{tr2} + 10k_{tr}^4 J_{tr1}J_{tr} + 10J_{tr}^2 k_{tr}^4 + 10k_{tr}^4 J_{tr}J_{tr2})$$
$$+s^2(5k_{tr}^4 C_{tr1}J_{tr2} + 10k_{tr}^4 J_{tr}C_{tr2} + 5k_{tr}^4 J_{tr1}C_{tr2} + 10k_{tr}^4 C_{tr2}J_{tr})$$
$$+s(15k_{tr}^5 J_{tr2} + 4k_{tr}^5 J_{tr} + k_{tr}^5 J_{tr1} + 5k_{tr}^4 C_{tr1}C_{tr2}) + k_{tr}^5 C_{tr1} + k_{tr}^5 C_{tr2}$$

(17)

$$
\begin{aligned}
T_{mrt}(t) &= J_{mr1}D^2\theta_{mr1}(t) + C_{mr1}D\theta_{mr1}(t) + k_{mr1}(\theta_{mr1}(t) - \overline{\theta_{mr2}}(t)) \\
0 &= \overline{J}_{mr1}D^2\overline{\theta}_{mr2}(t) + k_{mr2}(\overline{\theta}_{mr2}(t) - \overline{\theta_{mr3}}(t)) + k_{mr1}(\theta_{mr1}(t) - \overline{\theta_{mr2}}(t)) \\
0 &= \overline{J}_{mr2}D^2\overline{\theta}_{mr3}(t) + k_{mr3}(\overline{\theta}_{mr3}(t) - \overline{\theta_{mr4}}(t)) + k_{mr2}(\overline{\theta}_{mr2}(t) - \overline{\theta_{mr2}}(t)) \\
0 &= \overline{J}_{mr3}D^2\overline{\theta}_{mr4}(t) + k_{mr4}(\overline{\theta}_{mr4}(t) - \overline{\theta_{mr3}}(t)) + k_{mr3}(\overline{\theta}_{mr3}(t) - \overline{\theta_{mr2}}(t)) \\
0 &= \overline{J}_{mr4}D^2\overline{\theta}_{mr5}(t) + k_{mr5}(\overline{\theta}_{mr5}(t) - \overline{\theta_{mr4}}(t)) + k_{mr4}(\overline{\theta}_{mr4}(t) - \overline{\theta_{mr2}}(t)) \\
0 &= \overline{J}_{mr5}D^2\overline{\theta}_{mr2}(t) + C_{mr2}D\theta_{mr2}(t) + k_{mr5}(\overline{\theta}_{mr5}(t) - \theta_{mr3}(t))
\end{aligned}
$$

(18)

Where $D\overline{\theta}_j(t) = \overline{\omega_j}(t), 2 \le j \le 5 - and - D\theta_k(t) = \omega_k(t), 1 \le k \le 2.$ Following

Laplace transformation, with zero initial conditions equations (15) become:

$$
\left[T_{mrt}(S) \quad 0 \quad 0 \quad 0 \quad 0 \quad 0\right]^T = \left[J_{mr}s^2 + C_{mr}s + K_{mr}\right] \times \left[\theta_{mr1}(s) \quad \overline{\theta}_{mr2}(s) \quad \overline{\theta}_{mr3}(s) \quad \overline{\theta}_{mr4}(s) \quad \overline{\theta}_{mr5}(s) \quad \overline{\theta}_{mr2}(s)\right]^T
$$

(19)

$$
k_{mr} = \begin{bmatrix}
k_{mr1} & -k_{mr1} & 0 & 0 & \cdots & 0 \\
-k_{mr1} & k_{mr1} + k_{mr2} & -k_{mr2} & 0 & \cdots & 0 \\
0 & -k_{mr2} & k_{mr2} + k_{mr3} & -k_{mr3} & \cdots & 0 \\
\vdots & 0 & & & & \vdots \\
\vdots & \vdots & & & & -k_{mr3} \\
0 & 0 & \cdots & 0 & -k_{mr5} & -k_{mr5}
\end{bmatrix}
$$

(20)

$$
J_{mr} = Diag(J_{mr1}, \overline{J}_{mr1}, \overline{J}_{mr2}, \overline{J}_{mr3}, \overline{J}_{mr4}, J_{mr2})
$$

$$
C_{mr} = Diag(C_{mr1}, 0, 0, 0, 0, C_{mr2})
$$

If all the shaft sections are equal in length and diameter, then:

$\bar{J}_{mr1} = \bar{J}_{mr2} = \bar{J}_{mr3} = \bar{J}_{mr4} = \bar{J}_{mr}$ and $k_{mr1} = k_{mr2} = k_{mr3} = k_{mr4} = k_{mr5} = k_{mr}$

The time response, frequency response characteristics for the subject system may be calculated from:

$$\omega_{mr}(s) = s\left[J_{mr}s^2 + C_{mr}s + k_{mr}\right]^{-1}\begin{bmatrix} T_{mrt} & 0 & 0 & 0 & 0 & 0 \end{bmatrix}^T$$

(21)

Where

$$\omega_{mr}(s) = \begin{bmatrix} \omega_{mr1}(s) & \bar{\omega}_{mr2}(s) & \overline{\omega_{mr3}}(s) & \overline{\omega_{mr4}}(s) & \bar{\omega}_{mr5}(s) & \omega_{mr2}(s) \end{bmatrix}^T$$

(22)

Therefore, it can be stated that,

$$\frac{\omega_{mr1}(s)}{T_{mrt}} = \frac{num2}{\square_1(s)}$$

(23)

$$\frac{\omega_{mr2}(s)}{T_{mrt}} = \frac{k_{mr}^5}{\square_1(s)}$$

(24)

Where:

$$num2 = s^{10}J_{mr}^4 J_{mr2} + s^9 J_{mr}^4 C_{mr2} + s^8(8k_{mr}J_{mr}^3 J_{mr2} + kJ_{mr}^4) + s^7 8k_{mr}J_{mr}^3 C_{mr2} +$$
$$s^6(7J_{mr}^3 k_{mr}^2 + 21k_{mr}^2 J_{mr2}) + s^5 21k_{mr}^2 J_{mr}^2 C_{mr2} + s^4(15J_{mr}^2 k_{mr}^3 + 20k_{mr}^3 J_{mr} J_{mr2}) +$$
$$s^3 20k_{mr}^3 J_{mr} C_{mr2} + s^2(5k_{mr}^4 J_{mr2} + 10k_{mr}^4 J_{mr}) + 5k_{mr}^4 C_{mr2} s + k_{mr}^5$$

(25)

$$\square_1(s) = J_{mr1}J_{mr}^4 J_{mr2}s^{11} + s^{11}(C_{mr1}J_{mr}^4 J_{mr2} + J_{mr1}J_{mr}^4 C_{mr2})$$
$$+s^9(k_{mr}J_{mr}^4 J_{mr2} + 8k_{mr}J_{mr1}J_{mr}^3 J_{mr2} + k_{mr}J_{mr1}J_{mr}^4 + C_{mr1}J_{mr}^4 C_{mr2})$$
$$+s^8(k_{mr}C_{mr1}J_{mr}^4 + 8k_{mr}C_{mr1}J_{mr}^3 J_{mr2} + 8k_{mr}J_{mr}^3 C_{mr2} + k_{mr}J_{mr}^4 C_{mr2})$$
$$+s^7(7J_{mr1}J_{mr}^3 k_{mr} + 21k_{mr}^2 J_{mr1}J_{mr}^2 J_{mr2} + k_{mr}^2 J_{mr}^4 + 8k_{mr}C_{mr1}J_{mr}^3 C_{mr2} + 7k_{mr}^3 J_{mr}^3 J_{mr2})$$
$$+s^6(21k_{mr}^2 J_{mr1}J_{mr1}^2 C_{mr2} + 7C_{mr1}J_{mr}^3 k_{mr}^2 + 21k_{mr}^2 C_{mr1}J_{mr}^2 J_{mr2} + 7k_{mr}^2 J_{mr}^3 C_{mr2})$$
$$+s^5(15k_{mr}^3 J_{mr}^2 J_{mr2} + 20k_{mr}^3 J_{mr1}J_{mr}J_{mr2} + 6J_{mr}^3 k_{mr}^3 + 15k_{mr}^3 J_{mr1}J_{mr}^2 + 21k_{mr}^2 C_{mr1}J_{mr}^2 C_{mr2})$$
$$+s^4(15k_{mr}^3 J_{mr1}J_{mr}^2 + 15k_{mr}^3 J_{mr}^2 C_{mr2} + 20k_{mr}^3 C_{mr1}J_{mr}J_{mr2} + 20k_{mr}^3 J_{mr1}J_{mr}C_{mr2})$$
$$+s^3(5k_{mr}^4 J_{mr1}J_{mr2} + 20k_{mr}^3 C_{mr1}J_{mr}C_{mr2} + 10k_{mr}^4 J_{mr1}J_{mr} + 10J_{mr}^2 k_{mr}^4 + 10k_{mr}^4 J_{mr}J_{mr2})$$
$$+s^2(5k_{mr}^4 C_{mr1}J_{mr2} + 10k_{mr}^4 J_{mr}C_{mr2} + 5k_{mr}^4 J_{mr1}C_{mr2} + 10k_{mr}^4 C_{mr2}J_{mr})$$
$$+s(15k_{mr}^5 J_{mr2} + 4k_{mr}^5 J_{mr} + k_{mr}^5 J_{mr1} + 5k_{mr}^4 C_{mr1}C_{mr2}) + k_{mr}^5 C_{mr1} + k_{mr}^5 C_{mr2}$$

(26)

3.5.1. Finite Element Models blocks diagram

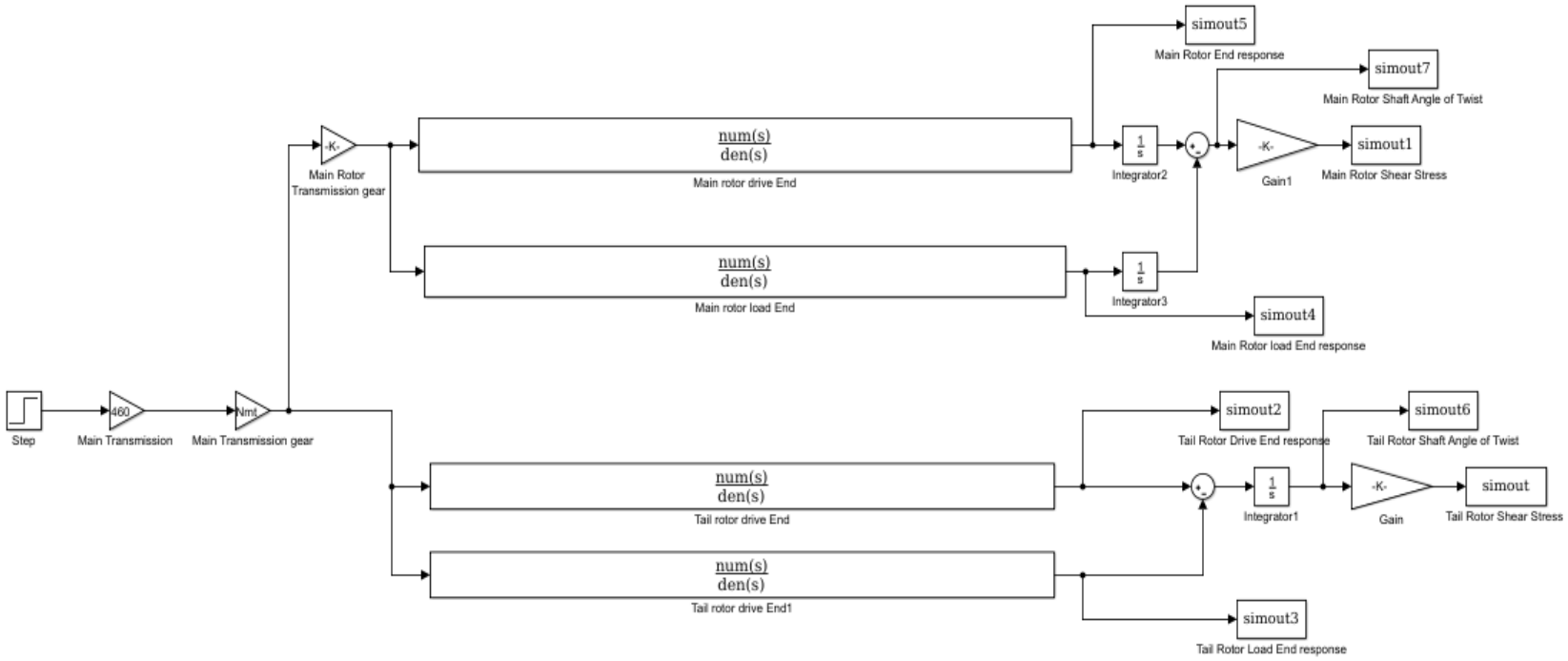

Figure 24 Finite Element Models blocks diagram

3.6. Hybrid Parameter model

In this section, a hybrid, distributed-lumped model for MD 500E helicopter drive shaft is developed based on R Whalley, M Ebrahimi and Z Jamil paper "The Torsional response of rotor systems."

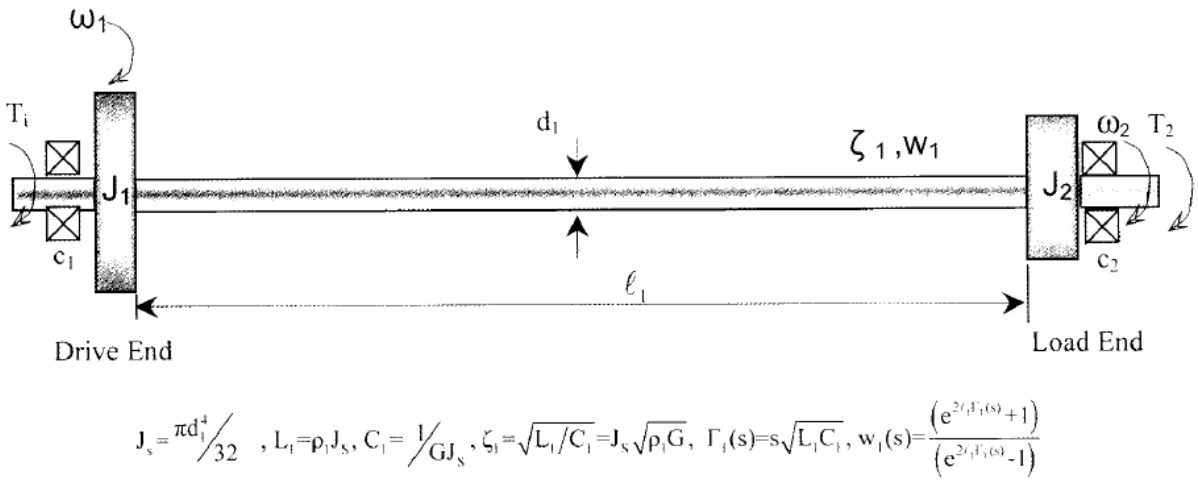

$$J_s = \pi d_1^4/32 \quad , L_1=\rho_1 J_S,\ C_1 = 1/GJ_s \ , \zeta_1 = \sqrt{L_1/C_1} = J_S\sqrt{\rho_1 G},\ \Gamma_1(s)=s\sqrt{L_1C_1},\ w_1(s)=\frac{\left(e^{2\zeta_1\Gamma_1(s)}+1\right)}{\left(e^{2\zeta_1\Gamma_1(s)}-1\right)}$$

Figure 25 Lumped-Distributed parameter model (source: Whalley, Ebrahimi & Jamil 2005)

$$\begin{bmatrix} T_{mt}(s) - J_{tr1} s\omega_1(s) - C_1\omega_1(S) \\ J_{tr2} s\omega_{tr2}(s) + C_2\omega_2(s) + T_{tr2}(s) \end{bmatrix} = \begin{bmatrix} \zeta_1 w_1(s) & -\zeta_1 (w_1(s)^2 - 1)^{1/2} \\ \zeta_1 (w_1(s)^2 - 1)^{1/2} & -\zeta_1 w_1(s) \end{bmatrix} \begin{bmatrix} \omega_{tr1}(s) \\ \omega_{tr2}(s) \end{bmatrix}$$

(27)

$$\begin{bmatrix} T_{mt}(s) \\ 0 \end{bmatrix} = \begin{bmatrix} \zeta_1 w_1(s) + \gamma_1(s) & -\zeta_1 (w_1(s)^2 - 1)^{1/2} \\ \zeta_1 (w_1(s)^2 - 1)^{1/2} & -\zeta_1 w_1(s) - \gamma_2(s) \end{bmatrix} \begin{bmatrix} \omega_{tr1}(s) \\ \omega_{tr2}(s) \end{bmatrix}$$

(28)

Where:

$$\delta_1(s) = J_1 s + C_1$$

$$\delta_2(s) = J_2 s + C_2$$

$$L_1 = \rho_1 J_s$$

$$C_1 = 1/(G_1 J_s)$$

Therefore, it can be stated that:

$$\sqrt{(L_1 C_1)} = \sqrt{(\rho_1 G_1)}$$

$$\xi_1 = \sqrt{L_1} / \mathrm{C}_1 = J_s \sqrt{(\rho_1 G_1)}$$

and

$$w_1(s) = \frac{e^{2l_1\Gamma_1(s)} + 1}{e^{2l_1\Gamma_1(s)} - 1}$$

Where in equation (00)

$$\Gamma_1(s) = s\sqrt{L_1 C_1} = s\sqrt{\rho_1} / G_1$$

$$T = 2l_1\sqrt{LC}$$

$$\Gamma_1(s) = s\sqrt{L_1 C_1} = s\sqrt{\rho_1} / G_1$$

$$\Delta(s) = \zeta_1(\gamma_1(s) + \gamma_2(s))w_1(s) + \gamma_1(s) + \zeta_1^2$$

For simplification of the hybrid model diagram both $w_1(s) = \frac{e^{2l_1\Gamma_1(s)} + 1}{e^{2l_1\Gamma_1(s)} - 1}$ and $\sqrt{w_1^2}(s) - 1) = \frac{2e^{-l_1\Gamma_1(s)}}{(1 - 2e^{-l_1\Gamma_1(s)})}$ model as a subsystem.

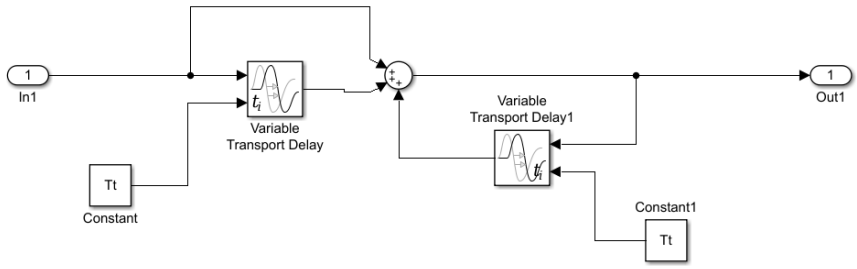

Figure 26 Block Diagram for W1(S)

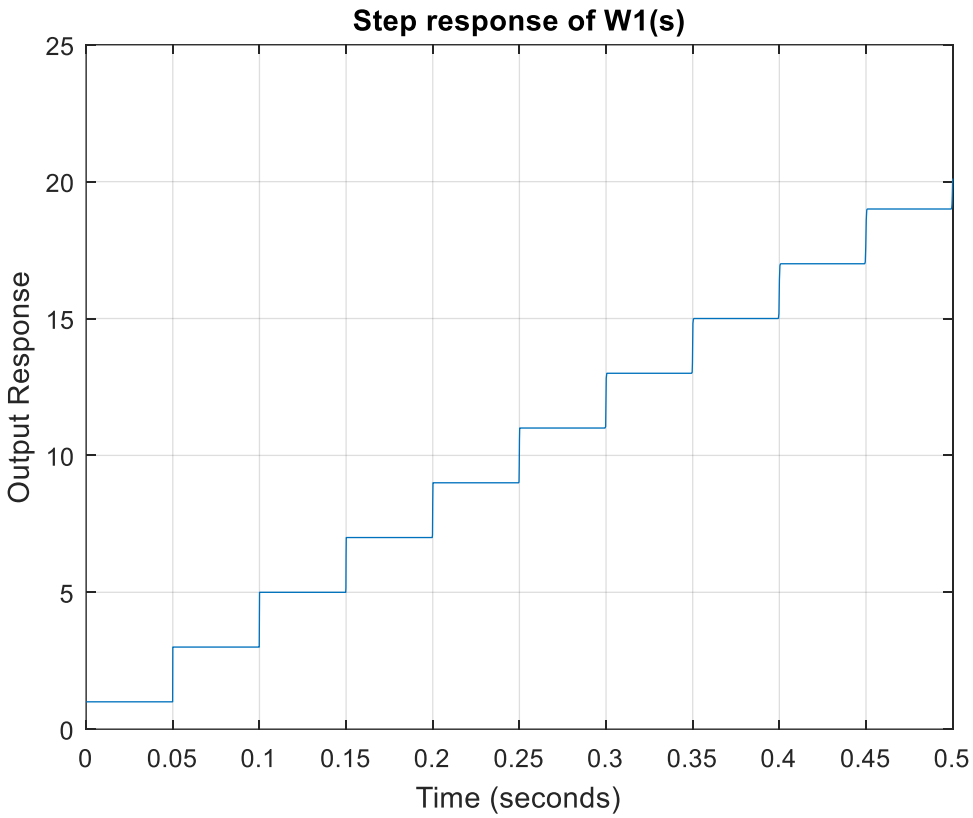

Figure 27 Unit step response of w1(s)

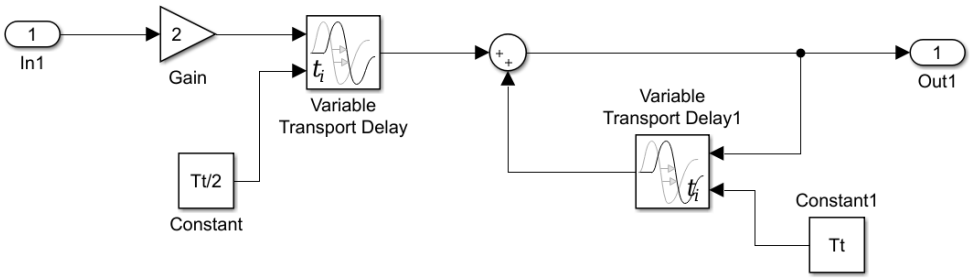

Figure 28 Block Diagram for (W^2(s)-1)^0.5

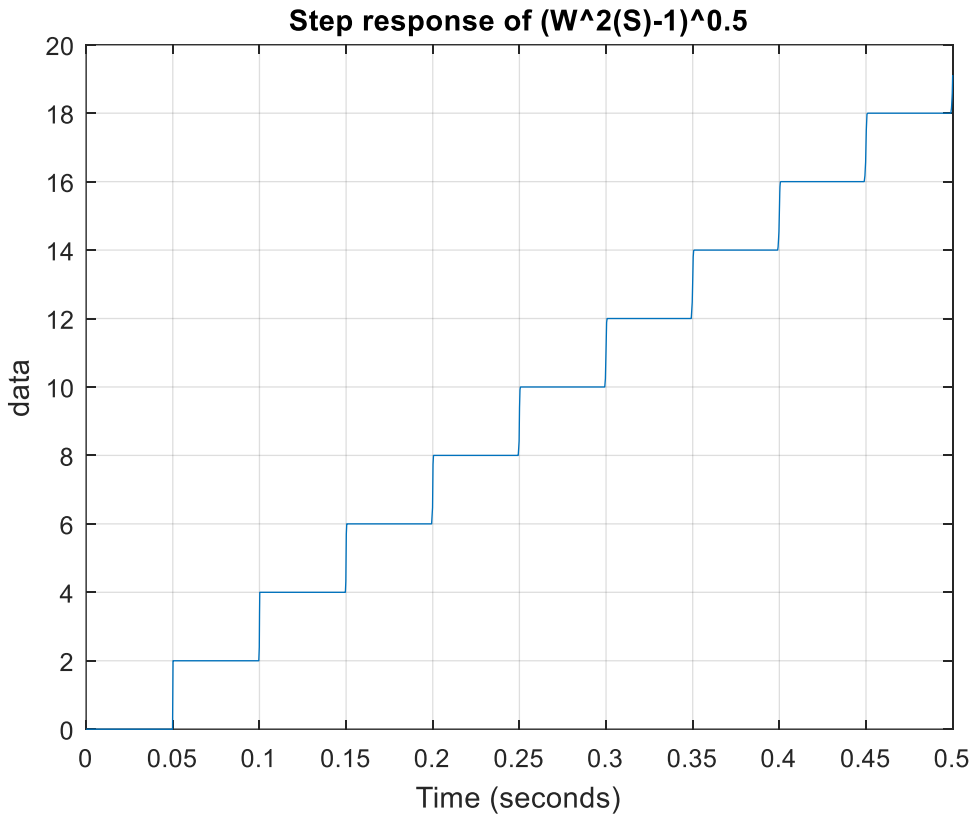

Figure 29 Unit Step response of (W^2(s)-1)^0.5

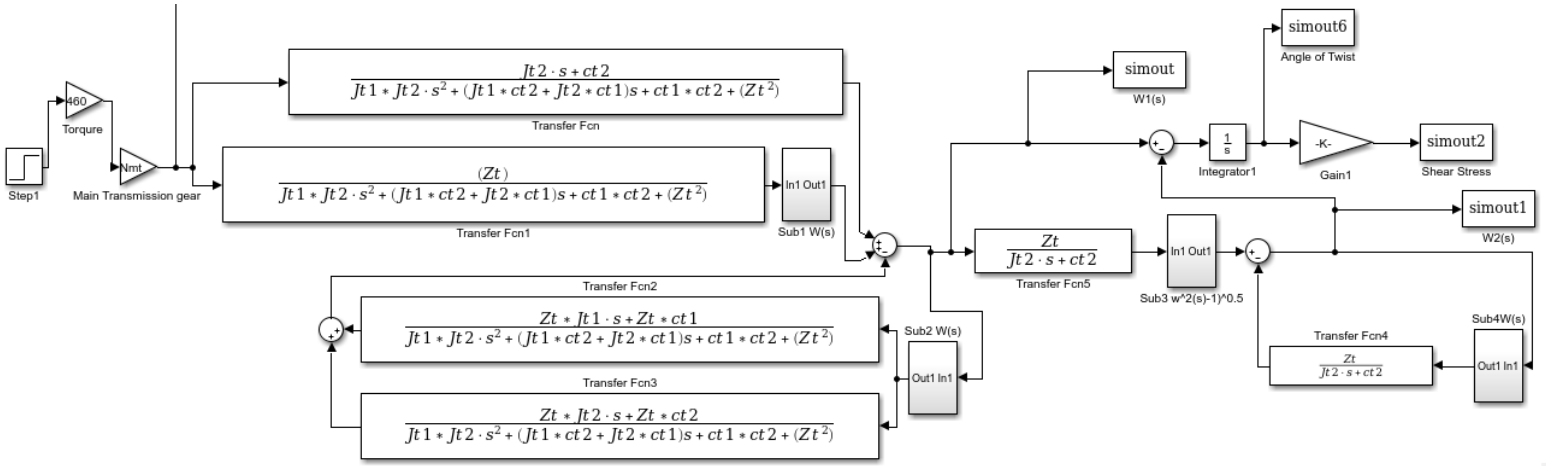

Figure 30 Tail Rotor Shaft Hybrid Model Block Diagram

Table 13: Shaft Material Properties

Property	Units	Aluminum Alloy T7075	Steel AISI 4340	Titanium Forging (6 A1-4V)
Ultimate tensile strength	psi	86,000	250,000	135,821
Yield tensile strength	psi	78,600	230,000	122,642
Shear yield stress	psi	39,300	115,000	61,321
Endurance strength	psi	20,000	100,000	20,000
Endurance limit	psi	14,280	71,400	14,280
Surface factor		1.00	1.00	1.00
Size factor		0.70	0.70	0.70
Load factor		1.00	1.00	1.00
Temperature factor		1.02	1.02	1.02
Miscellaneous effects		1.00	1.00	1.00
Total endurance factor		0.71	0.71	0.71
Density (weight)	lb/in^3	0.098	0.283	0.161
Modulus of Elasticity		10.3E6	30.0E6	15.5E6

Table 2 Shaft Material Properties

3.7.Calculating Model constant value

3.7.1. Calculating moment of inertia (J)

Helicopter rotor moment of inertia

A helicopter rotor blade can be considered as a long thin rod. The moment of inertia of a thin rod, rotating with reference to its end.

Figure 31 long thin rod moment of Inertia

Main rotor blades moment of inertia

Number of blades are N= 5

Length of blade L=4.03 M

Mass of each blade M=16.6 Kg

$$J_{MR} = 5(\frac{1}{3}ML^2) = 5(\frac{1}{3}16.6x4.03^2) = 5\,\text{x}\,89.87 = 449.33kg.m^2$$

Tail rotor blades moment of inertia

Length of blade L=0.035m

Mass of each blade M=0.7 Kg

$$J_{TR} = 4(\frac{1}{3}ML^2) = 4(\frac{1}{3}0.7x0.035^2) = 4\,\text{x}\,0.1225 = 0.0011433kg.m^2$$

Main rotor hub moment of inertia

Figure 32 Solid cylinder or disk moment of inertia

Main rotor hub mass is 20 Kg

R =0.3 m

$$J = \frac{1}{2}MR^2 = \frac{1}{2}x20x0.3^2 = 0.9kg.m^2$$

Main rotor total moment of inertia

$$J_{MRtotal} = J_{blades} + J_{MRH} = 449.33 + 0.9 = 450.23kg.m^2$$

Helicopter drive shafts moment of inertia

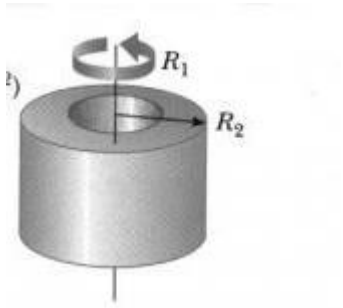

Figure 33 Hollow cylinder moment of inertia

Main rotor drive shaft moment of inertia

R_1= 0.042 m

R_2= 0.0575m

$$\rho = 2770kg/m^3$$

$$V = \pi h(\mathrm{R}_2^2 - R_1^2) = \pi x 0.34(0.0575^2 - 0.042^2) = 0.0016\,\mathrm{m}^3$$
$$M = \rho V = 4.432kg$$
$$J = \frac{1}{2}M(R_1^2 + R_2^2) = \frac{1}{2}4.432(0.042^2 + 0.0575^2) = 0.01124kg.m^2$$

Tail rotor drive shaft moment of inertia

R_1= 0.688m

R_2= 0.7m

$$\rho = 2770kg/m^3$$

$$V = \pi h(\mathrm{R}_2^2 - R_1^2) = \pi x 3.96(0.07^2 - 0.0688^2) = 0.00207\,\mathrm{m}^3$$
$$M = \rho V = 5.74kg$$
$$J = \frac{1}{2}M(R_1^2 + R_2^2) = \frac{1}{2}5.74(0.0688^2 + 0.07^2) = 0.02747kg.m^2$$

Engine drive shaft moment of inertia

Helicopter drive shaft's Gears and pins moment of inertia

Main rotor Gear moment of inertia

R =0.1m

h =0.02

$$\rho = 6800kg/m^3$$

$$V = \pi hR^2 = \pi x 0.02x 0.1^2 = 0.00063$$

M=4.284 kg

$$I = \frac{1}{2}MR^2 = \frac{1}{2}x4.284x0.1^2 = 0.02142kg.m^2$$

Tail rotor Gear moment of inertia

3.8.Calculating stiffness (k)

The shaft stiffness k is given by

$$k = \frac{GJ}{L}$$

$$J = \frac{\pi(D_{out}^4 - D_{in}^4)}{32}$$

Modulus of rigidity modulus G=28462 N/mm^2

3.9.Lumped parameter Model Stiffness (K)

3.9.1. Stiffness (K) of tail rotor shaft

$$Jts = \frac{\pi(0.07^4 - 0.068^4)}{32} = 2.58\times10^{-7}m^4$$

$$K_{ts} = \frac{(2.8462\times10^{10})(2.58\times10^{-7})}{3.96} = 1854.342424N.m$$

3.9.2. Stiffness (K_{ts}) of Main rotor shaft

$$Jms = \frac{\pi(0.0575^4 - 0.042^4)}{32} = 7.67\times10^{-7}m^4$$

$$K_{ms} = \frac{(2.8462\times10^{10})(7.67\times10^{-7})}{0.34} = 64206.92 N.m$$

3.10. Finite element model Stiffness (K)

3.10.1. Stiffness (K) of tail rotor shaft

$$Jts = \frac{\pi(0.07^4 - 0.068^4)}{32} = 2.58\times10^{-7} m^4$$

$$K_{ts} = \frac{(2.8462\times10^{10})(2.58\times10^{-7})}{0.792} = 8765.07 N.m$$

3.10.2. Stiffness (K_{ts}) of Main rotor shaft

$$Jms = \frac{\pi(0.0575^4 - 0.042^4)}{32} = 7.67\times10^{-7} m^4$$

$$K_{ms} = \frac{(2.8462\times10^{10})(7.67\times10^{-7})}{0.068} = 333870 N.m$$

3.11. Engine Model

Engine power is P=420 hp =313194watts

ω =6000 rpm = 628.31853 radian/ second

$$P = T\omega$$

$$T_e = \frac{P_e}{\omega_e} = \frac{313194}{628.31853} = 498.463733 N.m$$

1.1.1. Main Transmission gear model

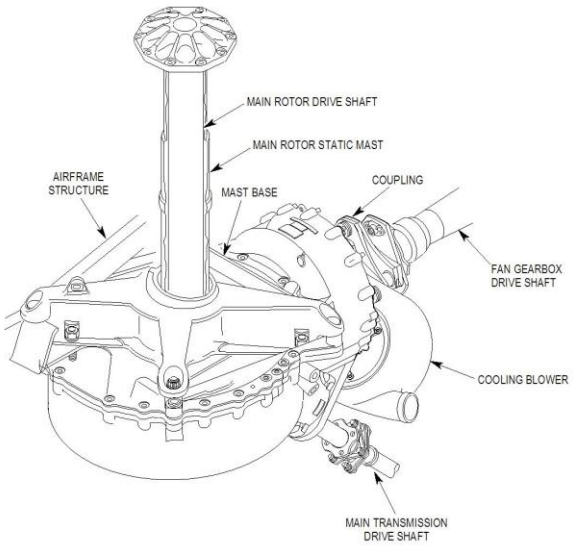

Figure 34 Main Transmission gear (Source Helicopters - MD 500E" 2018)

$$P_E = P_{tts}$$

$$T_E \omega_E = T_{tts} \omega_{tts}$$

$$T_E \frac{\omega_E}{\omega_{tts}} = T_{tts}$$

$$N_{mt} = \frac{\omega_E}{\omega_{tts}} = \frac{6000}{2040} = 2.9412$$

Therefore it can be stated that, Main Transmission gear model as Gain (Nmt = 2.9412)

1.1.2. Main Rotor Transmission gear

$$P_{mts} = P_{mrs}$$

$$T_{mts}\omega_{mts} = T_{mrs}\omega_{mrs}$$

$$T_{mts}\frac{\omega_{mts}}{\omega_{mrs}} = T_{mrs}$$

$$N_{mt} = \frac{\omega_{mts}}{\omega_{mrs}} = \frac{2040}{468} = 4.359$$

Therefore it can be stated that, Main Rotor Transmission gear model as gain (N_{mr}=4.359)

Gear ratio	
Parameter	Value
Main Transmission gear Nmt	2.9412
Main Rotor Transmission Nmr	4.359

Table 3 Summary of gear ratio constant

Tail Rotor Model					
Moment of Inertia ($Kg.m^2$)		Equivalent system damping (Nms/Rad)		Stiffness (Nm/rad)	
Parameter	Value	Parameter	Value	Parameter	Value
Main Transmission Jtr1	0.00045	Viscous damping coefficients Ctr1	0.6	Lumped system Stiffness Ktr	1753.014
Tail Rotor Jtr2	0.0011433	Viscous damping coefficients Ctr2	5	Finite element System Stiffness Ktr	8765.07

Table 4 Summary of tail Rotor Model constant

Main Rotor Model					
Moment of Inertia ($Kg.m^2$)		Equivalent system damping (Nms/Rad)		Stiffness (Nm/rad)	
Parameter	Value	Parameter	Value	Parameter	Value
Main Rotor Transmission Jmr1	0.009	Viscous damping coefficients Cmr1	10	Lumped system Stiffness Kmr	66774.12
Main Rotor Jm2	450.23	Viscous damping coefficients Cmr2	100	Finite element System Stiffness Kmr	333870

Table 5 Summary of Main Rotor Model constant

Lumped parameter transfer functions:

Tail Rotor drive end Transfer function:

$$\frac{0.933\ s^2 + 3\ s + 1753}{0.8397\ s^3 + 3.167\ s^2 + 3215\ s + 6136}$$

Tail Rotor load End transfer function:

$$\frac{1753}{0.8397\ s^3 + 3.167\ s^2 + 3215\ s + 6136}$$

Main Rotor drive end transfer function:

$$\frac{450.2\ s^2 + 100\ s + 6.677e04}{405.2\ s^3 + 315.1\ s^2 + 3.012e07\ s + 6.711e06}$$

Main Rotor load end transfer function:

$$\frac{6.677e04}{405.2\ s^3 + 315.1\ s^2 + 3.012e07\ s + 6.711e06}$$

3.12. MATLAB Simulink

Simulink is a software bundle for modelling, simulating, and analysing dynamic systems. It modelled in continuous time, discrete time or a hybrid of the two. In addition, it supports linear and nonlinear systems.

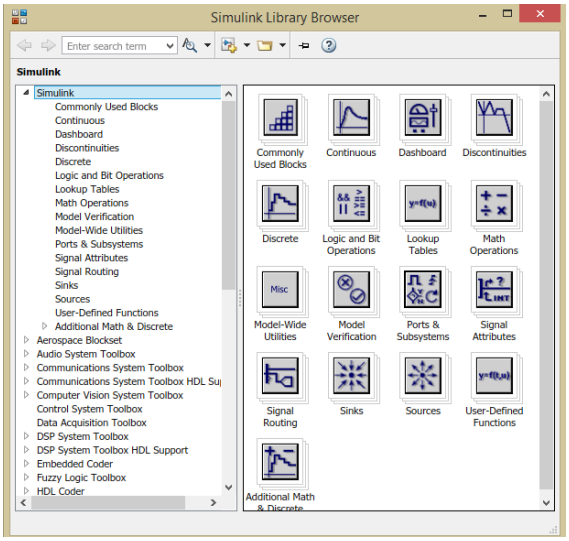

Figure 35 Simulink Library Browser (Source: "MATLAB"2018)

Simulink employs a graphical user interface (GUI) for building models as block diagrams, using click and drag operations from blocks library of linear and nonlinear components, sources, sinks and connectors. Furthermore, customise blocks can be created using S-Functions. Models are hierarchical. Modes can be both top-down and bottom-up. The model can be view at a high level and then double-click on blocks to go down through the various levels to see an increasing amount of detail. This approach allows insight into how the model is organised and how its components interact.

Simulink and MATLAB are integrated; System can be models, simulate and analyse in either environment at any point. System Model can be entered as commands in MATLAB's command window or simulated in Simulink from interacted block diagrams. The command-line approach is particularly convenient for running a batch of simulations while Simulink library menus are very useful for interactive work. Simulation result can be obtained using Simout and other display blocks for post-processing and visualisation.

3.13. Test completed

1. Step input response for MD500E Helicopter drivetrain lumped model
2. Step input response for MD500E Helicopter drivetrain finite element model
3. Step input response for MD500E helicopter drivetrain hybrid, distributed-lumped model

Plot obtain from Simulink Matlab

- Time response
- Bode diagram

Chapter IV

Simulation Results and Discussions

4.1.Introduction

In this chapter, MD500E helicopter drive-train system which consists of Rolls-Royce Model 250 Turboshaft Engine, main drive shaft, main transmission gear, main rotor transmission gear, main rotor shaft, tail rotor shaft, main rotor and tail rotor is considered. The drive-train simulated in Simulink for comparison purpose using lumped, finite element, and lumped-distributed parameter hybrid models.

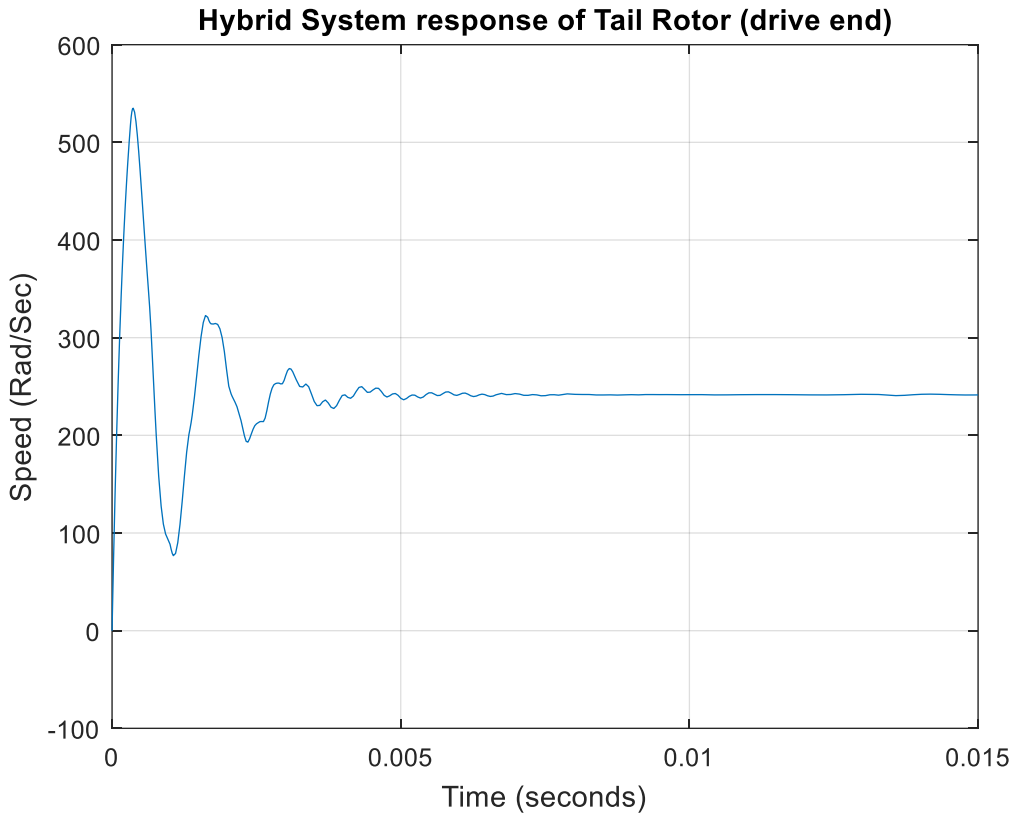

Figure 36 Hybrid System response of Tail Rotor (drive end)

Figure 36 shows that the hybrid system response of the Tail rotor at the drive end. From the figure, it can be discerned that there is an overshoot to speed greater than 500Rad/sec almost instantly. Then there is a sharp decline which then fluctuates for a short time period and then stabilises between 0.005 seconds and 0.01 seconds.

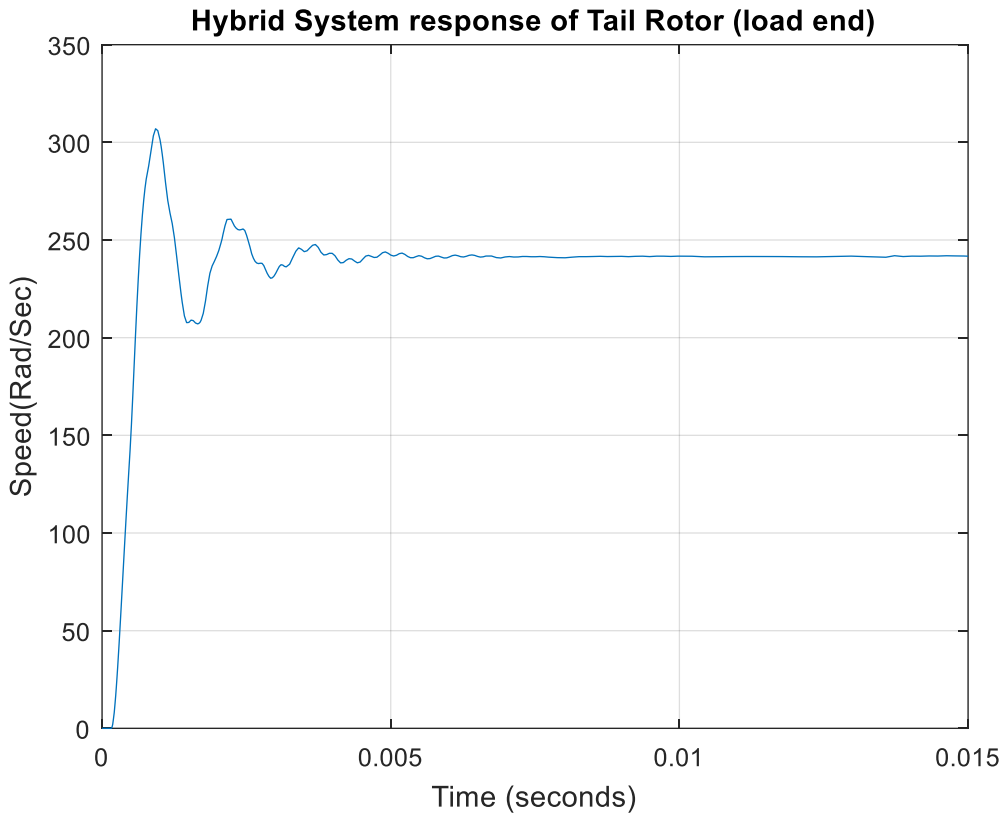

Figure 37 Hybrid System response of Tail Rotor (Load End)

The above figure 36 shows the hybrid system response of the tail rotor at the load end. As is evident from the diagram, the overshoot happens almost instantaneously to the speed of 300 Rad/sec and then has a smaller decline to around 200 rad/sec. After a little fluctuation, the response stabilises and at around the 0.007 seconds mark.

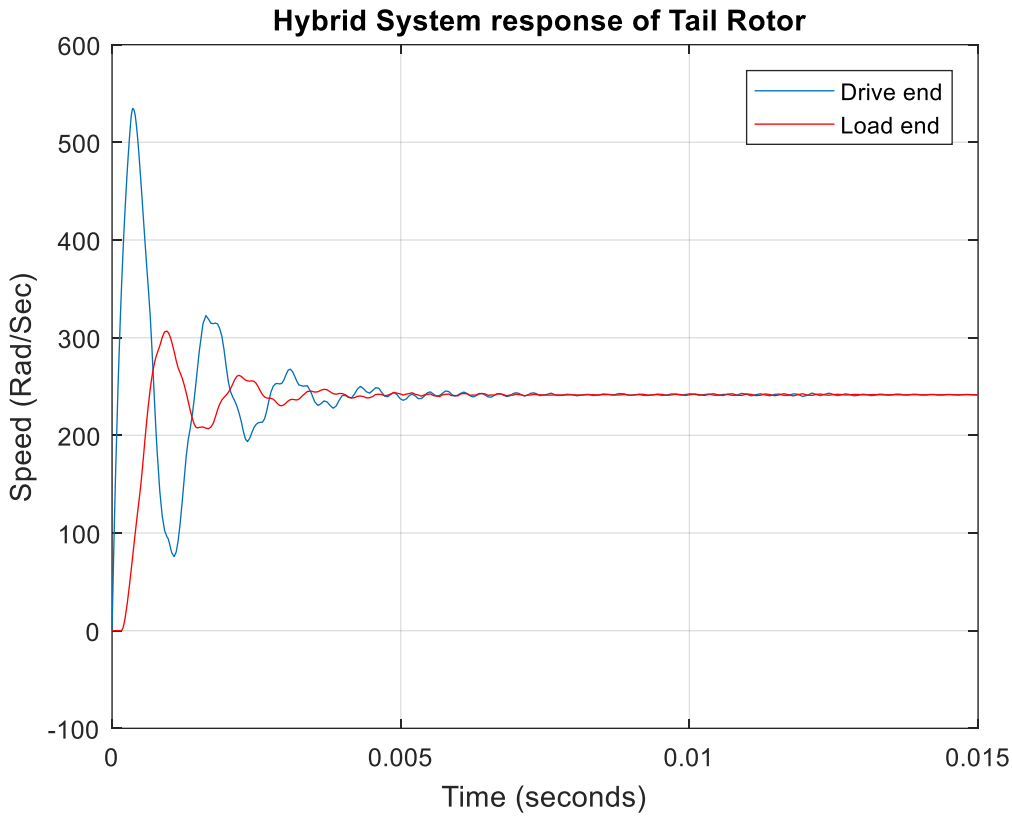

Figure 38 Hybrid System response of Tail Rotor (Drive and Load end)

The above figure 37 provides a comparison of the hybrid system response at the drive end (depicted by the blue line) and the load end (depicted by the red line). As can be seen from the above figure, the drive end experiences a higher overshoot and greater fluctuations in comparison to the load end. In addition, it can be seen that there is a more stable response generated in the load end in comparison to the drive end.

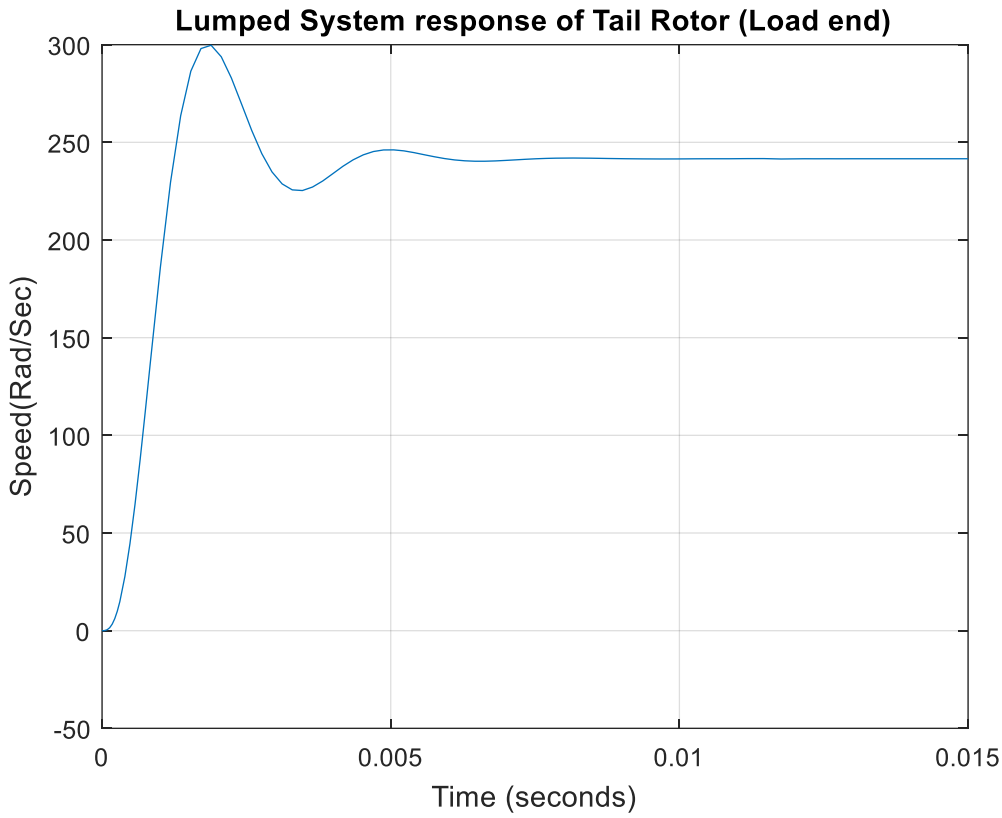

Figure 39 Lumped System response of Tail Rotor (Load End)

The above figure represents the Lumped system response of the tail rotor at the load end. It can be seen from Figure 38 that the overshoot is massive and sharp, happening to the speed of 300 Rad/Sec. However, the dip is not too extreme as well as the fluctuations are not major. The response stabilises quite quickly at the 0.005 marks.

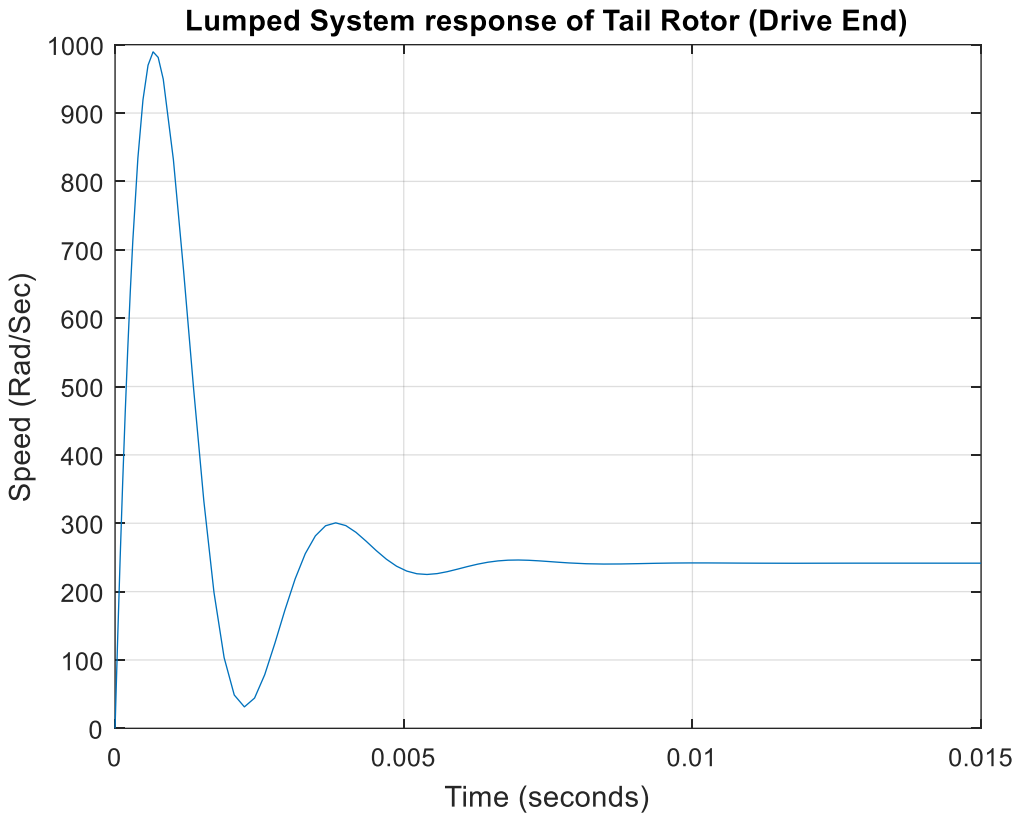

Figure 40 Lumped System response of Tail Rotor (Drive End)

Figure 39 depicts the lumped system response of a tail rotor at the drive end. As the figure represents, there is a massive overshoot that rises sharply at the speed of almost 1,000 Rad/sec and then follows an almost equally sharp decline. After the sharp increase and decrease the response stabilises beyond the 0.007 seconds mark.

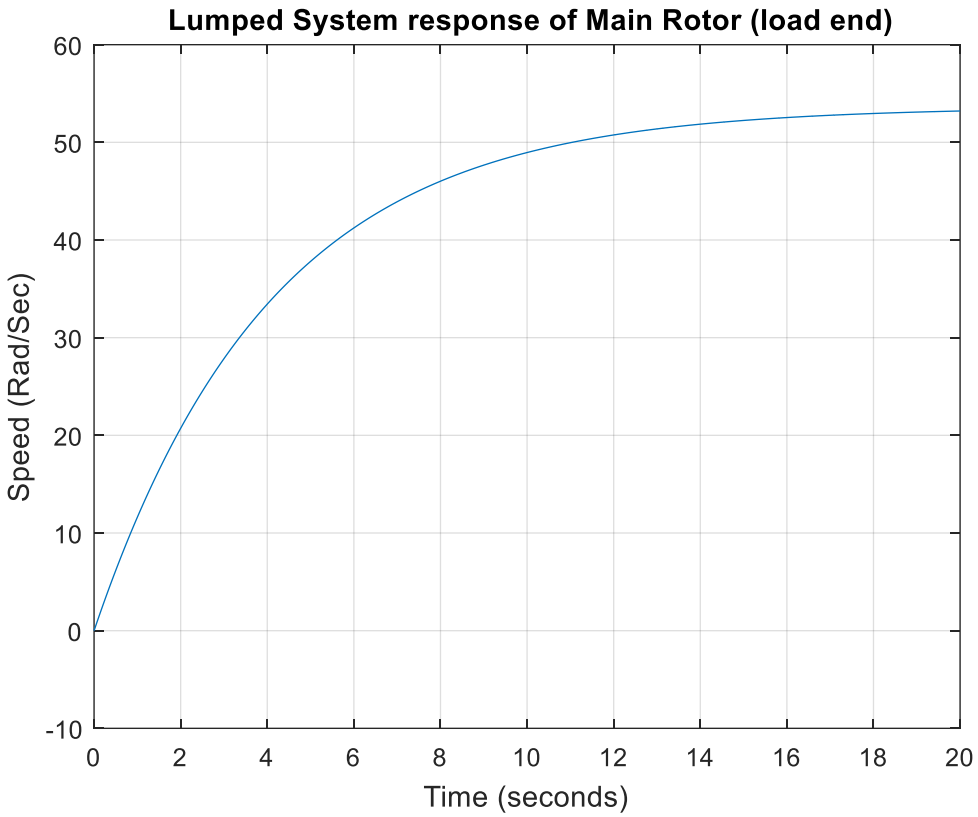

Figure 41Lumped System response of Main Rotor (Load End)

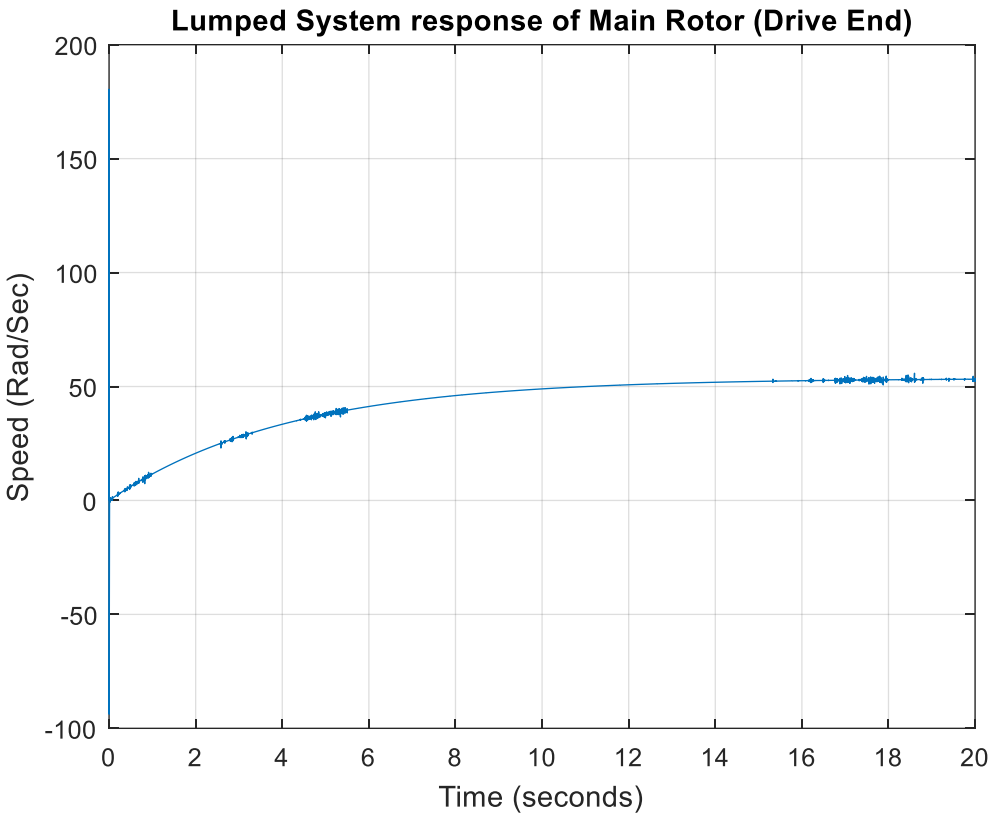

Figure 42 Lumped System response of Main Rotor (Drive End)

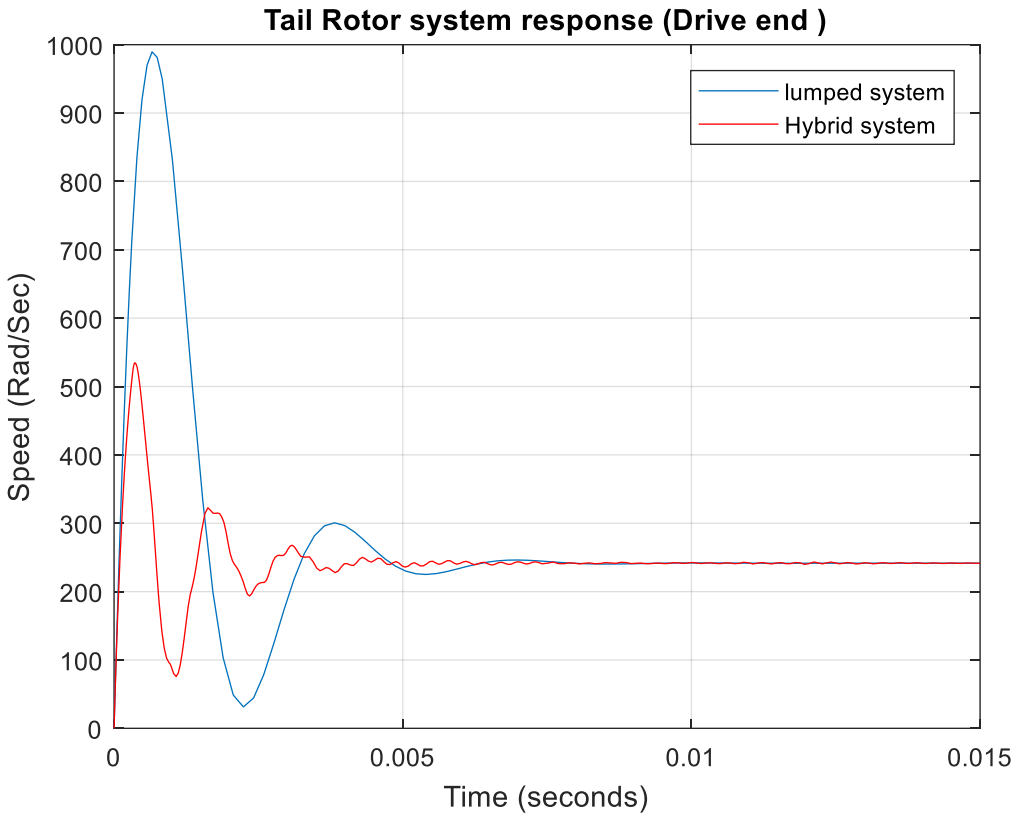
Tail Rotor system response (Drive end)
lumped system
Hybrid system
Speed (Rad/Sec)
Time (seconds)
0
100
200
300
400
500
600
700
800
900
1000
0
0.005
0.01
0.015

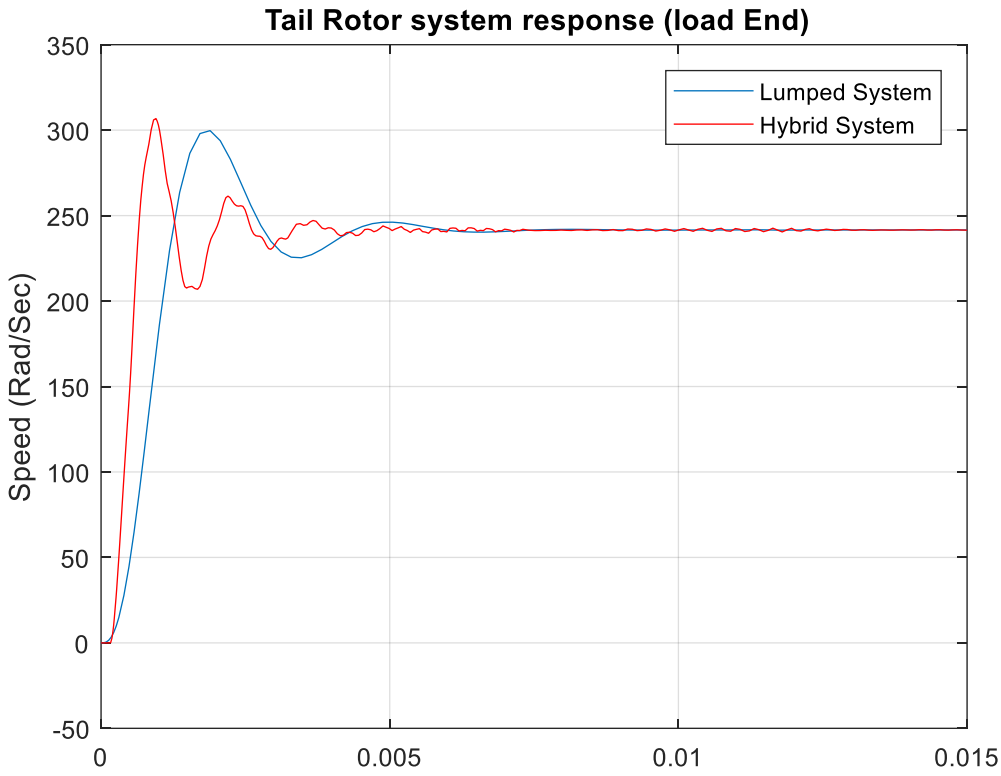
Tail Rotor system response (load End)
Lumped System
Hybrid System
Speed (Rad/Sec)
350
300
250
200
150
100
50
0
-50
0
0.005
0.01
0.015

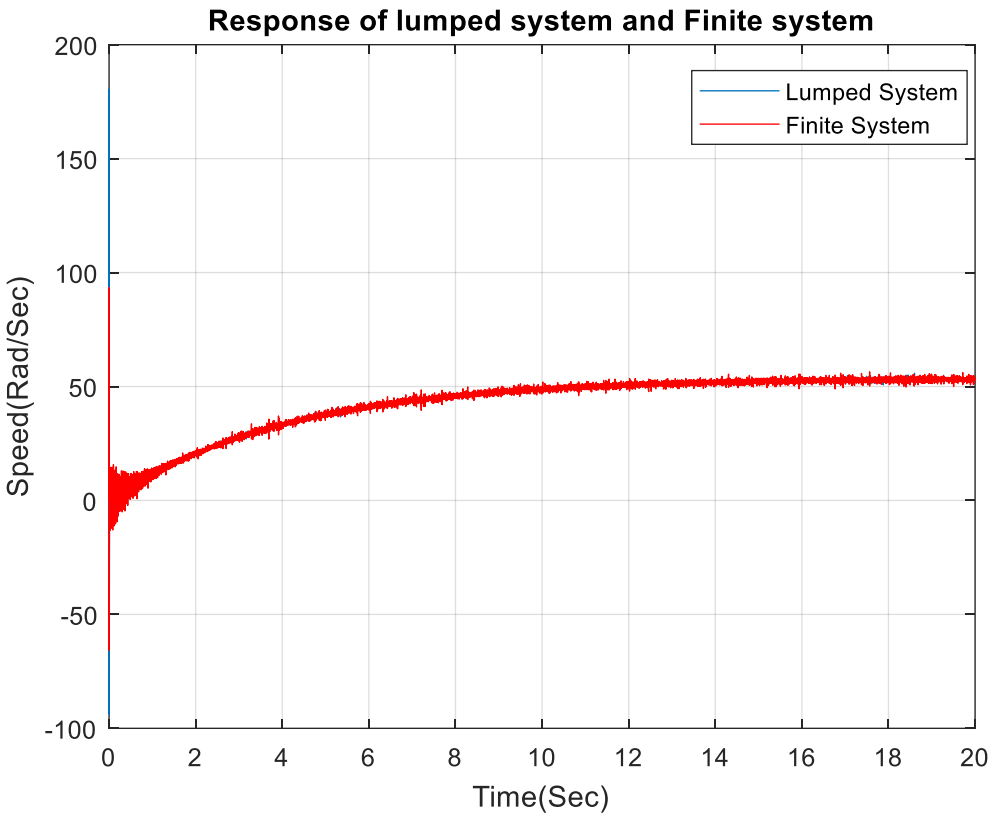
Response of lumped system and Finite system
Lumped System
Finite System
Speed(Rad/Sec)
Time(Sec)
200
150
100
50
0
-50
-100
0
2
4
6
8
10
12
14
16
18
20

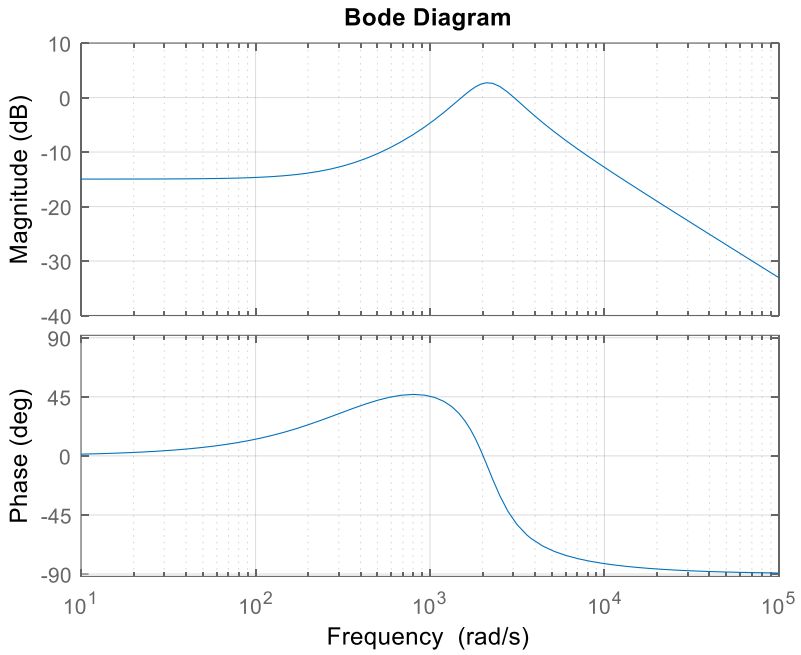

Figure 43 Bode diagrams for Tail Rotor Lumped System (Drive end)

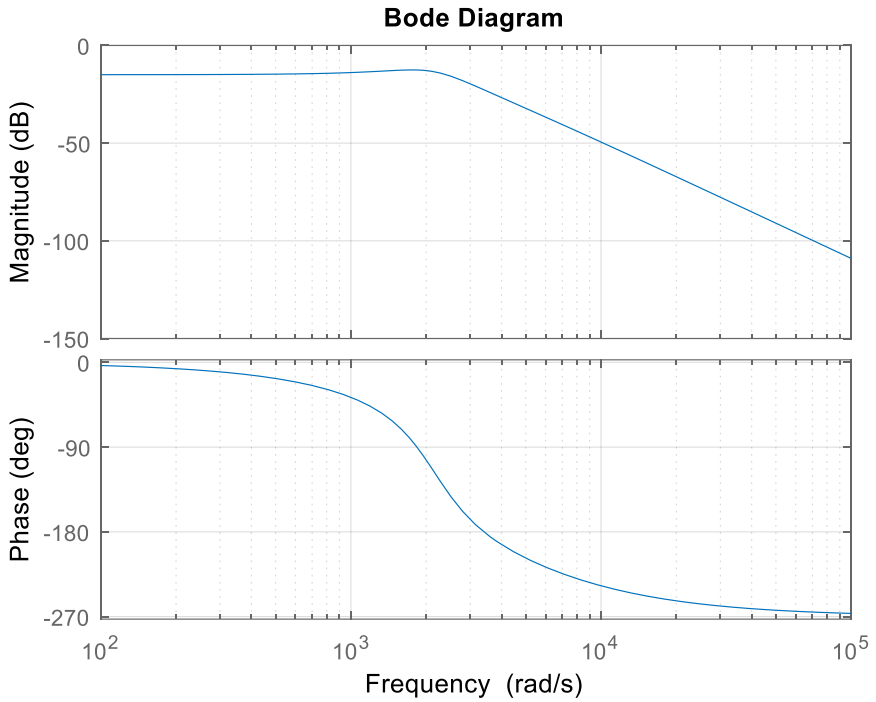

Figure 44 Bode diagrams for Tail Rotor lumped System (Load End)

The resonant frequency for Tail Rotor lumped system can be estimated based on the following formation:

Resonance is achieved when the amplitude of the output-input ratio reaches a maximum, and the phase at the load end is Φ_2=-π/2

$$\square(i\omega) = k_{tr}(C_{tr1} + C_{tr2}) - (J_{tr1}C_{tr2} + J_{tr1}C_{tr1})\omega_{tr}^{\ 2} + [(J_{tr1} + J_{tr2})k_{tr} + C_{tr1}C_{tr2} - J_{tr1}J_{tr2}\omega_{tr}^{\ 2}]i\omega$$

(29)

Therefore, it can be stated that, Resonant Frequency

$$\phi_2(\omega) = -\tan^{-1}\frac{(J_{tr1}+J_{tr2})k_{tr}+C_{tr1}C_{tr2}-J_{tr1}J_{tr2}\omega^2)\omega_{tr}}{K_{tr}(C_{tr1}+C_{tr2})-(J_{tr1}C_{tr2}+J_{tr2}C_{tr1})\omega_{tr}{}^2}$$

(30)

$$\omega_{tr}{}^2 = \frac{k_{tt}(c_{tr1}+c_{tr2})}{J_{tr1}c_{tr2}+J_{tr2}c_{tr1}}$$

(31)

$$\omega_{tr} = 44.0187$$

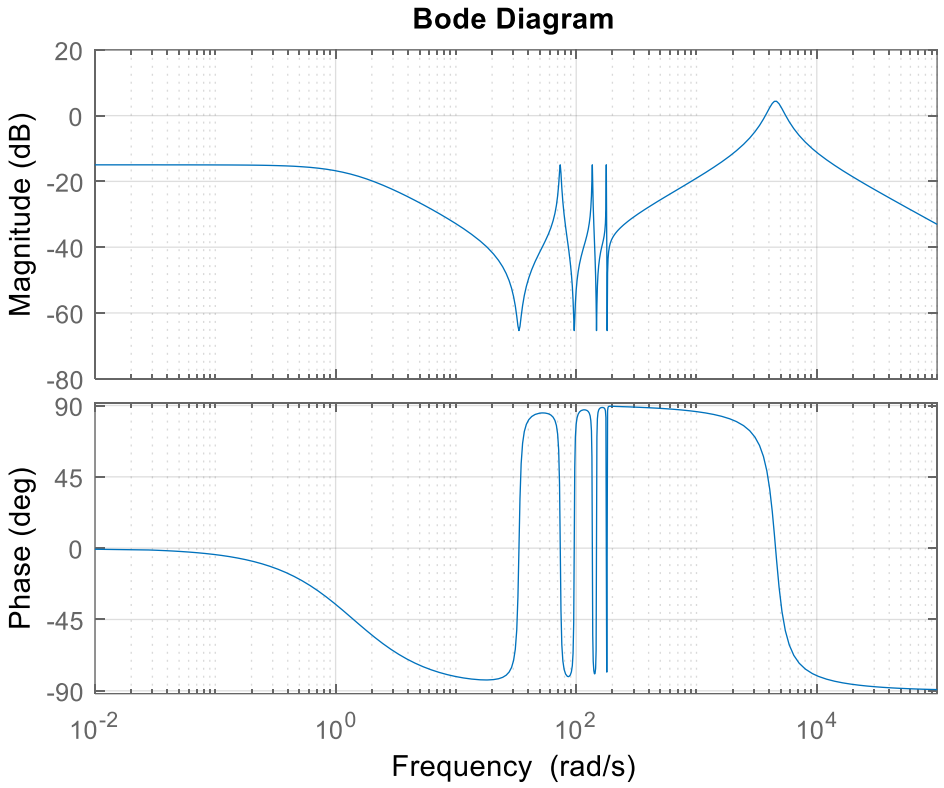

Figure 45 Bode diagram for Tail Rotor finite Element system (Drive End)

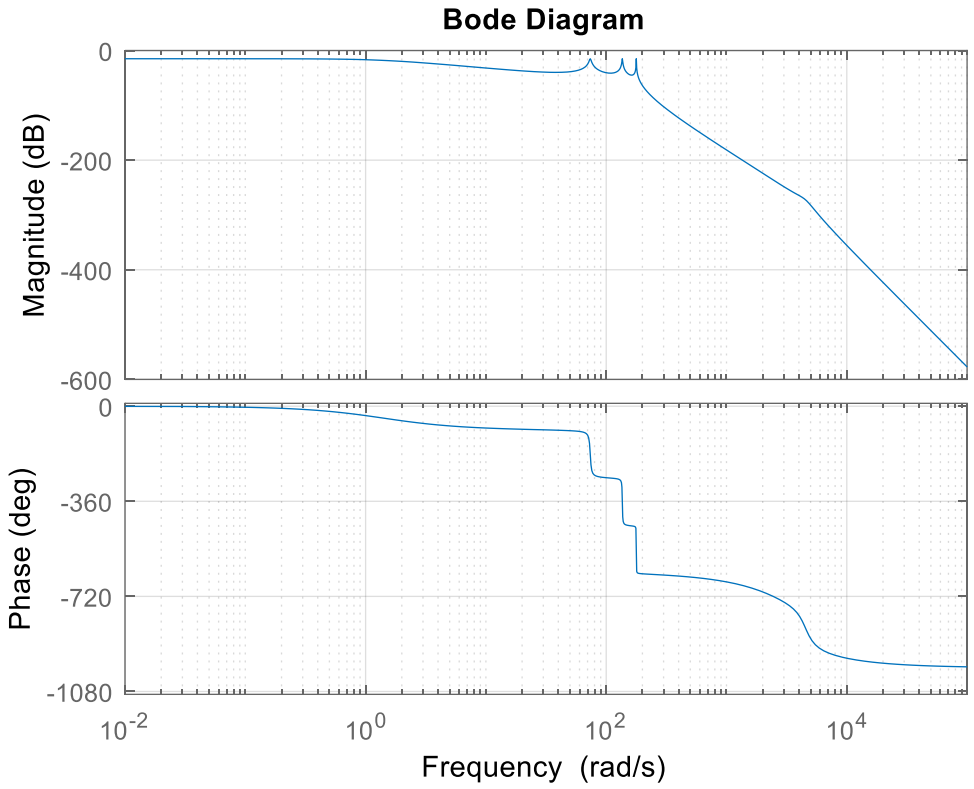

Figure 46 Bode diagrams for Tail Rotor system finite element system (Load End)

wtr = 1.8367e+03

Main rotor drive end

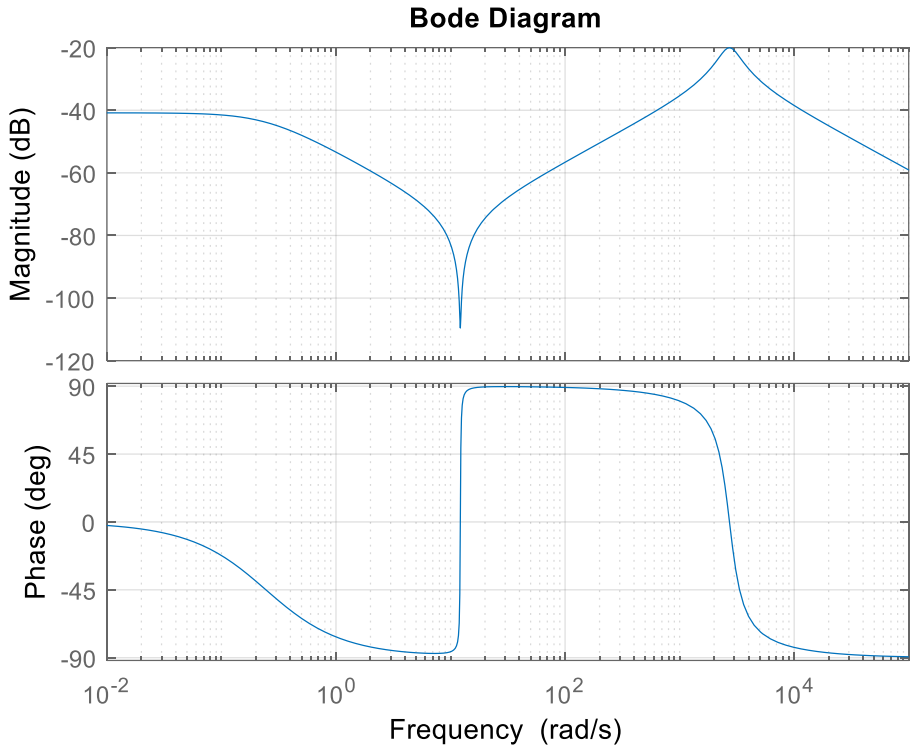

Figure 47 Bode diagrams for Main Rotor shaft lumped system (Drive End)

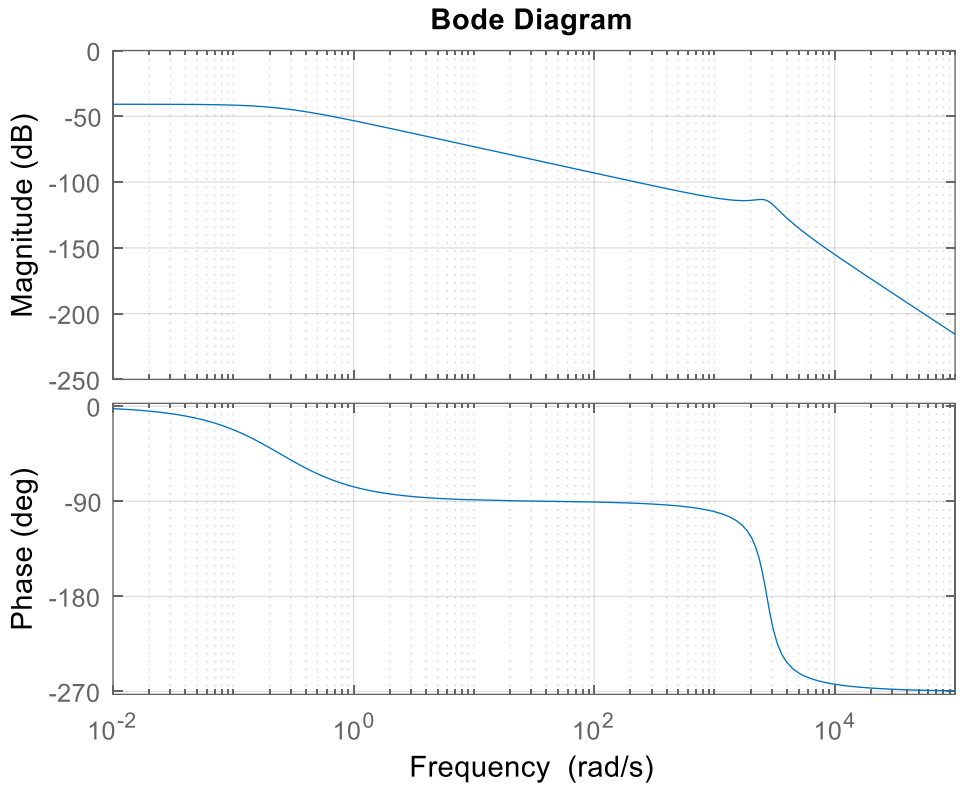

Figure 48 Bode diagrams for Main Rotor shaft lumped system (Load End)

The resonant frequency for Main Rotor lumped system can be estimated based on the following formation:

Resonance is achieved when the amplitude of the output-input ratio reaches a maximum, and the phase at the load end is Φ_2=-π/2

$$\square(i\omega) = k_{mr}(C_{mr1} + C_{mr2}) - (J_{mr1}C_{mr2} + J_{mr1}C_{mr1})\omega_{mr}{}^2 + [(J_{mr1} + J_{mr2})k_{mr} + C_{mr1}C_{mr2} - J_{mr1}J_{mr2}\omega_{mr}{}^2]i\omega_{mr}$$

(32)

Resonant Frequency

$$\phi_2(\omega) = -\tan^{-1}\frac{(J_{mr1}+J_{mr2})k_{mr}+C_{mr1}C_{mr2}-J_{mr1}J_{mr2}\omega_{mr}{}^2)\omega_{mr}}{K_{mr}(C_{mr1}+C_{mr2})-(J_{mr1}C_{mr2}+J_{mr2}C_{mr1})\omega_{mr}{}^2}$$

(33)

$$\omega_{mr}{}^2 = \frac{k_{mr}(C_{mr1}+C_{mr2})}{J_{mr1}C_{mr2}+J_{mr2}C_{mr1}}$$

(34)

$$\omega_{mr} = 145.9327$$

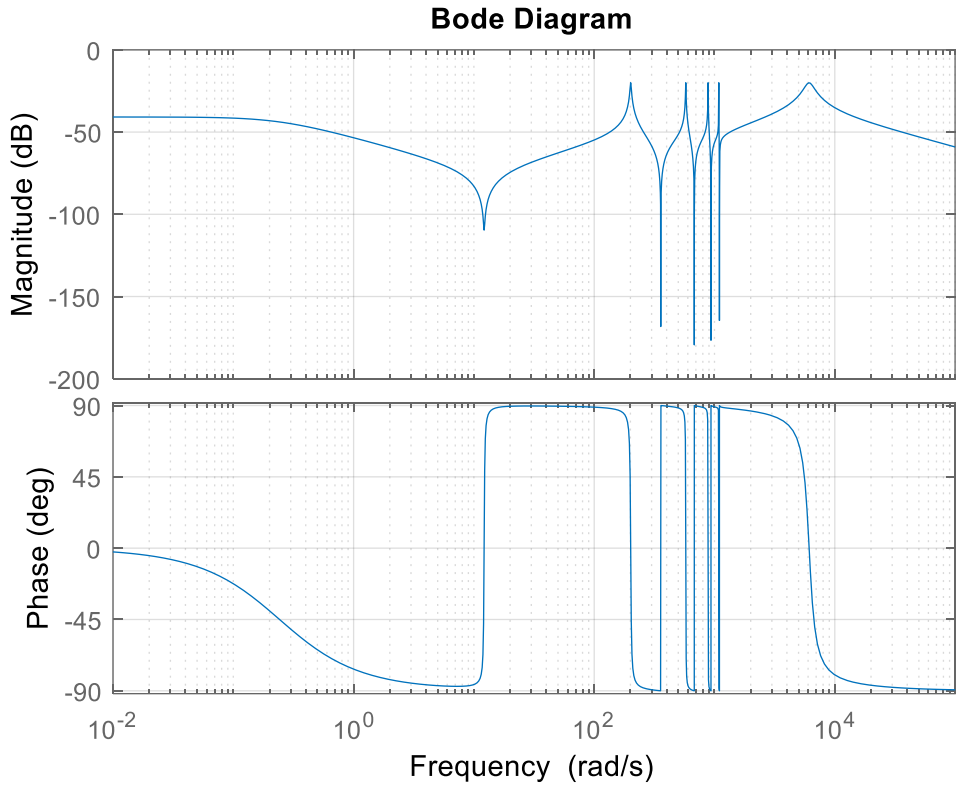

Figure 49 Bode diagrams for Main Rotor shaft finite element system (Drive End)

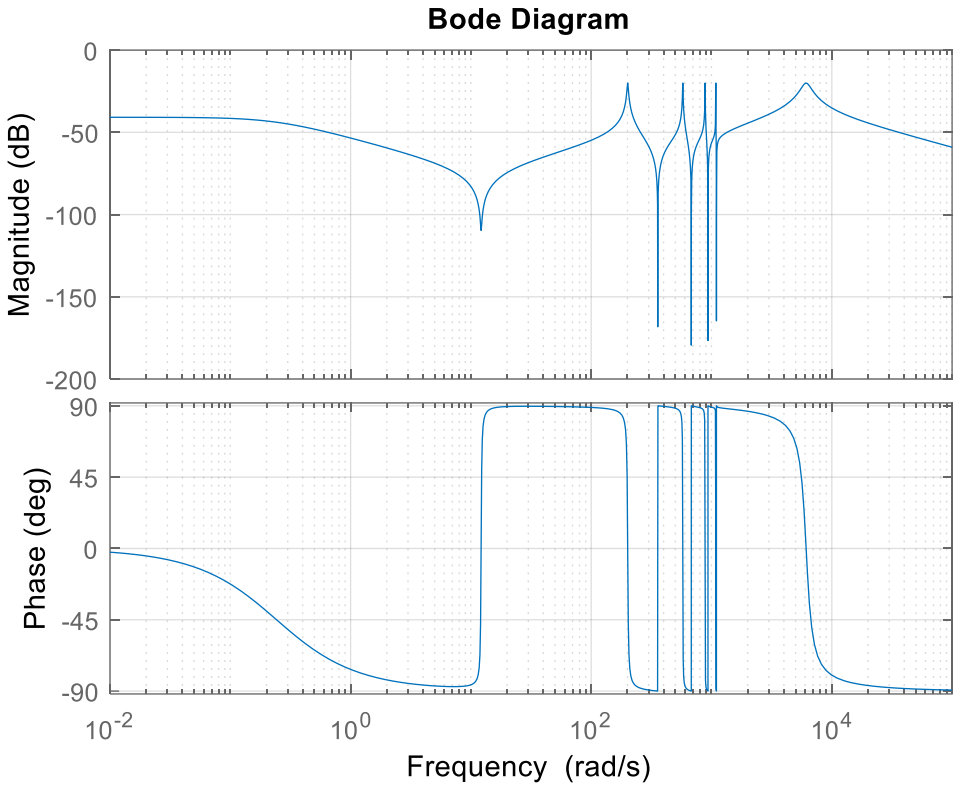

Figure 50 Bode diagrams for Main Rotor shaft finite element system (Load End)

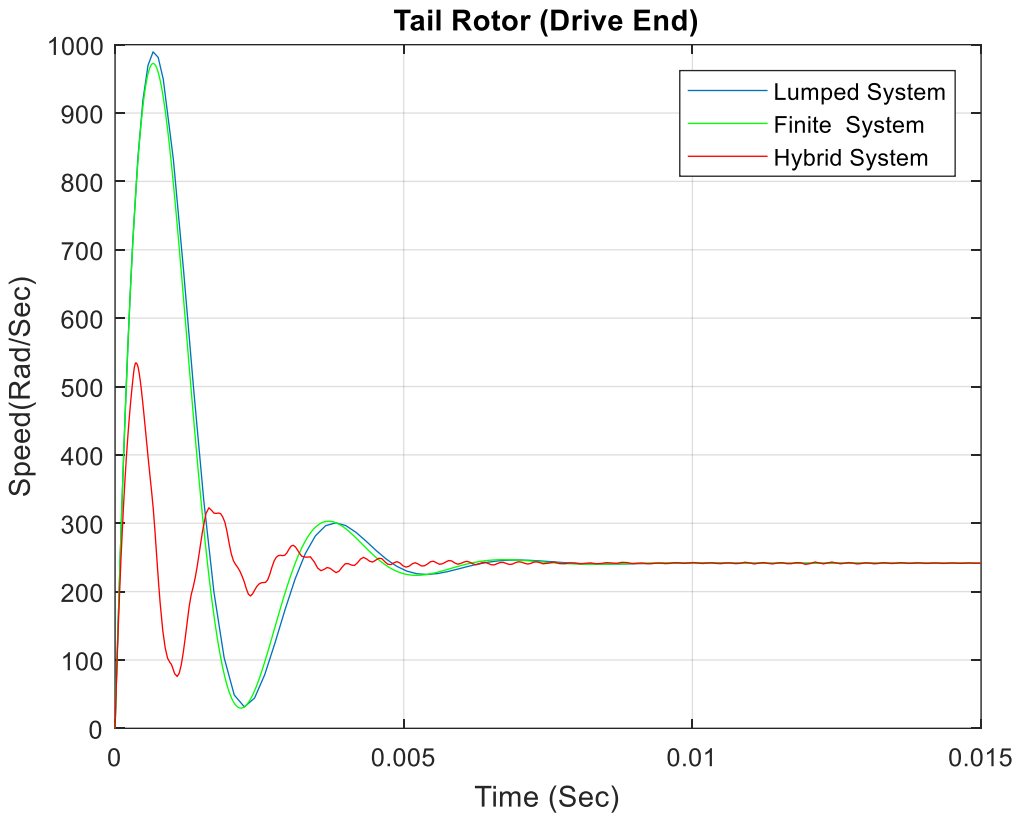

Figure 51 Comparison between lumped, finite element and Hybrid system following step input change (Drive End)

Figure 51 shows the comparison between the lumped, finite element and hybrid system. From the above figure, it is observed that both lumped, finite element systems show exaggerated overshoot and settling time characteristics compared to the hybrid system which is considered as more realistic realisation. In addition, the finite element representation illustrates some improvement over the purely lumped model. However, some uncertainties begin to appear regarding the accuracy of the results due to the generation of addition eigenvalues.

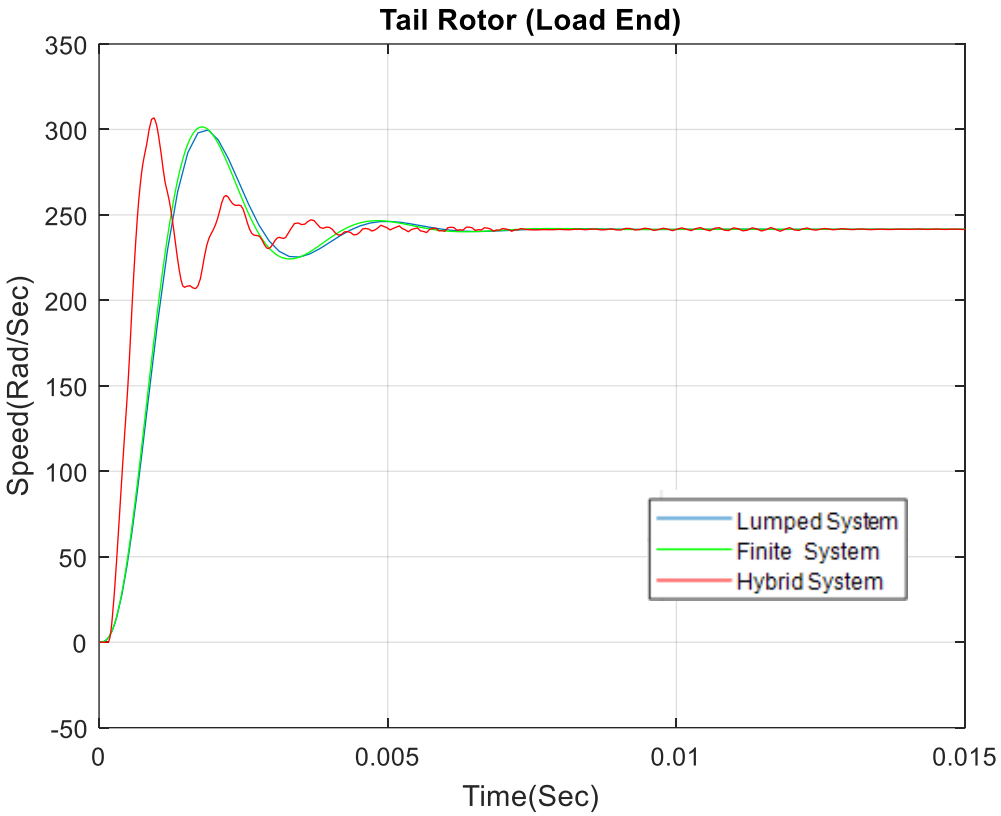

Figure 52 Comparison between lumped, finite element and Hybrid system following step input change (Load End)

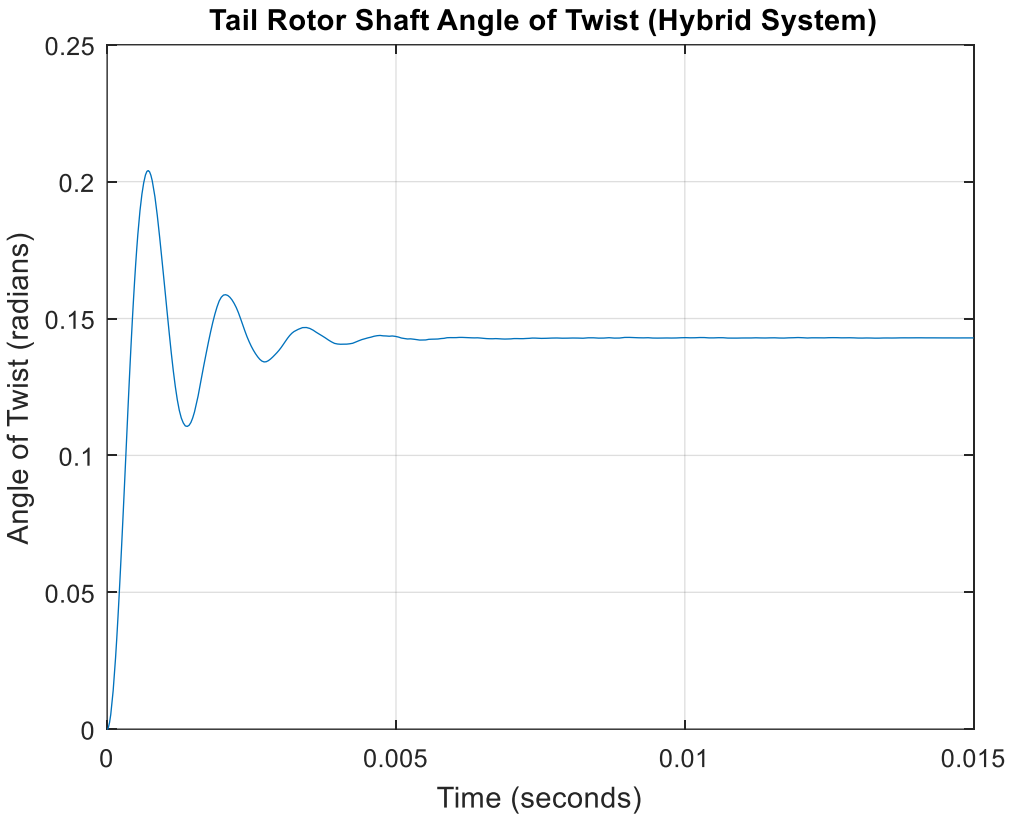

Figure 53 Tail Rotor Shaft Angle of Twist Transient Following a Step Input Torque Change

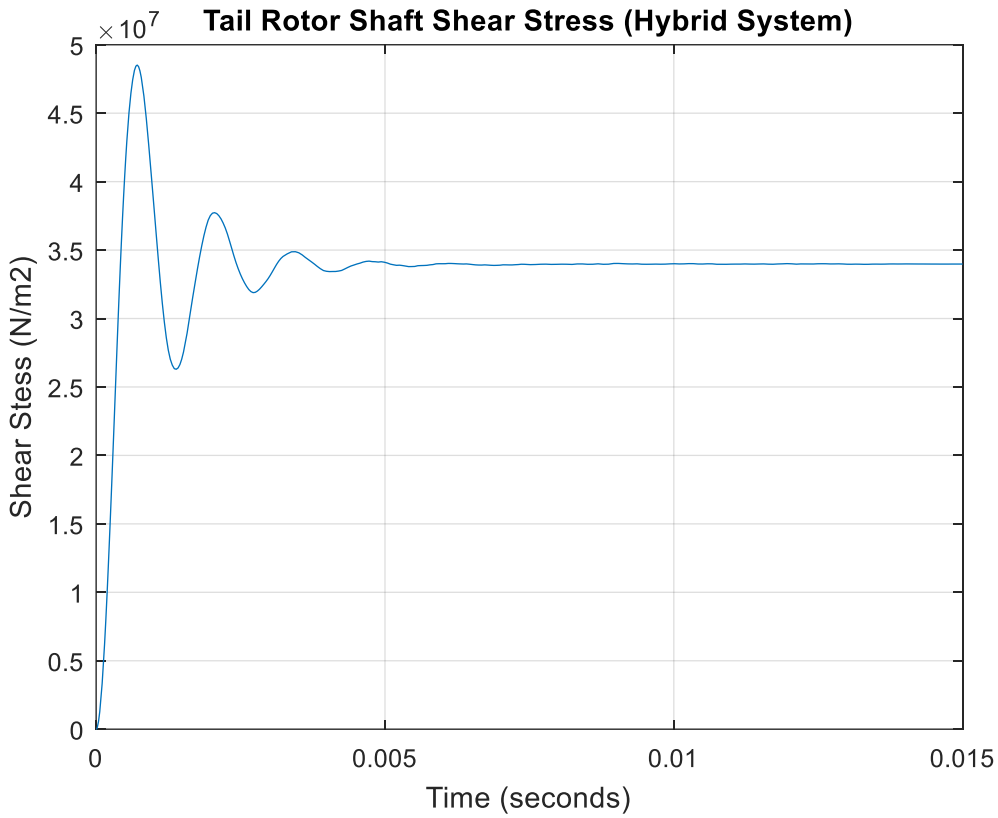

Figure 54 Tail Rotor Shaft Shear Stress Transient Following a Step Input Torque Change

Chapter V

Conclusions and Recommendations

5.1. Conclusions

In this dissertation, MD500E helicopter drive-train system model which consists of Rolls-Royce Model 250 Turboshaft Engine, main drive shaft, main transmission gear, main rotor transmission gear, main rotor shaft, tail rotor shaft, main rotor and tail rotor was derived based on technique develop by R Whalley, M Ebrahimi and Z Jamil paper “The Torsional response of rotor systems”.

Three Models were derived for the same system lumped, finite element and hybrid. Then, the models were simulated in MATLAB-Simulink for purposes of comparison. In addition, the resonant frequency, for each model was calculated and compared with it bode plot.

The lumped model was the simplest analytical realization, but it also provided the least accurate result. In lumped model mass-inertia, stiffness and damping model as single, undefined point in space.

On the other hand, finite element models provided improved prediction in comparison to lumped parameter models. However, some uncertainties started to appear regarding the accuracy of the results obtained. It appeared that the integrity of the model reduces as dimensions of the mass, damping and stiffness matrices increase because of the fact that of the increase generation of eigenvalues, eigenvectors and hence decay rates and

mode shapes. Therefore it can be stated that increasing finite element sections, would eventually result in increased computational errors.

In hybrid distributed-lumped parameter model, rotors and bearings modelled as pointwise unit same as the lumped model. However, shafts modelled as a distributed parameter where the inertia and stiffness are continuous functions of shaft length which proving to be more realistic representation.

It was observed from the simulation results that all three models share identical steady-state response and they are only dissimilar in transient behaviour. The transient characteristics of the lumped model have little in common with hybrid representations. In addition, it was observed that finite element transient response was moving in the direction toward the characteristics produced by the hybrid realisation.

The following table summarises the comparison between the three techniques used in modelling the MD500E helicopter drive-train.

	Lumped parameter model	Finite element model (five sections)	Hybrid (lumped-distributed parameter model)
Accuracy	Low	Medium	High
Integrity	Excellent	Reduce with increasing number of sections	Good

Computational efficiency	High	Reduce with increasing number of sections	Good

Table 6 Summary of the comparison of the three techniques

5.2. Recommendations

This dissertation illustrated one of the applications that hybrid, distributed-lumped parameter procedures developed by Whalley, Ebrahimi and Jamil (2005) could be utilised where system under investigation has some components that are significantly dispersed and others that exhibit a relatively lumped characteristic. In addition, this paper demonstrated the advantage of hybrid, distributed-lumped parameter procedures over lumped and finite element representation in such a system. Therefore, it can be stated that it is recommended to use a hybrid, distributed-lumped parameter procedures where such conditions exist. For example, long thin ships drive-train or earth drilling equipment.

It is suggested to develop the Hybrid, distributed-lumped parameter procedures to user friend software package to simulate a system that has some components that significantly dispersed and other that exhibit relative lumped characteristic such as helicopters and ships drive-train. This software can be used in troubleshooting as well as design.

5.3. Limitations

There are several limitations to this study. First, while attempts were made by the researcher to make the model as accurately as possible of the MD 500E, complete accuracy

could not be assumed because of the fact that many of the measurements were confidential and were not accessible. In such a scenario where the measurements were not available, the researcher has made assumptions into the same while trying to be as accurate as possible.

The second limitation is that of the main rotor drive shaft. This main rotor drive shaft of this helicopter was not modelled using the hybrid, lumped-distributed system because of the fact that MD 500E's drive shaft has a smaller length to width ratio. One of the preconditions of this model is that the drive shaft's length to width ratio is high and the drive shaft itself be longer. Therefore, only finite element analysis and the lumped model were used for this purpose.

With respect to the finite element analysis model, there is an inherent limitation. What this means is that one can get carried away with the breaking of a component into several sections. There is also the matter where the more sections that are created, the more eigenvalues and eigenvectors will be generated. Not only will this become increasingly complicated, but also lead to several errors.

References

A-Ameer, A. (2010). *Distributed Parameter System Modelling (SYS1504) Leacture_1*.

A-Ameer, A. (2010). *Distributed Parameter System Modelling (SYS1504) Leacture_2*.

A-Ameer, A. (2010). *Distributed Parameter System Modelling (SYS1504) Lecture_3 Case Study*.

Australian Transport Safety Bureau. (2005). *In-Flight Failure of a Tail rotor Drive Shaft*. Fig Tree Pocket, Qld.

Achinstein, P., 1965. Theoretical models. *The British journal for the philosophy of science*, *16*(62), pp.102-120.

Aström, K.J. and Murray, R.M., (2010). *Feedback systems: an introduction for scientists and engineers*. Princeton university press.

Berry, J., and Houston, K., (1995). *Mathematical modelling*. Gulf Professional Publishing.

Catling, H. and De Barr, A.E., (1956). Torsional Vibrations of Rotating Shafts. *Nature*, *178*(4542), p.1114.

Cheng, K.A., (2001). Teaching mathematical modelling in Singapore schools. *The Mathematics Educator*, *6*(1), pp.63-75.

Das, A.S., Dutt, J.K. and Ray, K., (2010). Active vibration control of unbalanced flexible rotor–shaft systems parametrically excited due to base motion. *Applied Mathematical Modelling*, *34*(9), pp.2353-2369.

Farshidianfar, A., Ebrahimi, M., Rahnejat, H. & Menday, M. (2002). High frequency torsional vibration of vehicular driveline systems in clonk. *International Journal of Heavy Vehicle Systems*, vol. 9 (2), p. 127.

Galbraith, P.L. and Clatworthy, N.J., (1990). Beyond standard models—meeting the challenge of modelling. *Educational Studies in Mathematics*, *21*(2), pp.137-163.

Hale, J.K. and LaSalle, J.P., (1963). Differential equations: Linearity vs. nonlinearity. *SIAM Review*, *5*(3), pp.249-272.

Hazelrigg, G.A., (1999). On the role and use of mathematical models in engineering design. *Journal of Mechanical Design*, *121*(3), pp.336-341.

Hughes Tool Company. (1972). *OH-6A PHASE II Quiet Helicopter Program*. Culver city, California : NTIS National Technical Information Service.

Kaiser, G. and Sriraman, B., (2006). A global survey of international perspectives on modelling in mathematics education. *Zdm*, *38*(3), pp.302-310.

Lewicki, D. & Coy, J. (1987). *Vibration Characteristics of OH 58A Helicopter Main Rotor Transmission*. Ohio: National Aeronautics and Space Administration (NASA). [Accessed 5 November 2018].

Ljung, L., 1997. System identification. In *Signal analysis and prediction* (pp. 163-173). Birkhäuser, Boston, MA.

"MD Helicopters - MD 500E". (2018). [Accessed 30 May 2018]. Available at: http://melm-md.com/MD500E.html

MDHI. (2014). *MD Helicopters Technical Description*. Mesa, AZ.

Magnus, P. (1996). *Driveline Modeling and Principles for Speed Control and Gear-Shift Control*. Linkoping University.

Nelson, H.D. and McVaugh, J.M., (1976). The dynamics of rotor-bearing systems using finite elements. *Journal of Engineering for Industry*, *98*(2), pp.593-600.

Pettersson, M., 1997. *Driveline modelling and control*. Department of Electrical Engineering, Linköping University.

Rosenberg, R. & Karnopp, D. (1983). *Introduction to physical system dynamics*. McGraw-Hill, Inc.

Ruhl, R.L. and Booker, J.F., (1972). A finite element model for distributed parameter turborotor systems. *Journal of Engineering for Industry*, *94*(1), pp.126-132.

Schichl, H., 2004. Models and the history of modeling. In *Modeling languages in mathematical optimization* (pp. 25-36). Springer, Boston, MA.

Stein, J. & Louca, L. (1995). A component based modeling approach for system design: Theory and implementation. *Proceedings of the 1995 International Conference on Bond Graph Modeling and Simulation*. [Accessed 5 November 2018].

Veershetty, D. (2018). [Accessed 26 October 2018]. Available at: https://www.quora.com/What-is-difference-between-CFD-and-FEA-Which-one-is-widely-used-in-automotive-industry

Whalley, R., (1988). The Response of Distributed—Lumped Parameter Systems. *Proceedings of the Institution of Mechanical Engineers, Part C: Journal of Mechanical Engineering Science*, vol. *202*(6), pp.421-429.

Whalley, R., Ebrahimi, M.& Jamil, Z., (2005). The torsional response of rotor systems. *Proceedings of the Institution of Mechanical Engineers, Part C: Journal of Mechanical Engineering Science*, vol.*219*(4), pp.357-380.

Whalley, R., Ebrahimi, M. & Jamil, Z. (2005). The torsional response of rotor systems. *Proceedings of the Institution of Mechanical Engineers, Part C: Journal of Mechanical Engineering Science*, vol. 219 (4), pp. 357-380.

Whalley, R., Ebrahimi, M. & Abdul-Ameer, A. (2007). High-speed rotor-shaft systems and whirling identification. *Proceedings of the Institution of Mechanical Engineers, Part C: Journal of Mechanical Engineering Science*, vol. 221 (6), pp. 661-676.

Appendix

5.4.Matlab Code

```
%Lumped Model

%tail rotor model
Jt1=0.00045
Jt2=0.0011
Ct1=0.6
Ct2=5
Kt=1753.014

%Main rotor model
Jm1=0.009
Jm2=450.23
Cm1=10
Cm2=100
Km=66774.12


G=26.9*10^9
Rt=0.035
```

```
Rm=0.0287

Lt=3.96

Lm=0.34

Nmt=2.9412

Nmr=4.359


% Lumped Model bode plot



% Tail rotor drive end

num=[Jt2 Ct2 Kt]

den=[Jt1*Jt2 (Jt1*Ct2+Jt2*Ct1) (Jt1*Kt+Jt2*Kt+Ct1*Ct2) (Ct1+Ct2)*Kt]

A=tf(num,den)

bode (A)



% Tail rotor load end

num=[Kt]

den=[Jt1*Jt2 (Jt1*Ct2+Jt2*Ct1) (Jt1*Kt+Jt2*Kt+Ct1*Ct2) (Ct1+Ct2)*Kt]

B=tf(num,den)

bode (B)


% wtr =
```

```
wtr=sqrt((Kt*(Ct1+Ct2))/(Jt1*Ct2+Jt2*Ct1))

% Main rotor drive end

num=[Jm2 Cm2 Km]

den=[Jm1*Jm2 (Jm1*Cm2+Jm2*Cm1) (Jm1*Km+Jm2*Km+Cm1*Cm2)

(Cm1+Cm2)*Km]

C=tf(num,den)

bode (C)



% Main rotor load end

num=[Km]

den=[Jm1*Jm2 (Jm1*Cm2+Jm2*Cm1) (Jm1*Km+Jm2*Km+Cm1*Cm2)

(Cm1+Cm2)*Km]

D=tf(num,den)

bode (D)

%Main rotor Resonant frequency

wmr=sqrt((Km*(Cm1+Cm2))/(Jm1*Cm2+Jm2*Cm1))
```

```
%FInite Element Models

%tail rotor model

Jt=2.58*10^-7  %0.02747

Jt1=0.00045

Jt2=0.0011

Ct1=0.6

Ct2=5

Kt=9271.7 %1753.014


%Main rotor model

Jm=1%7.67*10^-7 %0.01124

Jm1=0.009

Jm2=450.23

Cm1=10

Cm2=100

Km=333870 %66774.12


G=26.9*10^9

Rt=0.35

Rm=0.0287

Lt=3.96

Lm=0.34
```

Nmt=2.94117

Nmr=4.3589

%finite element bode plot

% Tail rotor drive end

numa=[(Jt^4)*Jt2 (Jt^4)*Ct2 8*Kt*(Jt^3)*Jt2+Kt*(Jt^4) 8*Kt*(Jt^3)*Ct2

7*(Jt^3)*(Kt^2)+21*(Kt^2)*(Jt^2)*Jt2 21*(Kt^2)*(Jt^2)*Ct2

15*(Kt^3)*(Jt^2)+20*(Kt^3)*Jt*Jt2 20*(Kt^3)*Jt*Ct2 5*(Kt^4)*Jt2+10*(Kt^4)*Jt

5*(Kt^4)*Ct2 Kt^5]

dena=[Jt1*(Jt^4)*Jt2 Ct1*(Jt^4)*Jt2+Jt1*(Jt^4)*Ct2

Kt*(Jt^4)*Jt2+8*Kt*Jt1*(Jt^3)*Jt2+Kt*Jt1*(Jt^4)+Ct1*(Jt^4)*Ct2

Kt*Ct1*(Jt^4)+8*Kt*Ct1*(Jt^3)*Jt2+8*Kt*Jt1*(Jt^3)*Ct2+Kt*(Jt^4)*Ct2

7*Jt1*(Jt^3)*(Kt^2)+21*(Kt^2)*Jt1*(Jt^2)*Jt2+(Kt^2)*(Jt^4)+8*Kt*Ct1*(Jt^3)*Ct2+7*(K

t^2)*(Jt^3)*Jt2

21*(Kt^2)*Jt1*(Jt^2)*Ct2+7*Ct1*(Jt^3)*(Kt^2)+21*(Kt^2)*Ct1*(Jt^2)*Jt2+7*(Kt^2)*(Jt^

3)*Ct2

15*(Kt^3)*(Jt^2)*Jt2+20*(Kt^3)*Jt1*Jt*Jt2+6*(Jt^3)*(Kt^3)+15*(Kt^3)*Jt1*(Jt^2)+21*(

Kt^2)*Ct1*(Jt^2)*Ct2

15*(Kt^3)*Ct1*(Jt^2)+15*(Kt^3)*(Jt^2)*Ct2+20*(Kt^3)*Ct1*Jt*Jt2+20*(Kt^3)*Jt1*Jt*Ct

2

5*(Kt^4)*Jt1*Jt2+20*(Kt^3)*Ct1*Jt*Ct2+10*(Kt^4)*Jt1*Jt+10*(Jt^2)*(Kt^4)+10*(Kt^4)

*Jt*Jt2 5*(Kt^4)*Ct1*Jt2+10*(Kt^4)*Jt*Ct2+5*(Kt^4)*Jt1*Ct2+10*(Kt^4)*Ct1*Jt

(Kt^5)*Jt2+4*(Kt^5)*Jt+(Kt^5)*Jt1+5*(Kt^4)*Ct1*Ct2 (Kt^5)*Ct1+(Kt^5)*Ct2]

A=tf(numa,dena)

% Tail rotor load end

numb=[Kt^5]

denb=[Jt1*(Jt^4)*Jt2 Ct1*(Jt^4)*Jt2+Jt1*(Jt^4)*Ct2

Kt*(Jt^4)*Jt2+8*Kt*Jt1*(Jt^3)*Jt2+Kt*Jt1*(Jt^4)+Ct1*(Jt^4)*Ct2

Kt*Ct1*(Jt^4)+8*Kt*Ct1*(Jt^3)*Jt2+8*Kt*Jt1*(Jt^3)*Ct2+Kt*(Jt^4)*Ct2

7*Jt1*(Jt^3)*(Kt^2)+21*(Kt^2)*Jt1*(Jt^2)*Jt2+(Kt^2)*(Jt^4)+8*Kt*Ct1*(Jt^3)*Ct2+7*(Kt^2)*(Jt^3)*Jt2

21*(Kt^2)*Jt1*(Jt^2)*Ct2+7*Ct1*(Jt^3)*(Kt^2)+21*(Kt^2)*Ct1*(Jt^2)*Jt2+7*(Kt^2)*(Jt^3)*Ct2

15*(Kt^3)*(Jt^2)*Jt2+20*(Kt^3)*Jt1*Jt*Jt2+6*(Jt^3)*(Kt^3)+15*(Kt^3)*Jt1*(Jt^2)+21*(Kt^2)*Ct1*(Jt^2)*Ct2

15*(Kt^3)*Ct1*(Jt^2)+15*(Kt^3)*(Jt^2)*Ct2+20*(Kt^3)*Ct1*Jt*Jt2+20*(Kt^3)*Jt1*Jt*Ct2

5*(Kt^4)*Jt1*Jt2+20*(Kt^3)*Ct1*Jt*Ct2+10*(Kt^4)*Jt1*Jt+10*(Jt^2)*(Kt^4)+10*(Kt^4)*Jt*Jt2 5*(Kt^4)*Ct1*Jt2+10*(Kt^4)*Jt*Ct2+5*(Kt^4)*Jt1*Ct2+10*(Kt^4)*Ct1*Jt

(Kt^5)*Jt2+4*(Kt^5)*Jt+(Kt^5)*Jt1+5*(Kt^4)*Ct1*Ct2 (Kt^5)*Ct1+(Kt^5)*Ct2]

B=tf(numb,denb)

% Main rotor drive end

numc=[(Jm^4)*Jm2 (Jm^4)*Cm2 8*Km*(Jm^3)*Jm2+Km*(Jm^4) 8*Km*(Jm^3)*Cm2

7*(Jm^3)*(Km^2)+21*(Km^2)*(Jm^2)*Jm2 21*(Km^2)*(Jm^2)*Cm2

```
15*(Km^3)*(Jm^2)+20*(Km^3)*Jm*Jm2 20*(Km^3)*Jm*Cm2
5*(Km^4)*Jm2+10*(Km^4)*Jm 5*(Km^4)*Cm2 Km^5 ]
denc=[Jm1*(Jm^4)*Jm2 Cm1*(Jm^4)*Jm2+Jm1*(Jm^4)*Cm2
Km*(Jm^4)*Jm2+8*Km*Jm1*(Jm^3)*Jm2+Km*Jm1*(Jm^4)+Cm1*(Jm^4)*Cm2
Km*Cm1*(Jm^4)+8*Km*Cm1*(Jm^3)*Jm2+8*Km*Jm1*(Jm^3)*Cm2+Km*(Jm^4)*Cm
2
7*Jm1*(Jm^3)*(Km^2)+21*(Km^2)*Jm1*(Jm^2)*Jm2+(Km^2)*(Jm^4)+8*Km*Cm1*(J
m^3)*Cm2+7*(Km^2)*(Jm^3)*Jm2
21*(Km^2)*Jm1*(Jm^2)*Cm2+7*Cm1*(Jm^3)*(Km^2)+21*(Km^2)*Cm1*(Jm^2)*Jm2+
7*(Km^2)*(Jm^3)*Cm2
15*(Km^3)*(Jm^2)*Jm2+20*(Km^3)*Jm1*Jm*Jm2+6*(Jm^3)*(Km^3)+15*(Km^3)*Jm1
*(Jm^2)+21*(Km^2)*Cm1*(Jm^2)*Cm2
15*(Km^3)*Cm1*(Jm^2)+15*(Km^3)*(Jm^2)*Cm2+20*(Km^3)*Cm1*Jm*Jm2+20*(Km
^3)*Jm1*Jm*Cm2
5*(Km^4)*Jm1*Jm2+20*(Km^3)*Cm1*Jm*Cm2+10*(Km^4)*Jm1*Jm+10*(Jm^2)*(Km
^4)+10*(Km^4)*Jm*Jm2
5*(Km^4)*Cm1*Jm2+10*(Km^4)*Jm*Cm2+5*(Km^4)*Jm1*Cm2+10*(Km^4)*Cm1*Jm
(Km^5)*Jm2+4*(Km^5)*Jm+(Km^5)*Jm1+5*(Km^4)*Cm1*Cm2
(Km^5)*Cm1+(Km^5)*Cm2]
C=tf(numc,denc)
% Main rotor load end
numd=[Km^5]
```

```
dend=[Jm1*(Jm^4)*Jm2 Cm1*(Jm^4)*Jm2+Jm1*(Jm^4)*Cm2
Km*(Jm^4)*Jm2+8*Km*Jm1*(Jm^3)*Jm2+Km*Jm1*(Jm^4)+Cm1*(Jm^4)*Cm2
Km*Cm1*(Jm^4)+8*Km*Cm1*(Jm^3)*Jm2+8*Km*Jm1*(Jm^3)*Cm2+Km*(Jm^4)*Cm
2
7*Jm1*(Jm^3)*(Km^2)+21*(Km^2)*Jm1*(Jm^2)*Jm2+(Km^2)*(Jm^4)+8*Km*Cm1*(J
m^3)*Cm2+7*(Km^2)*(Jm^3)*Jm2
21*(Km^2)*Jm1*(Jm^2)*Cm2+7*Cm1*(Jm^3)*(Km^2)+21*(Km^2)*Cm1*(Jm^2)*Jm2+
7*(Km^2)*(Jm^3)*Cm2
15*(Km^3)*(Jm^2)*Jm2+20*(Km^3)*Jm1*Jm*Jm2+6*(Jm^3)*(Km^3)+15*(Km^3)*Jm1
*(Jm^2)+21*(Km^2)*Cm1*(Jm^2)*Cm2
15*(Km^3)*Cm1*(Jm^2)+15*(Km^3)*(Jm^2)*Cm2+20*(Km^3)*Cm1*Jm*Jm2+20*(Km
^3)*Jm1*Jm*Cm2
5*(Km^4)*Jm1*Jm2+20*(Km^3)*Cm1*Jm*Cm2+10*(Km^4)*Jm1*Jm+10*(Jm^2)*(Km
^4)+10*(Km^4)*Jm*Jm2
5*(Km^4)*Cm1*Jm2+10*(Km^4)*Jm*Cm2+5*(Km^4)*Jm1*Cm2+10*(Km^4)*Cm1*Jm
(Km^5)*Jm2+4*(Km^5)*Jm+(Km^5)*Jm1+5*(Km^4)*Cm1*Cm2
(Km^5)*Cm1+(Km^5)*Cm2]
D=tf(numd,dend)

%Resonant frequency

%syms w
```

```
%eqn = (-Ct1*Jt*Jt2-
Jt1*(Jt^4)*Ct2)*(w^10)+(Kt*Ct1*(Jt^4)+8*Kt*Jt1*(Jt^3)*Ct2+Kt*(Jt^4)*Ct2)*(w^8)+(-
7*Ct1*(Jt^3)*(Kt^2)-21*(Kt^2)*Jt1*(Jt^2)*Ct2-7*(Kt^2)*(Jt^3)*Ct2-
21*(Kt^2)*Ct1*(Jt^2)*Jt2)*(w^6)+(15*(Kt^3)*Ct1*(Jt^2)+15*(Kt^3)*(Jt^2)*Ct2+20*(Kt
^3)*Ct1*Jt*Jt2+20*(Kt^3)*Jt1*Jt*Ct2)*(w^4)+(-10*(Kt^4)*Ct1*Jt-5*(Kt^4)*Ct1*Jt2-
10*(Kt^4)*Ct2-5*(Kt^4)*Jt1*Ct2)*(w^2)+(Kt^5)*Ct1+(Kt^5)*Ct2 ==0
%solve(eqn, w)



% Fi-Rotor System Hybrid Models


G1=26.9*10^9

p1=2770


%Main rotor model

Jm1=0.9

Jm2=450.23

cm1=10

cm2=100

Km=1.6362*10^4 %66774.12

Lm=0.34

rm=0.0287335
```

```
Jms=(3.141592654*((0.057467^4)-(0.042037^4))/32)

Lm=p1*Jms

Cm=1/(G1*Jms)

Zm=sqrt(Lm/Cm)

Tm=sqrt(Lm*Cm)


%tail rotor model

Jt1=0.00045

Jt2=0.0011

ct1=0.6

ct2=5

Kt=1753.014

Lt=3.96

rt=0.035


Jts=(3.141592654*((0.07^4)-(0.0688^4))/32)

Lt=p1*Jts

Ct=1/(G1*Jts)

Zt=sqrt(Lt/Ct)

Tt=sqrt(Lt*Ct)
```

Nmt=2.9412

Nmr=4.359